



# Review of High-Power Electrostatic and Electrothermal Electric Propulsion

David R. Jovel\* and Mitchell L. R. Walker†  
*Georgia Institute of Technology, Atlanta, Georgia 30332*

and

Daniel Herman‡  
*NASA John H. Glenn Research Center, Cleveland, Ohio 44135*

<https://doi.org/10.2514/1.B38594>

## Nomenclature

$g$	=	Earth's gravitational constant, 9.80665 m/s <sup>2</sup>
$I_{\text{beam}}$	=	beam current of gridded ion engines, A
$I_{\text{dis}}$	=	discharge current of Hall effect thrusters, A
$I_{\text{sp}}$	=	total specific impulse, s
$I_{\text{sp,dis}}$	=	discharge specific impulse, s
$\dot{m}_a$	=	anode mass flow rate, mg/s

$\dot{m}_c$	=	cathode mass flow rate, mg/s
$\dot{m}_n$	=	neutralizer mass flow rate of gridded ion engines, mg/s
$\dot{m}_{\text{tot}}$	=	total mass flow rate, mg/s
$P_{\text{beam}}$	=	beam power of gridded ion engines, kW
$P_{\text{dis}}$	=	discharge power of Hall effect thrusters, kW
$P_{\text{in}}$	=	total thruster input power, kW
$P_{\text{tot}}$	=	total power processing unit input power, kW



David R. Jovel is a Southern Regional Education Board and National Consortium for Graduate Degrees for Minorities in Engineering and Science (GEM) Fellow working toward his Ph.D. at the High-Power Electric Propulsion Laboratory in the School of Aerospace Engineering at the Georgia Institute of Technology. He earned his B.S. in Aerospace Engineering from the University of Texas at Austin in 2012 and went on to serve in various technical roles at organizations such as NASA Goddard Space Flight Center, Orbital ATK, Intelsat, and The Aerospace Corporation. His primary research focus is on the characterization of electrical facility effects of vacuum chambers on the performance and stability of Hall effect thrusters. Other research interests include radio frequency ion thrusters, thermal management of high-power electric propulsion devices, and nonequilibrium plasma.



Mitchell L. R. Walker is a Professor of Aerospace Engineering and Associate Chair of Graduate Studies at the Georgia Institute of Technology, where he directs the High-Power Electric Propulsion Laboratory. His primary research interests include both experimental and theoretical studies of advanced plasma propulsion concepts for spacecraft and fundamental plasma physics. Dr. Walker received his Ph.D. in Aerospace Engineering from the University of Michigan, where he specialized in experimental plasma physics and advanced space propulsion. His training includes rotations at Lockheed Martin and NASA Glenn Research Center. In 2005, he founded the electric propulsion program at the Georgia Institute of Technology. Dr. Walker's research activities include Hall effect thrusters, gridded ion engines, magnetoplasmadynamic thrusters, diagnostics for plasma interrogation and thruster characterization, vacuum facility effects, helicon plasma sources, plasma–material interactions, and electron emission from carbon nanotubes.



Dan Herman has been performing electric propulsion system research and development for 21 years. His doctoral thesis focused on internal ion thruster discharge plasma characterizations to understand and mitigate discharge cathode erosion in NSTAR and NEXT ion thrusters. He has been employed at the NASA Glenn Research Center for 16 years performing and leading electric propulsion projects. He led the life test, the centerpiece of the ion thruster life qualification, for the NEXT ion thruster, which will fly on the NASA DART mission. He was the technical lead for the 12 kW electric propulsion system development for the Solar Electric Propulsion Technology Demonstration Mission (SEP TDM) Project for 5.5 years. This effort was initially an in-house development activity of a 12.5 kW Hall thruster and HP-120 V PPU and has since transitioned to the Advanced Electric Propulsion System (AEPS) Contract to complete the 13 kW Hall thruster system development and to qualify and deliver three flight 12 kW Hall thrusters. Currently he is the Ion Propulsion Subsystem Lead for the NASA Power and Propulsion Element (PPE) and the Electric Propulsion System Manager for the NASA Gateway Program. The PPE is the 50 kW solar electric propulsion vehicle, flying three 12 kW AEPS Hall thrusters and four 6 kW Hall thrusters, and the first element of NASA's Gateway, the cornerstone of NASA's Artemis lunar exploration program.

Received 16 July 2021; revision received 15 July 2022; accepted for publication 5 August 2022; published online 9 September 2022. Copyright © 2022 by David Jovel, Mitchell Walker, and Daniel Herman. Published by the American Institute of Aeronautics and Astronautics, Inc., with permission. All requests for copying and permission to reprint should be submitted to CCC at [www.copyright.com](http://www.copyright.com); employ the eISSN 1533-3876 to initiate your request. See also AIAA Rights and Permissions [www.aiaa.org/randp](http://www.aiaa.org/randp).

\*Graduate Research Assistant, School of Aerospace Engineering; [david.r.jovel@gatech.edu](mailto:david.r.jovel@gatech.edu). Member AIAA.

†Professor, School of Aerospace Engineering; [mitchell.walker@ae.gatech.edu](mailto:mitchell.walker@ae.gatech.edu). Associate Fellow AIAA.

‡Electric Propulsion Systems Branch; [daniel.a.herman@nasa.gov](mailto:daniel.a.herman@nasa.gov). Associate Fellow AIAA.

$T$	=	thrust, mN
$T_{\text{emit}}$	=	thermionic emission temperature of a cathode insert, K
$T/P$	=	thrust-to-power ratio, mN/kW
$V_{\text{beam}}$	=	beam or screen grid voltage of gridded ion engines, V
$V_{\text{dis}}$	=	discharge voltage of Hall effect thrusters, V
$V_{\text{in}}$	=	spacecraft bus input voltage, V
$\eta_{\text{dis}}$	=	discharge efficiency, %
$\eta_{\text{PPU}}$	=	power processing unit electrical energy conversion efficiency, %
$\eta_{\text{tot}}$	=	total thruster efficiency, %

## I. Introduction

**H**IGH-POWER electric propulsion (EP) systems with input power levels greater than 10 kW are now being considered and implemented on various space missions. This is primarily because over the last 25 years there have been substantial advancements in solar array technology in which the specific power generated on-board spacecraft has increased from 30 to 100 W/kg [1]. Indeed, the spacecraft manufacturing community has demonstrated a shift toward all-electric spacecraft platforms that utilize midpower EP systems such as the 702SP, Eurostar E3000, 1300-class, and the ETS-9 [2–5]. In the next 5–10 years, the specific power ratio is projected to further increase to values up to 200 W/kg with a commensurate impact on spacecraft power budgets for telecommunication satellite constellations, sustainable space architectures for human exploration beyond low Earth orbit (LEO), and deep space exploration type missions [1]. With these larger spacecraft power budgets, mission designers and satellite operators are well postured to leverage the benefits of high-power EP systems. In preparation for this, the EP community has engaged in a range of activities aimed at characterizing the performance of high-power EP thrusters and their supporting segments to varying degrees. In fact, the realization of high-power EP is readily confirmed when we consider the recent progress made by government and commercial space sector stakeholders in the United States and abroad as they continue to support the development and flight qualification of high-power EP systems.

In the United States, Congress unanimously approved the NASA Transition Authorization Act of 2017 that specifically names high-power EP as an enabling space technology for various planned space missions. This act has motivated and sustained the development and flight qualification of two well-known high-power EP systems: the 12.5 kW Advanced Electric Propulsion System (AEPS) and the 6.9 kW NASA's Evolutionary Xenon Thruster—Commercial (NEXT-C). AEPS will serve as the primary propulsion system aboard the Power and Propulsion Element (PPE) mission to support the U.S.'s goal of achieving a sustainable space transportation system between the Earth, moon, and Mars [6,7]. Additionally, PPE will utilize four 6 kW BHT-6000 Hall effect thrusters (HETs) that provide mission-critical capabilities and have been identified as a strategic benefit to further commercializing high-power EP [8]. On the other hand, the NEXT-C gridded ion engine (GIE) is the primary propulsion system used on the Double Asteroid Redirection Test mission, which launched on Nov. 24, 2021. Implementation of the NEXT-C on this mission marks the culmination of almost 20 years of research and development on gridded ion thruster technology.

The maturation of high-power EP technology for future applications is also being pursued at an international level. In Europe, much progress has been made toward the development of high-power HETs and GIEs through various long-term, government-sponsored programs. For example, two 5 kW and two 20 kW HETs are being matured to meet the needs of large satellite operators to reduce the transfer time during electric orbit raising (EOR) [9–11]. In parallel, the initial development of the 6.4 kW T7 GIE and flight qualification of the well-established 5 kW RIT 2X GIE are underway to advance their technology readiness levels (TRLs) and facilitate their use in geostationary orbits and space exploration mission applications [12,13]. It should be noted that these high-visibility projects are also finding solutions to problems associated with hardware manufacturability, production costs, and qualification testing of the thruster and its supporting segments for eventual commercialization.

To achieve the practical application of high-power EP in the near term, we must consider the thruster and all the supporting segments necessary for its operation. At a system level, an EP thruster aboard a spacecraft requires a cathode, a power processing unit (PPU), and a propellant management system (PMS). Each of these segments must be extensively characterized and undergo the same level of hardware maturity to ensure full compatibility with its associated thruster. The combination of the thruster, cathode(s), PPU, and PMS comprise the EP string.

A thorough literature review identified a gap in addressing the challenges associated with further realizing the potential of EP strings with thruster input powers  $\geq 6$  kW. Petro and Sedwick conducted a survey of midpower HETs and GIEs with maximum input power levels of 8 and 13 kW, respectively, and their potential use on space exploration mission applications [14]. Wollenhaupt et al. published a review on the design and performance of arcjet thrusters ranging between 0.02 and 200 kW [15]. In another review by Lev et al., we are given a wholesome perspective on the various applications of low to midpower EP strings and their projected future use [16]. Lastly, Dale et al. identify and discuss many of the remaining challenges in EP for a wide range of thruster technologies and provide recommendations for future research [17]. However, none of these surveys provide a rigorous focus on thrusters of input power levels greater than 6 kW or discuss their evolution from prototype to flight. Furthermore, these surveys place emphasis on the thruster and do not provide sufficient insight on the state-of-the-art (SOA) and obstacles associated with maturing the cathode, PPU, and PMS segments. Thus, we believe that such a review is necessary to meet the space sector's growing interest in the high-power EP regime.

In this work, we define high-power as an EP thruster that requires input electrical power values of 6 kW or greater. The total input power  $P_{\text{in}}$  is the main parameter for this review as it is commonly used by the EP community to identify the power requirements to achieve a particular performance profile in thrust  $T$  and total specific impulse  $I_{\text{sp}}$ . Our review found a total of 46 high-power electrostatic and electrothermal devices of different technology maturity levels that have been developed since the 1980s. Of the 46 thrusters identified, less than a third of them are supported by active research and development campaigns focused on thruster performance characterization. The rest of the EP devices were developed as lab prototypes to demonstrate proof-of-concept and/or study plasma phenomenology with limited or no plans of transitioning into an EP string. Presently, three high-power thrusters are being flight qualified as fully integrated EP strings for government space applications. Furthermore, only one high-power EP string  $> 6$  kW has ever flown. Thus, we note a disparity between high-power EP thrusters and their ability to achieve EP string or flight qualification status. To this end, we aim to identify as many high-power EP strings as possible, beginning with the thruster segment and moving on to the cathode, PPU, and PMS segments required for space flight operation.

The main objective of this review paper is to identify the gaps in the current SOA of high-power EP strings that meet the criteria of  $P_{\text{in}} \geq 6$  kW. In Sec. II, we define the scope of high-power EP types reviewed in this paper. We break down the EP string architecture into four segments and define their respective SOA. In Sec. III, we provide the reader with a brief overview of midpower EP strings in the range of 1–5 kW with flight heritage as they serve as the natural starting point for enabling the high-power regime. In Sec. IV, we present a high-level summary of the performance and hardware maturity level of all the electrostatic and electrothermal high-power thrusters identified, among other technical details. As a complement to Sec. IV, we tabulate the nominal and demonstrated performance range of each thruster for a variety of parameters, such as input power, thrust, specific impulse, total efficiency, and more along with references in the Appendix. In Sec. V, we introduce the high-power EP strings in development as of 2021, and the corresponding cathode, PPU, and PMS segments along with their respective performance metrics. The hardware maturity and qualification state of all segments of the EP string in the high-power regime are assessed when applicable. In Sec. VI, we share some insight and discussion points regarding recent programmatic and technological advances we believe to be vital

in enabling the development of high-power EP strings. Finally, in Sec. VII, we identify critical gaps in the current SOA and offer recommendations, when possible, to serve as a vector for the EP community to follow in order to realize the potential of high-power EP for future space applications.

## II. Scope and Definition of SOA High-Power EP

In this section, we discuss the scope of thrusters reviewed and define the four segments of the EP string. We restrict our review to only electrostatic and electrothermal EP types and briefly explain our exclusion of electromagnetic devices. Following this discussion, we decompose the EP string into the thruster, cathode, PPU, and PMS segments and provide a short description of each along with qualities that define their SOA. The objective of this section is to orient the reader with the vocabulary and terminology used throughout this paper and provide a clear definition of SOA.

### A. Scope of EP Types Reviewed

The EP string is typically categorized by the thruster's total input power  $P_{in}$  and the plasma acceleration mechanism employed. The acceleration mechanisms are generally grouped into three thruster types: 1) electrothermal, 2) electrostatic, and 3) electromagnetic. Detailed descriptions of each type can be found in the works of Jahn [18] and Goebel and Katz [19]. In this paper, the scope of EP strings reviewed was limited to electrothermal and electrostatic EP types. This is primarily due to their growing flight heritage in recent LEO and geostationary equatorial orbit (GEO) missions utilizing EP for EOR and station-keeping [16]. Electrothermal devices such as arcjets and resistojets have been widely used since the early 1980s for station-keeping maneuvers. Their proliferation to the commercial sector was mainly due to their competitive pricing and simplicity in integration and on-orbit operations. Electrostatic thrusters offered higher system efficiency and constant thrust operations, making EOR and in-orbit station-keeping maneuvers a more practical option for large satellite operators. Both EP thruster types have significant flight heritage in a diverse range of space applications with fully characterized cathode, PPU, and PMS segments.

Electromagnetic thruster types are not included in this review due to their lower technology maturity levels and limited experience in EP string integration testing. Significant research has been conducted on devices such as pulsed plasma thrusters (PPTs), pulsed inductive thrusters (PITs), field-reversed configuration (FRC) thrusters, and magnetoplasmadynamic thrusters (MPDTs). High-power electromagnetic devices such as steady-state applied-field (AF) MPDTs exist in the hundreds of kilowatts levels and have been tested on various types of propellants other than xenon [20]. Indeed, Kodys et al. provide a development timeline of MPDTs dating back to the 1960s [20]. Notable AF-MPDT research and development programs in the 100 kW class as of 2019 include the MAT-100 [21], SX3 [22], and the AF 2D-MPD [23]. Accurate characterization of the performance of such high-power devices remains a challenge due to the elevated facility operational pressures above the 0.05 Pa requirement, severe degradation rates of the cathode, and thermal loading on magnetic coils and other thruster components when operating at steady state [22]. However, the authors of this paper acknowledge that much progress has been made in recent years in addressing such challenges as discussed by Boxberger et al. [24]. AF-MPDTs may be operated in different modes to achieve competitive performance profiles in thrust and total efficiency while mitigating the various challenges associated with this thruster technology type. For example, the SX3 was operated in the hybrid Hall-effect centric acceleration mode producing 2.75 N of thrust,  $I_{sp}$  of 4665 s, and a thrust efficiency of 62% at a discharge power of 101.5 kW and facility pressure of 0.4 Pa [24]. Additionally, lanthanum hexaboride ( $LaB_6$ ) hollow cathodes have been used in relatively low-power MPDT applications of up to 8.6 kW demonstrating proof-of-concept as shown in [24,25]. Recent advancements in superconducting, high-temperature coil technology also have the potential of reducing the structural mass and input power required for generating the external magnetic fields. Thus, optimizing between the various operational modes, the use of

high-amperage  $LaB_6$  hollow cathodes, and superconductor technology make AF-MPDTs a promising technology for high-power EP strings.

High-power PITs, FRCs, and PPTs remain relatively technologically immature compared to electrostatic and electrothermal high-power EP devices. The first notable high-power PIT prototype, the PIT MkV, was introduced in 1993 with performance levels with performance around 20 kW [26]. A more recent paper reviewing the current SOA in PITs is given in [27]. However, high-power PITs are limited by the current SOA in electrical energy storage and switching technology [27–29]. FRCs originally developed in the United Kingdom in the 1960s are designed for an input power range of 10–100 kW, but thruster performance characteristics such as thrust and specific impulse have never been collected [30,31]. PPTs are a compelling option for the SmallSat community, given their simplicity in solid propellant ablative technology. Still, they remain at a relatively low maturity level in the high-power regime with few performance metrics as reported by Kazeev and Kozlov [32]. These factors combined make MPDTs, PITs, FRCs, and high-power PPTs less practical than the other types of EP thrusters reviewed in this paper. From this base, we define our scope to be only high-power electrostatic and electrothermal EP devices and strings.

### B. Overview of the EP String Architecture

In this paper, an EP string is defined as the ensemble consisting of the thruster, cathode, PPU, and PMS. An EP system includes the EP string, propellant storage tanks, deployment mechanism, and thrust vector orientation controls such as multi-axis gimbals. The objective of this subsection is to provide the reader with a technical definition of the four segments and the qualities that define them as SOA. Figure 1 provides the reader with a high-level schematic of the four EP segments and their interfaces [33]. The figure serves as a visual aid as we address the different segments of the EP string. In the following subsections, each EP segment is described, and the qualitative metrics that define them as SOA are presented.

#### 1. Thruster

The thruster is the electromechanical device whose function is to convert the total input electrical power,  $P_{in}$ , into jet power, thereby producing thrust. The function of the thruster is to increase and convert the potential energy of the propellant into useful kinetic energy for momentum transfer. Depending on the thruster type, the potential energy of the propellant can be the total stagnation enthalpy of the gas or the electric potential energy of the plasma.

Electrothermal devices input electric energy via heating elements or a steady discharge plasma to raise the stagnation enthalpy of the propellant. The supplemented enthalpy of the working fluid is then converted into kinetic energy as the propellant expands through a nozzle. Resistojets and arcjets are both examples of electrothermal devices and are adequately described by Jahn [18].

Electrostatic thruster operation can be divided into three stages: 1) plasma generation, 2) ion acceleration, and 3) beam neutralization. In the first stage, the electronic energy state of the propellant must be elevated from the ground, neutral state to an excited, net positive charge state through a process called ionization. Typically, ionization occurs collisionally when neutral gas particles collide inelastically with highly energetic electrons. For the neutral particle to become an ion, the energy exchange during this collision must be equal to or greater than the first electronic energy level of the atom or particle. For xenon, the first electronic energy level is about 12.1 eV. Propellant ionization is achieved through various physical mechanisms, as outlined in Chapter 4 by Jahn [18]. In the second stage, external electric fields are used to accelerate the ion in a specific direction to produce thrust. In GIEs, a series of electrically biased grids are used to extract and accelerate the ions from the discharge chamber out of the thruster. In HETs, an electric potential drop between the anode and the local plasma potential near the exit plane serves as the accelerating electric field. The third stage consists of neutralizing the exhausted ion beam using electron sources called cathodes. The final stage is important to mitigate spacecraft–plasma plume interactions.

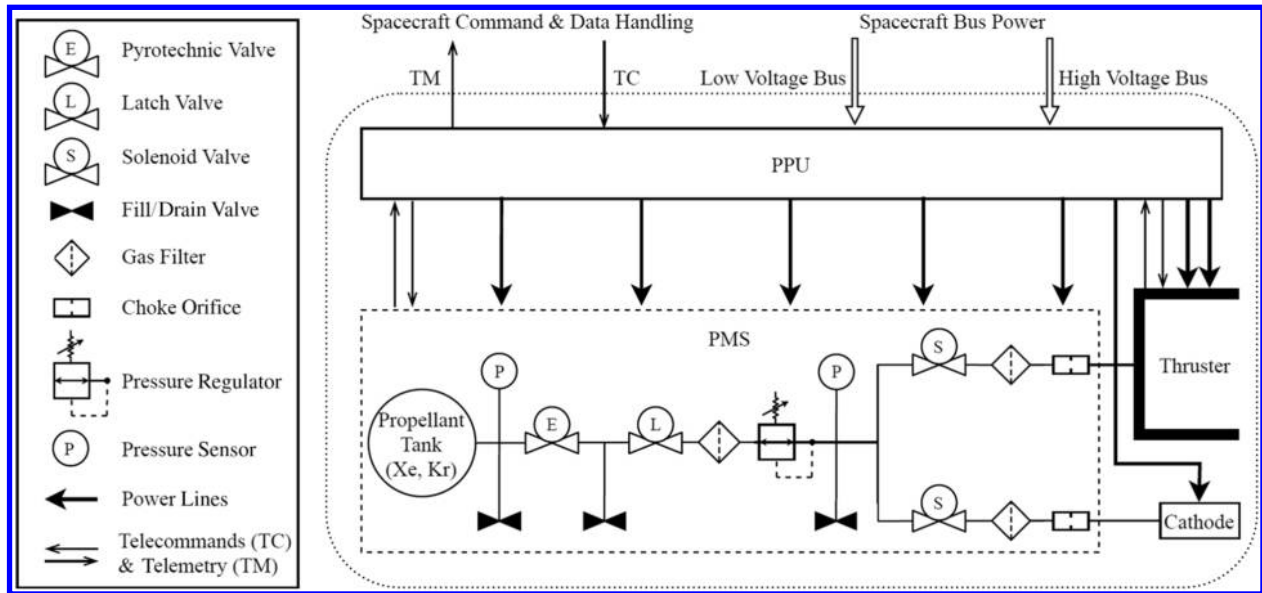


Fig. 1 Visual schematic of the EP string consisting of the thruster, cathode, PPU, and PMS segments.

An SOA high-power thruster is one that has achieved the following requirements. First, the thruster has been operated at  $P_{in} \geq 6$  kW and its performance measured in vacuum facilities capable of maintaining adequate pressure levels. At a minimum, performance measurements of thrust, specific impulse, mass flow rates, currents, and voltages are reported in publicly available resources. Second, a thruster must have demonstrated cumulative operation of 50 h or more proving sustainability in performance. Lastly, the thruster must have completed one or more flight qualification tests imposed by relevant industry standards that address mechanical, thermal, and/or electrical mission requirements. We note that high-power thrusters undergoing flight qualification will satisfy these and many more stringent requirements and thus are automatically considered SOA in this paper.

## 2. Cathodes

Cathode and neutralizers function as electron sources for gas ionization and plume neutralization downstream of the thruster exit plane. Thermionic hollow cathodes developed in the late 1960s are commonly used in EP systems today [34,35]. The operating principle of a hollow cathode is based on sufficiently heating a special insert, called the emitter, up to its thermionic emission temperature  $T_{emit}$  (the temperature at which energetic electrons escape the emitter surface). The two most common emitters used in hollow cathodes are barium-oxide-impregnated tungsten (BaO-W) or lanthanum hexaboride ( $LaB_6$ ). The BaO-W emitter is composed of a porous tungsten solid impregnated with earth metal oxide compounds like barium oxide, calcium oxide, and aluminum oxide. The  $LaB_6$  emitter consists of press-sintered lanthanum hexaboride powder [36]. Heat addition in a thermionic hollow cathode may be supplied one of two ways: 1) through an electrically resistive element called the cathode heater or 2) via a sustained discharge between the keeper and cathode body electrodes. The latter of the two methods is called a heaterless cathode, which is a recent and growing technology. Cathodes must generate the electrical currents required to maintain ionization and/or neutralization processes during nominal thruster operation. Goebel and Katz provide a detailed overview of the theory of hollow cathode operation in [19].

Cathodes are utilized differently depending on the EP thruster type. In DC discharge GIEs, two cathodes are utilized to support separate functions: propellant ionization and ion beam neutralization. First, a discharge cathode that resides inside the thruster's discharge chamber emits electrons necessary for propellant ionization. These electrons are magnetically confined using either permanent magnets or electromagnetic coils to enhance ionization efficiency [37]. The second cathode, called the neutralizer, is externally mounted downstream of the GIE grid assembly and neutralizes the exhausted ion

beam. Radiofrequency (RF) GIEs do not require a discharge cathode because propellant ionization is achieved via a time-varying electromagnetic field inside the thruster's discharge chamber and only use an externally mounted neutralizer. In HETs, a cathode mounted outside of the discharge channel, facing the plasma plume, supports both ionization and beam neutralization. A fraction of the HET's discharge current  $I_{dis}$  is utilized for propellant ionization while the rest is utilized for HET plume neutralization.

We note to the reader that the cathode segment is inherently part of the thruster and not a separate component. All electrostatic devices in this review paper must utilize a cathode to operate in the space environment. Both the thruster and cathode segments are codeveloped and operated together during performance characterization of EP strings. We may at times discuss the thruster and cathode independently, but it is implied that they are inextricably linked based on the operating principles of EP devices.

An SOA high-power cathode segment is one that satisfies the following requirements. First, the cathode must have been operated at the discharge or beam currents required by their respective high-power thruster in a relevant test environment at  $P_{in} \geq 6$  kW. Second, the cathode's emitter material properties must have been well characterized and compatible with the propellant of the thruster. Third, the cathode must have completed one or more flight qualification tests imposed by relevant industry standards that address mechanical, thermal, and/or electrical mission requirements.

## 3. Power Processing Unit

The function of the PPU is to provide all the power conditioning and logic necessary to operate, control, monitor, and protect the EP string during nominal thruster operation. As shown in Fig. 1, the PPU interfaces directly with the spacecraft bus and conditions spacecraft power to meet the input power requirements of the thruster and its supporting segments. In general, the PPU must supply power to support five tasks: 1) thruster electrode operations, 2) PMS valve and flow controls, 3) cathode(s) operations, 4) EP string health monitoring and control, and 5) spacecraft bus communications for EP string commanding and telemetry relay. To do this, the PPU physically connects to the spacecraft's low- and high-voltage power distribution buses and conditions the available power to supply regulated electrical energy necessary to operate the EP string. The low-voltage bus is typically regulated between 22 and 34 V and is mainly used to power PPU electronics, routine housekeeping functions, sensor telemetry, and other low-power EP string elements such as the PMS and its components. The high-voltage bus serves as the primary energy source for thruster operation. For heritage NASA deep space missions, the high-voltage bus ranges between 80 and

160 V, while standard spacecraft buses used by industry are 36, 70, or 100 V and typically regulated within  $\pm 2$  V. For telecom satellites that offer only one common 100 V power bus, the PPU must internally regulate and output the power necessary to support both thruster and low-power EP string operations. The PPU uses isolated DC/DC converters to efficiently step up the supplied spacecraft bus voltages to the voltages and currents necessary to operate the EP device.

The total PPU input power  $P_{\text{tot}}$  is the net electrical energy consumed by the PPU for thruster operations. The PPU converts this input power to the voltages and currents required to operate the thruster. The total input power to the thruster,  $P_{\text{in}}$ , includes all the electrical energy necessary to create, sustain, and accelerate the plasma. In HETs,  $P_{\text{in}}$  consists of the discharge power  $P_{\text{dis}}$  between the anode and cathode, power delivered to the electromagnetic coils, and, if used, power to the cathode heater element and keeper electrode. In GIEs,  $P_{\text{in}}$  consists of the beam power  $P_{\text{beam}}$  between the discharge chamber anode and the neutralizer, power to sustain the plasma inside the discharge chamber,<sup>§</sup> power to auxiliary grids such as the accelerating and decelerating grids, and if used, power to electromagnetic coils. In arcjets,  $P_{\text{in}}$  is the electric power needed to sustain a steady discharge between the nozzle electrode and coaxially mounted cathode. Often, the discharge power,  $P_{\text{dis}} = V_{\text{dis}} I_{\text{dis}}$ , for HETs and arcjets or the beam power,  $P_{\text{beam}} = V_{\text{beam}} I_{\text{beam}}$ , for GIEs is presented in the literature as they consist of  $> 85\%$  of  $P_{\text{in}}$ . Ultimately, we use  $\eta_{\text{PPU}} = P_{\text{in}}/P_{\text{tot}}$  to measure how efficient the PPU converts the available spacecraft energy to meet the total input power demands of the thruster.

The power to the PMS segment includes power to operate electro-mechanical components such as pyrotechnic valves, solenoid valves, proportional control or chopping valves, pressure regulators, and heaters that maintain mass flow rates. Power to the cathode (or neutralizer) segment is composed of two circuits: 1) a DC power supply energizing a resistive heating element with respect to the cathode body and 2) a current source in series with the keeper electrode with respect to the cathode body. Power to the cathode and keeper are usually observed during thruster startup operations.

In addition to electrical power functions, the PPU also serves as the communication interface between the spacecraft's command and data handling subsystem and the EP string. In this role, the PPU uses various sensors to monitor, control, and implement fault detection, isolation, and recovery (FDIR) commands to recover nominal thruster operations [6,38,39]. The PPU receives, consolidates, and transmits EP string telemetry during thruster operations to the spacecraft's command and data handling subsystem [6,40]. Communication with the string is typically executed via a MIL-STD-1553B bus; however, other bus architectures such as SpaceWire and Controller Area Network (CAN) may also be used depending on data transmission speed, power, and budget requirements.

Various flight PPUs have been developed by both thruster manufacturers and the commercial space sector to support the midpower regime as discussed in Sec. III. Typically, the PPU is uniquely designed and manufactured for an EP device to support specific throttle points, defined as a specific set of discharge or beam voltages and currents, with  $\eta_{\text{PPU}}$  in the 90% range.

An SOA high-power PPU is defined as having achieved the following requirements. First, the PPU must have demonstrated performance in supplying input powers  $\geq 6$  kW to all the segments of the EP string in a relevant test environment. Second, PPU performance measurements consisting of energy conversion efficiency, output currents and voltages to the thruster, and associated instabilities must have been reported. Lastly, the PPU must have completed one or more flight qualification tests imposed by relevant industry standards that address mechanical, thermal, and/or electrical mission requirements.

#### 4. Propellant Management System

The function of the PMS is to supply the thruster with the correct amount of neutral gas required for ionization and beam neutralization. The PMS is propellant specific and can be decomposed into two sequential operations: pressure regulation and flow control. As shown in Fig. 1, the PMS interfaces directly with the high-pressure propellant storage tank typically 2175 psia and above [41,42]. Pressure regulation is required to reduce the high pressure in the storage tank down to the operating pressures of the various electromechanical devices that enable flow control downstream. Usually, high-pressure regulation in the PMS segment is achieved through a traditional mechanical pressure regulator or a "bang-bang" solenoid valve and plenum assembly [33,43]. After the pressure has been regulated, low-pressure flow control is implemented either actively or passively to supply the nominal mass flow rates of gas to the thruster and cathode segments within a prescribed uncertainty. Active flow control consists of using a closed feedback loop based on the measured  $I_{\text{dis}}$ ,  $I_{\text{beam}}$ , or setpoint offset as measured by flow sensors near the inlet of the thruster/cathode segments. Passive flow control uses compressible flow concepts to size flow restrictors to choke the gas flow at the nominal flow rates required. In addition to this, solenoid and/or latch valves are included throughout the PMS to ensure flow isolation between various plumbing sections. Lastly, micron filters are utilized at multiple points in the PMS to remove any contaminants trapped inside the propellant lines inherent from assembly, integration, and processing. Usually, EP string developers qualify the pressure regulation and flow control hardware separately. As Snyder et al. outlined in [33], several different PMS architectures have flown as part of various low and midpower EP systems.

An SOA of PMS segment in the high-power regime is defined by the following qualities. First, the PMS must be able to supply the flow rates required to operate thrusters at input powers  $\geq 6$  W. Second, the performance of the PMS segment indicating high-to-low pressure regulation and active flow control must have been measured. Third, the PMS must be compatible with the propellants used on the thruster. Lastly, the PMS must have completed one or more flight qualification tests imposed by relevant industry standards that address mechanical, thermal, and/or electrical mission requirements.

### III. Flight-Qualified EP Systems Near the High-Power Regime

This section provides a brief overview of the flight-qualified EP systems operating near the high-power regime and their use in space architectures today. The EP community has produced a variety of EP systems in the midpower regime, 1–5 kW, with well-characterized performance to support the changing needs of stakeholders in the space sector. However, our literature review indicates that only one EP string greater than 6 kW has flown while only a few others have embarked on formal flight-qualification test campaigns. Therefore, we find it useful to introduce the six fully integrated EP systems operating in the midpower regime that have completed a formal flight qualification program and demonstrated on-orbit performance. These systems were selected based on their operating conditions near the 6 kW input power level, frequency of use since the 2000s, and/or their function as a baseline design for a high-power thruster counterpart. The six midpower EP systems operate between 0.46 and 4.5 kW discharge/beam power and are given in Table 1. The nominal operating points of each EP system are mission specific and typically target either a high-thrust mode for EOR or high- $I_{\text{sp}}$  mode for station-keeping maneuvers. Included in this table are the EP system's thruster, EP device type, nominal discharge/beam power(s), primary developers, the number of satellites incorporating the EP system, and the notable mission and year that established its status within the EP community. We also include the orbit type, which is either GEO or science-based missions requiring a unique orbit trajectory (SCI). The authors of this paper believe that these EP systems will serve as the baseline in further enabling high-power EP.

Understanding how the six EP systems evolved from prototype to flight serves as an indicator for the continued development of the high-power thrusters in Sec. IV. The main observation from Table 1 is

<sup>§</sup>This power is either the power to support discharge cathode operations in DC discharge-type GIEs or RF generator power in RF-type GIEs.

**Table 1** Midpower EP systems with flight heritage in ascending  $P_{\text{dis}}$  or  $P_{\text{beam}}$ 

EP system thruster	Type	$P_{\text{dis}}$ or $P_{\text{beam}}$ , kW	Developers	No. of satellites (orbit)	Notable mission (year)	References
PPS <sup>®</sup> 1350 <sup>a</sup>	HET	0.46–1.19	Fakel/Safran	2 (SCI)	SMART-1 (2003)	[16,44]
SPT-100 <sup>b</sup>	HET	1.35	Fakel, Fakel/Maxar	84 (GEO)	Gals 1 (1994) MBSAT (2004)	[16,45]
XIPS-25	GIE	1.7, 3.7 <sup>c</sup>	L-3 ETI/Boeing	35 (GEO)	Galaxy XI (1999)	[16,46,47]
T6	GIE	2–4 <sup>c</sup>	QinetiQ	1 (SCI)	BepiColombo (2018)	[48,49]
SPT-140 <sup>d</sup>	HET	3, 4.5	Fakel/Maxar, Fakel/Airbus DS	5 (GEO)	Telstar 19 VANTAGE (2018) Eutelsat 172B (2017)	[4,16,50,51]
XR-5	HET	3, 4.5	Aerojet Rocketdyne	7 (GEO)	AEHF-1 (2010)	[16,52,53]

<sup>a</sup>PPS<sup>®</sup>1350 was qualified at two different nominal input powers up to 1.5 kW. The values shown here are based on the throttled performance demonstrated on the SMART-1 mission.

<sup>b</sup>SPT-100 was initially qualified in Russia and first flown on the 1994 Gals 1 mission and then qualified to Western standards as part of a joint effort between Fakel and Maxar (formerly known as SS/L).

<sup>c</sup>Calculated based on reported values.

<sup>d</sup>SPT-140 prototype models were initially developed in Russia as a high-power alternative for Western spacecraft manufacturers. Both Maxar and Airbus collaborated with Fakel to qualify and fly SPT-140 variants on their GEO platforms.

that all thrusters are scaled-up versions of their lower power counterparts. The SPT-100 was the next-generation upgrade to the low-power SPT-70 EP system that was mainly used for orbit insertion and east–west station-keeping of Russian GEO satellites [54]. The SPT-100 served as the baseline design for both the PPS<sup>®</sup>1350 and the SPT-140. The PPS<sup>®</sup>1350 HET was derived from the SPT-100 in the mid-1990s but implemented a new magnetic field topology, cathode design and location, and overall mechanical design essentially improving performance and lifetime [55]. Originally, PPS<sup>®</sup>1350 was qualified to a discharge power of 1.5 kW but ultimately flew as a variable input power thruster on the SMART-1 mission [44,55]. The PPS<sup>®</sup>1350 is the baseline for three subsequent thruster versions as well as the 5-kW-class PPS<sup>®</sup>5000 Hall thruster. The 4.5 kW SPT-140 leveraged much of the extensive flight heritage of the SPT-100's, primarily used for north–south station-keeping activities and momentum wheel unloads, to support a wider performance range targeting EOR operations [50]. The scaled-up SPT-140 uses a conceptually similar PMS segment but a higher current cathode and newly designed PPU [50]. The T6 design is based on the 700-W T5 engine and also demonstrated variable thrust performance in the beam power range of 2.1–3.5 kW on the BepiColombo mission [56,57]. Similarly, the XIPS-25 is the high-power successor of the 300-W XIPS-13 with a modified PPU, all other segments the same [47,58]. The XIPS-25 was qualified at two operational beam power modes, 1.7 and 3.7 kW, to support on-orbit station-keeping and orbit insertion operations [59]. Finally, the XR-5 HET is the culmination of a series of midpower qualification tests ranging from 1.7 to 4.5 kW based on the performance of the BPT-1, BPT-2000, and the BPT-4000 [60,61].

Table 1 confirms that the maximum power of flown electrostatic devices is limited to 4.5 kW. In contrast, the high-power thrusters discussed in the next section scale up to 100 kW, suggesting a large disparity between what the community has flown versus what has been tested in vacuum test facilities. This gap will be addressed in detail in Sec. VII.

Next, we introduce the midpower-class cathodes with flight heritage in Table 2. The table includes the cathode name or function, associated thruster from Table 1, cathode discharge current ( $I_{\text{dis}}$ )

range, emitter material, ignition method, and developer. For the emitter materials listed, we used the abbreviations defined in Sec. II. Table 2 reveals that only heater-based cathodes primarily consisting of BaO-W emitter material have flown. Furthermore, we observe that the maximum  $I_{\text{dis}}$  flown is 18 A and corresponds to the discharge cathodes used in the XIPS-25 and T6 GIEs. In addition, each of these cathodes was paired with the thruster early in development phase and matured together through flight qualification. On this basis, we identify a gap in the ability of midpower cathodes to readily support high-power EP thrusters, specifically HETs. Our review found the average discharge currents demonstrated on high-power HETs to be 22 A for 6–9 kW, 34 A for 10–18 kW, 39 A for the 25 kW class, and more than 88 A for >30 kW thrusters. We also learned that much work is being done on characterizing high-current LaB<sub>6</sub> cathodes as well as heaterless ignition methods for high-power EP applications. These findings are discussed further in Secs. V and VI.

The midpower PPUs with flight heritage are shown in Table 3. The information presented in Table 3 is based on the relevant performance metrics discussed in Sec. II and is as follows: PPU segment name, supported thruster(s), nominal discharge/beam power range, discharge voltage range for HETs ( $V_{\text{dis}}$ ), screen grid voltage range for GIEs ( $V_{\text{beam}}$ ), discharge current range for HETs ( $I_{\text{dis}}$ ), beam current range for GIEs ( $I_{\text{beam}}$ ), spacecraft bus input voltages ( $V_{\text{in}}$ ), total mass, efficiency, and primary developer(s).

The main observation we make of midpower PPUs with flight heritage is that they are designed to support specific thruster operating conditions with respect to the available spacecraft bus power. Based on the data collected, a spacecraft bus input voltage of 100 V DC is a common design point for commercial PPU developers. However, as the available power onboard a spacecraft change, PPU developers must modify and requalify the PPU segment to support the new input voltages. This is readily evident based on PPU Mk1 and the XR-5 PPU, both requalified for lower input voltage buses to support different satellite power buses [65,66]. Power conversion efficiencies  $\eta_{\text{PPU}}$  for the PPUs in Table 3 are all greater than 90%. The mass of the PPU is generally larger for GIEs as they contain more electronics to support more power supply functions than HETs and operate at higher voltages that results in more complex and heavier

**Table 2** Midpower cathodes with flight heritage in ascending  $I_{\text{dis}}$ 

Cathode	Thruster	$I_{\text{dis}}$ , A	Emitter material	Ignition method	Developer	References
Neutralizer	T6	1–2.2	BaO-W	Heater	QinetiQ	[35]
Neutralizer	XIPS-25	1.5–3	BaO-W	Heater	L-3 ETI	[35]
KN-3	SPT-100	4.5	LaB <sub>6</sub>	Heater	Fakel	[35]
K1, K2	PPS <sup>®</sup> 1350-G	2.1–3.8	LaB <sub>6</sub>	Heater	Safran/Fakel	[35,55]
—	SPT-140	3–15	LaB <sub>6</sub>	Heater	Fakel	[35]
HCA <sup>a</sup>	XR-5	5–15	BaO-W	Heater	Aerojet Rocketdyne	[62]
Discharge	T6	5–18	BaO-W	Heater	QinetiQ	[35,57]
Discharge	XIPS-25	7.6, 18	BaO-W	Heater	L-3 ETI	[35,63]

<sup>a</sup>HCA was initially tested on the BPT-4000 thruster, which was eventually renamed XR-5 [64].

**Table 3** Midpower PPU with flight heritage in ascending  $P_{\text{dis}}$  or  $P_{\text{beam}}$ 

PPU name	Thruster	$P_{\text{dis}}$ or $P_{\text{beam}}$ , kW	$V_{\text{dis}}$ or $V_{\text{beam}}$ , V	$I_{\text{dis}}$ or $I_{\text{beam}}$ , A	$V_{\text{in}}$ , V	Mass, kg	$\eta_{\text{PPU}}$ , %	Developers	References
PPU-100	SPT-100	1.35	300	4–5	100	7.5	90.8	Maxar	[38,68]
PPU Mk1	PPS <sup>®</sup> 1350-G, SPT-100	1.5	220–350	3–4.5	50/100	10.9	91/92	Thales Alenia Space Belgium	[65,69]
36 V PPU	XR-5	3	300, 400	7.5, 10	36	<19	>90	Aerojet Rocketdyne/Northrop Grumman	[66]
XPC	XIPS-25	1.7, 3.7 <sup>a</sup>	1215	1.43, 3.01	100	21.3	91/93	L-3 ETI	[47]
PSCU	T6	2.1–4	1850	1.1–2.2 <sup>a</sup>	100	23	92–95	Airbus DS Crisa	[43,69,70]
HTPS PPU	XR-5	2–4.5	150–400	5.6–15	70	12.8	>94	Aerojet Rocketdyne/Lockheed Martin	[71,72]
PPU-140	SPT-140	3, 4.5	300	10, 15	100	15	94	Maxar	[43,50,73]
PPU <sup>b</sup> Mk3	SPT-140D, PPS <sup>®</sup> 5000	1.5, 4.7	100–400	2–15.5	100	18.6	>94.5	Thales Alenia Space Belgium	[65]

<sup>a</sup>Calculated based on reported values.

<sup>b</sup>PPU Mk3-demonstrated performance during the flight qualification test campaign is presented.

power converters. By inspection we see that midpower HET PPUs have been flight-qualified up to a maximum  $V_{\text{dis}}$  of 400 V and a maximum  $I_{\text{dis}}$  of 15 A while midpower GIE PPUs have been flight-qualified up to a maximum  $V_{\text{beam}}$  of 1850 V and maximum  $I_{\text{beam}}$  of 3 A. These metrics will prove to be limiting factors for the high-power regime in Sec. IV as they have discharge/beam power requirements as high as 800 V/80 A for HETs and 4740 V/4.1 A for GIEs.

Commercial developers have embarked on flight qualification test campaigns of other PPUs in addition to the hardware captured in Table 3. Bourguignon and Fraselle share their efforts in qualifying and testing the PPU Mk2, the successor to PPU Mk1, compatible with the SPT-100 and PPS<sup>®</sup>1350 with a maximum discharge power of 2.5 kW [65]. They also introduce the PPU Mk3 along with its full performance range as it was designed to interface with the growing portfolio of HETs of discharge powers up to 5 kW [65]. As another example, Pintó et al. are developing the Elektro, a PPU compatible with various 5-kW-class HETs, and a highly modular PPU for GIEs in the midpower regime [67].

Table 4 lists the PMS segments supporting midpower EP systems with flight heritage. The information provided in Table 4 consists of PMS segment name, corresponding thruster, anode flow rate range as it constitutes >90% of the total flow rate, the pressure reduction ratio denoted as reservoir storage tank pressure to flow control unit pressure, compatible propellants, and primary developer(s). As described in Sec. II, the PMS is often decomposed into a pressure regulation unit and flow control unit. For this reason, in the first column of Table 4, the PMS segment name is given by the pressure regulation name first, followed by the flow control unit.

We highlight a few trends based on Table 4. First, the maximum anode flow rate demonstrated on-orbit is at most 20 mg/s on xenon. This maximum flow rate corresponds to the midpower HETs, as expected. Second, although the pressure reduction ratio is generally larger for HETs, most flow controllers required a regulated input pressure of about 37 psia. Lastly, only xenon-compatible flow controllers have flown. Together with the performance data of high-power thrusters presented in the Appendix, these trends suggest that

midpower PMS segments with flight heritage cannot readily support high-power EP operations. For example, 20-kW-class HETs demonstrate an average  $\dot{m}_a$  of 34 mg/s, whereas HETs  $\geq 47$  kW exhibited an average  $\dot{m}_a$  of 97 mg/s on various propellants, such as krypton, iodine, and bismuth. Overall, the main observation we make in this section is that all the midpower EP systems and many of their segments are scaled-up versions of their respective lower power counterparts. Thus, in terms of flight-qualifying high-power EP strings, a lower power design baseline facilitates the process. We also note that flying midpower EP systems >4 kW is a relatively new concept with the first flight in 2010 with limited in-flight experience available in the public domain. Moreover, cathode, PPU, and PMS segments in the midpower regime cannot readily support many of the high-power EP devices identified in this review. Thus, an equivalent level of effort is required in developing and maturing these segments for operation in the high-power regime. In the remaining sections of this paper, we will direct our focus to the current SOA of high-power EP strings. We start with the thrusters and lead into the string addressing the corresponding cathode, PPU, and PMS segments when possible.

#### IV. Current SOA of High-Power EP Thrusters

Historically, the development of many EP strings began with the design and testing of the thruster and cathode segments with little consideration of the PPU or PMS. Once the thruster and cathode design achieved an adequate level of maturity in performance, the development of the supporting segments at the breadboard level followed. Conforming to this order, we begin this section by first introducing all the high-power electrostatic and electrothermal thrusters that have demonstrated performance with  $P_{\text{in}} \geq 6$  kW. We describe the data collection methodology employed throughout the literature review process in determining the nominal and demonstrated performance range for each thruster. We then share general performance trends of thrusters in the high-power regime and determine their hardware maturity and qualification state. The objective of

**Table 4** Midpower PMSs with flight heritage in ascending  $\dot{m}_a$ 

PMS names	Thruster	$\dot{m}_a$ , mg/s	Pressure reduction ratio, psia/psia	Compatible propellants	Developer(s)	References
HPRS, FCU	T6	0.8–3	2175/36	Xe	Astrium, Moog Bradford	[56,74]
BPRU, XFC	PPS <sup>®</sup> 1350-G	3.9–4.5 <sup>a,b</sup>	2175/29	Xe	Safran/IberEspacio, N/A	[44,75]
50–741, <sup>c</sup>	XIPS-25	2.4, 4.8 <sup>a,d</sup>	2175/37	Xe	Moog	[76,77]
PMA, XFC-100	SPT-100	5.1 <sup>a</sup>	2000/37	Xe	Moog, Fakel	[38,68,78]
N/A, XFC	XR-5	8.4–14.8	2700/37	Xe	Lockheed Martin, Moog	[52,79]
PMA, XFC-140	SPT-140	10.7, 15.1	2700/37	Xe	Moog, Fakel	[80–82]
PMA, XFC	XR-5	6–20 <sup>e</sup>	2700/37	Xe	Moog, Moog	[66]

<sup>a</sup>Calculated based on reported values.

<sup>b</sup>XFC total mass flow rates were not directly measured during the SMART-1 mission but can be estimated from thrust and  $I_{\text{sp}}$  flight data.

<sup>c</sup>After pressure regulation, flow control on XIPS-25 is achieved passively using flow restrictors.

<sup>d</sup>Total flow rates for the XIPS-25 are presented.

<sup>e</sup>Only the full range of the XFC from the qualification test campaign is shown.

this section is to acquaint the reader with the high-power thrusters in this review, and set up the transition to EP strings discussed in Sec. V.

### A. Data Collection Methodology

The list of high-power thrusters in this review was generated based on publicly available information disseminated by academic research groups, commercial organizations in the space industry, and government space programs. Only thrusters at a breadboard maturity level with initial performance data reported via a publicly available resource are considered in this paper. The performance metrics of total thruster input power  $P_{in}$ , thrust  $T$ , total specific impulse  $I_{sp}$ , and total efficiency  $\eta_{tot}$  were collected for each thruster at a steady-state, nominal operating condition. Typically, a thruster's nominal operating condition, also known as throttle or design point, is defined by its developer to meet specific mission requirements. For EP strings undergoing flight qualification, throttle points are explicitly defined in a throttle table such as high-thrust or high- $I_{sp}$  mode. For simplicity, we report the nominal total input power throttle point and tested performance range in this paper. When the total input power is not available, we report the discharge/beam power. In most cases throughout our literature review, a thruster's performance was characterized over a range of operating conditions in which  $V_{dis}$ ,  $V_{beam}$ ,  $I_{dis}$ ,  $I_{beam}$ ,  $\dot{m}_a$ ,  $\dot{m}_c$ , grid assembly voltages, and/or electromagnetic coil currents were varied. In these instances, we used our best judgment to select a nominal operating condition using the context provided in the corresponding references but generally selected the maximum power performance point.

For cases where only some of the performance metrics are provided, Eqs. (1) and (2) were used to determine missing parameters.

$$\eta_{tot} = \frac{T^2}{2\dot{m}_{tot}P_{in}} \quad (1)$$

$$I_{sp} = \frac{T}{\dot{m}_{tot}g} \quad (2)$$

In Eqs. (1) and (2),  $\dot{m}_{tot}$  is the total mass flow rate supplied to the thruster during nominal operations. For HETs,  $\dot{m}_{tot}$  is the sum of the anode and cathode flow rates. For GIEs,  $\dot{m}_{tot}$  is the sum of  $\dot{m}_a$ ,  $\dot{m}_c$ , and neutralizer,  $\dot{m}_n$ , flow rates. In Eq. (1),  $P_{in}$  is the total thruster input power as defined for each device type in Sec. II. The resources leveraged during this review primarily consisted of proceedings of the International Electric Propulsion Conference (IEPC) and the AIAA conferences, white papers found in manufacturer websites, doctoral dissertations, and journal publications.

### B. High-Power EP Thrusters

A total of 46 high-power EP thrusters have been identified as being developed to a breadboard hardware maturity level or greater and tested. The period of electrostatic and electrothermal type high-power thrusters begins in 1978 and is on-going. Thrusters have been developed with nominal input powers ranging between 5.65 and 200 kW. Many of these thrusters were tested over a range of input powers demonstrating breadth in thrust and total specific impulse performance. Multiple propellants were used to test high-power devices such as xenon, krypton, bismuth, and iodine; however, xenon was the primary option for 43 thrusters. Table 5 offers a summary of nominal performance range in  $T$ ,  $I_{sp}$ , and  $\eta_{tot}$  for all the high-power

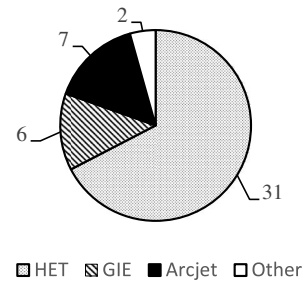


Fig. 2 Distribution of high-power thrusters by device type.

thrusters identified in this review. The complete list, along with various performance metrics of each thruster, is documented in the Appendix. Figure 2 shows the breakdown of thrusters by EP type. The 31 HETs comprised more than 67% of this power class, followed by seven arcjets, six GIEs, and two Other.

In Fig. 3, we present the total efficiency as a function of the nominal thrust-to-power ratio,  $T/P$ , of high-power EP thrusters. The  $T/P$  of each thruster was calculated by dividing the measured thrust by  $P_{in}$  at the nominal operating point. Total efficiency was determined to be an appropriate measure of thruster performance as it relates jet power production to the total input power at the target  $T/P$  ratio. A few observations can be made in Fig. 3. First, thrusters of the same EP type can be grouped together as they demonstrate similar performance in total efficiency at their nominal  $T/P$ . As a visual aid, dashed ellipses are placed inside Fig. 3, grouping the thrusters into the three device types. The total efficiency for high-power HETs ranges between 57 and 67%, with an average of 62%. High-power arcjets demonstrated the lowest total efficiencies ranging between 14 and 37% with an average of 30%. GIEs in the high-power class exhibited the highest total efficiencies with values between 68 and 78% and an average of 74%. Second, arcjets achieved broad coverage in  $T/P$  performance spanning from 40 to 117 mN/kW although at low  $\eta_{tot}$  values. Third, HETs offered more diversity in total efficiency versus  $T/P$  performance for input powers between 5.9 and 98.4 kW. For example, most of the HETs between 6 and 8 kW achieved higher  $T/P$  values than 20-kW-class HETs, given the same total efficiency of 60%. It should be noted that these thrusters operated on various propellants other than xenon and that their total efficiency performance may not have been maximized as part of the objectives of their test campaigns. Generally, GIEs and HETs rendered total efficiency values greater than 50% that can address the current needs of satellite operators and mission designers requiring high specific impulse for station-keeping, space exploration missions, or high thrust for EOR. Additionally, we did not find any active research programs supporting the development of the high-power arcjets identified since 2000. As for thrusters classified as Other, their unique technology and performance thus far makes them unsuitable for direct comparison to other EP devices. This motivated us to understand and comment on the total efficiency performance of high-power GIEs and HETs further.

Figure 4 shows the total efficiency of high-power GIEs and HETs as a function of time, specifically the year in which the performance of the thruster was initially reported. Only thrusters operating on xenon were plotted over time to ensure direct comparison. In this subset of thrusters, high-power GIEs and HETs have spanned from 1997 until now, although some references imply that these systems were developed and tested to powers above 100 kW earlier than the 1990s [83,84]. From Fig. 4, the reader can see that the average total thruster efficiency of HETs in the high-power regime has increased from 57% to about 62% since the late 1990s. However, HETs have maintained an approximately constant value of 62% since 2007, serving as an indicator for the current SOA in this power class. GIEs have shown a more consistent performance in the same time frame remaining more efficient with a total efficiency SOA value of 72%. Uncertainty in the reported total efficiency values from references was not considered for this analysis and can be as large as  $\pm 5\%$ . Regardless of this shift, both thruster types indicate the total

Table 5 Range of nominal high-power EP thruster performance<sup>a</sup>

EP type	$P_{in}$ , kW	$T$ , mN	$I_{sp}$ , s	$\eta_{tot}$ , %
HET	5.9–98.7	290–5420	1120–3472	57–67
Arcjet	9.8–100	568–4000	400–1400	14–37
GIE	5.7–20.8	175–446	3555–7650	68–78
Other	10–200	332–5800	3154–4900	51–72

<sup>a</sup>Performance ranges are based only on the nominal operating points of each thruster and do not reflect their demonstrated range.

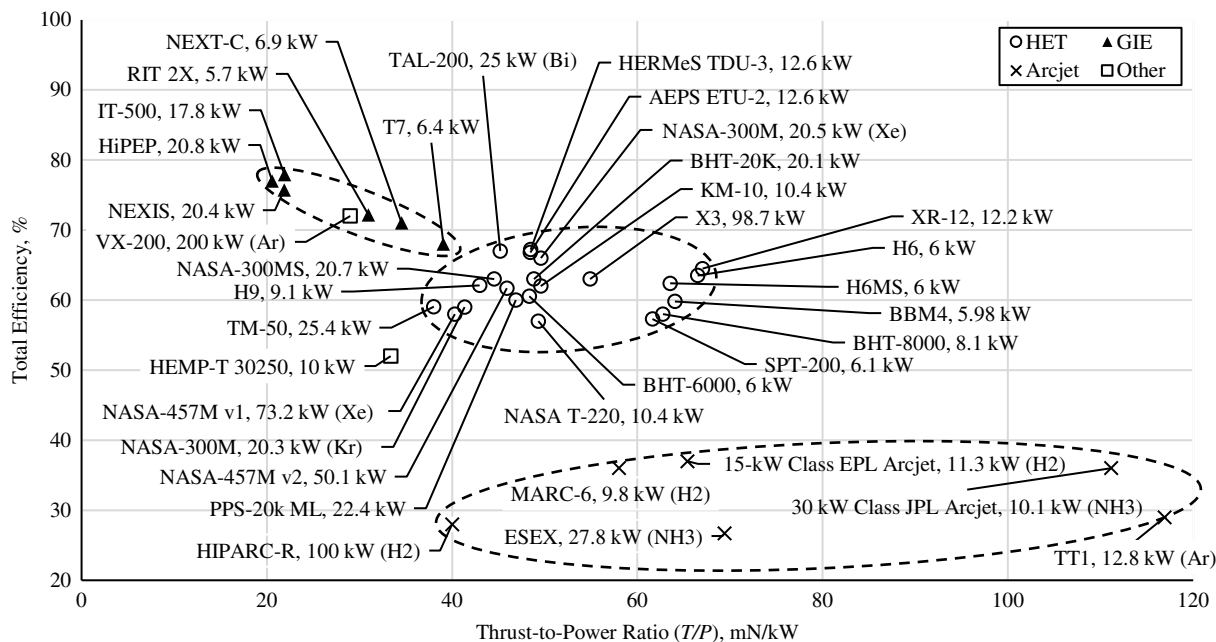


Fig. 3 Current SOA of high-power EP  $\eta_{tot}$  as a function of thrust-to-power ratio,  $T/P$ .

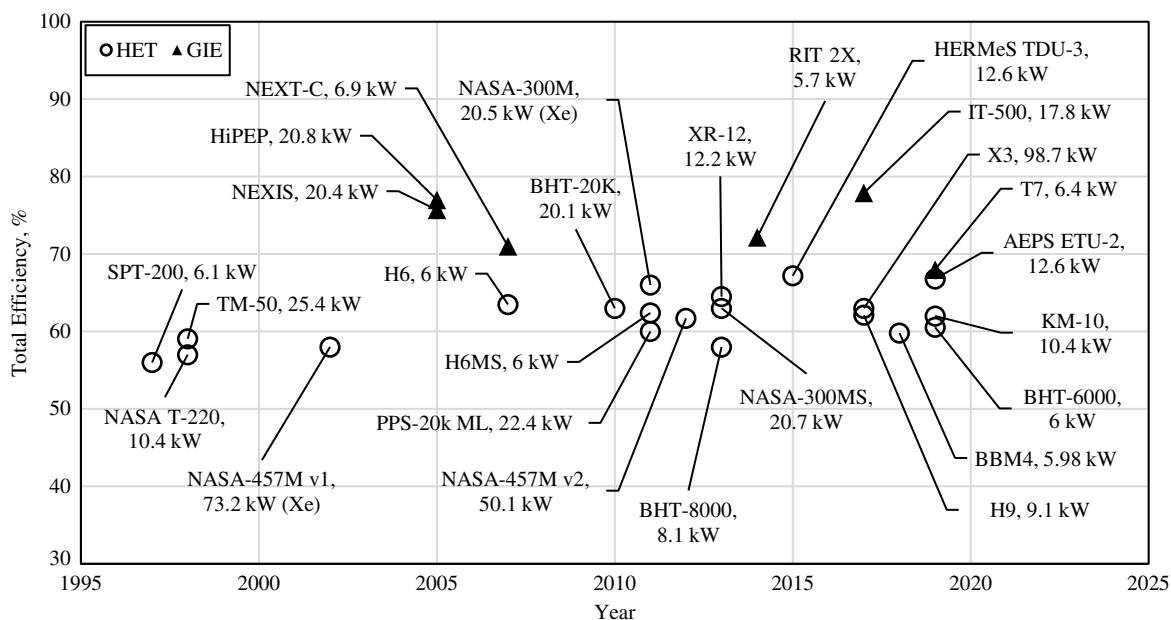


Fig. 4 Current SOA of  $\eta_{tot}$  of high-power HETs and GIEs over the last 30 years.

efficiency SOA value in the high-power regime to be limited to an approximately constant value.

In Table 6, we catalog the physical properties of mass, specific power at nominal operating point, and the mechanical envelope for many of the thrusters in this review. The motivation in doing so is to provide mission designers and spacecraft system engineers with estimates for mass and volume budget allocations when considering high-power EP options. In this paper, the mechanical envelope is a cylinder defined by a characteristic diameter and length based on thruster dimensions. The mass and mechanical envelope data in Table 6 provide useful information for spacecraft integration planning such as thruster installation locations, identifying possible spacecraft-plasma plume interacting surfaces, postlaunch thruster deployment mechanisms, and multi-axis gimbals for positioning and thrust vector control. Additionally, the SOA of specific power at the

nominal operating point is readily determined by dividing the thruster's nominal discharge or beam power by its total mass. We remark that the masses and mechanical envelopes presented for each thruster may not have been optimized since many of them are laboratory prototypes at low maturity levels. Generally, a high specific power is appealing as it measures a thruster's ability to support high-power discharge operations per unit mass of the thruster body.

Inspecting Table 6 affirms that high-power GIEs and HETs exhibit different physical properties in specific power and overall mechanical envelope. All GIEs had a larger mechanical envelope than their HET counterparts of the same power level with the RF ion thruster, RIT 2X, offering the smallest volume of the technology types. Furthermore, the average specific power for GIEs is 0.51 kW/kg while HETs display a larger variance, centered around 0.62 kW/kg, but ultimately depending on the technology type. For example, thrusters

**Table 6** Demonstrated physical properties of the SOA of high-power EP thrusters in ascending thruster mass

Thruster	Thruster mass, kg	Specific power, kW/kg	Envelope, $\varnothing$ (cm) $\times$ L (cm)
RIT 2X	<11.5	<0.46	33 $\times$ 22
KM-10	11.6	0.9	— —
SPT-200	12	0.50	26 $\times$ 20
BHT-6000	12.5	0.48	25 $\times$ 18
NEXT-C	12.7	0.50	53 $\times$ 38
ESEX	12.7	2.19	45 $\times$ 54
T7	13	0.44	44 $\times$ 38
HEMP-T 30250	14.5	0.69	14 $\times$ 25 <sup>a</sup>
D-150	18	0.83	34 $\times$ 13
SPT-290	18	1.00	37 $\times$ 23
H9	20	0.45	30 $\times$ 15 <sup>a</sup>
TAL-200	20	1.25	32 $\times$ 32 <sup>a</sup>
BHT-8000	25 <sup>a</sup>	0.32	38 $\times$ 18 <sup>a</sup>
PPS-20k ML	25 <sup>a</sup>	0.80	36 $\times$ 11
BBM4	26	0.23	— —
NEXIS	29	0.67	65 $\times$ 38
TM-50	30.5	0.83	31 $\times$ 16
IT-500	<40	<0.88	60 $\times$ 47 <sup>a</sup>
VHITAL-160	40	0.92	42 $\times$ 25 <sup>a</sup>
HT20k	40–50 <sup>a</sup>	0.4–0.5	40 $\times$ — <sup>a</sup>
BHT-20K	45 <sup>a</sup>	0.44	46 $\times$ 25
HiPEP	49.5	0.40	100 $\times$ 50 $\times$ 22 <sup>a,b</sup>
HERMeS TDU-3	50 <sup>a</sup>	0.25	— —
D-160	70	0.57	42 $\times$ 42 <sup>a</sup>
N30	100	0.32	50 $\times$ 15 <sup>a</sup>
X3	230	0.43	80 $\times$ 20 <sup>a</sup>
SMHT	— —	— —	26 $\times$ 10 <sup>a</sup>
H6	— —	— —	32 $\times$ 10
NASA T-220	— —	— —	31 $\times$ 20 <sup>a</sup>
NASA-300M	— —	— —	39 $\times$ 15 <sup>a</sup>
NASA-400M	— —	— —	53 $\times$ 20 <sup>a</sup>
NASA 457M v1	— —	— —	58 $\times$ 20 <sup>a</sup>

<sup>a</sup>Approximate mass and/or mechanical dimensions.

<sup>b</sup>HiPEP has a rectangular mechanical envelope.

with anode layer (TALs) demonstrated a higher specific power of 0.88 kW/kg, while nested HETs exhibited a lower specific power of 0.38 kW/kg. We note to the reader that nested HETs only begin to trade well against single-channel Hall thrusters at power levels above 50 kW and thus exhibit lower specific power values.

We share a few general observations that can be made thus far. First, the number of high-power HETs identified in this power class far exceeded other technology types. We believe this to be attributed to the relative ease in applying HET scaling laws during the design and manufacturing of the thruster. The consistent performance of HETs suggests that the EP community is proficient at scaling the design of HETs for high-power operating conditions. Second, we observed that hardware maturity level and flight qualification state, terms to be defined in the next subsection, of the thruster types varied. While many high-power HETs have been developed at the breadboard level, less than a fifth have engaged in activities to elevate its hardware maturity level or acceptance testing pursuant to flight qualification. The opposite is true for GIEs that were more readily matured with at least a lifetime test over 2000 h in preparation for EP string architectures. To capture this discrepancy, we define hardware maturity and qualification state next.

### C. Hardware Maturity Level and Qualification State Definitions

Each high-power thruster in this review has been developed to varying levels of hardware maturity and flight qualification state. In this subsection, we provide the definition of the two terms for a

thruster, but they can be generalized for the other EP string segments as well. The hardware maturity level of a thruster is a qualitative metric that aims to characterize its degree of technological advancement in achieving a specific performance profile that is repeatable in a relevant vacuum environment. The hardware maturity levels of a thruster are derived from NASA's Systems Engineering Handbook [85] and, for this paper, can be one of the following three levels.

A breadboard prototype (BB) is a working laboratory prototype that has been tested in a representative environment with initial performance metrics reported validating theoretical principles of the design. At this maturity level, the thruster is intended for R&D applications and is typically operated using laboratory power supplies, mass flow controllers, and cathode(s). In this review, 34 out of the 46 high-power thrusters are classified as breadboard prototypes.

An engineering test unit (EU) is a high-fidelity thruster unit that has undergone at least one design iteration and has been scaled and manufactured to demonstrate form, fit, and function pursuant of an EP string architecture or mission application. At this maturity level, the thruster has been paired with a cathode for operation. The thruster has been tested more than once, showing repeatable performance in a representative vacuum environment, and implemented structural, thermal, and/or electrical design modifications. In addition, the thruster has endured a wear test greater than 100 h characterizing the degradation of thruster components. In this review, eight high-power thrusters are classified as engineering test units.

A flight qualification unit (FQ) is a thruster whose design is either finalized or has undergone extensive design iterations and is ready to be integrated as part of the EP string. For flight qualification, this thruster is the same as the flight unit and will be used to complete the full range of acceptance tests as required by the mission. In this review, four thrusters are classified as flight qualification units. In the Appendix, we include the hardware maturity level of each thruster based on these definitions.

The qualification state of a thruster describes its advancement in completing flight-qualification acceptance tests per relevant industry standards in accordance with mission requirements. A thruster pursuant to flight qualification will undergo lifetime, mechanical, thermal, electrical, and string integration acceptance testing. Each acceptance test varies based on mission requirements and is defined within the scope of the thruster's qualification program. An outline of each acceptance test and what they encompass at the program level is provided in [86]. These tests have been adapted to EP string qualification testing as described in the next paragraph.

A thruster that has completed a lifetime test (LT) has successfully operated at a prescribed throttle point or set of throttle points in a vacuum facility for more than 100 h. Mechanical acceptance testing (ME) aims to validate the structural integrity of the thruster under static and dynamic loading. Usually, this consists of sinusoidal sweep vibration, random vibration, acoustics, shock, and/or pressure profile tests. In thermal acceptance testing (TH), the thruster has completed one or more tests such as thermal cycling and/or thermal balance. During electrical acceptance testing (EE), the thruster has completed electromagnetic interference (EMI) and electromagnetic compatibility (EMC) testing. In string integration testing (SIT), the thruster has been integrated into the string and successfully demonstrated end-to-end functionality over a set of conditions representative of the mission environment. Lastly, a thruster with flight heritage (FH) has flown and its operation validated in-orbit. The thruster's qualification state increases as LT, ME, TH, EE, and SIT acceptance tests are completed. The qualification state is maximized once the thruster, as part of an EP string, achieves flight heritage.

We found that many high-power thruster developers advanced the hardware maturity level of the thruster by engaging in a lifetime test motivated by the performance requirements imposed by a planned mission. The primary outcomes of a lifetime test are quantifiable metrics regarding the physical degradation of thruster components and thruster performance variation in  $T$  and  $I_{sp}$  at a prescribed  $P_{in}$ , as a function of time. Lifetime testing is particularly important for the high-power EP community due to the expected long operational h in space applications that can be as high as 50,000 h for some missions [87]. Of the 46 thrusters, 16 engaged in some form of long-duration

**Table 7** Accumulated lifetime hours of SOA of high-power EP in ascending  $P_{in}$

Thruster	EP type	$P_{in}$ , kW	Mission	Lifetime, h	References
BBM4	HET	5.98	ETS-9	4,048	[88]
BHT-6000	HET	6	PPE	>100	[8]
RIT 2X, QM1	GIE	2–6 <sup>a</sup>	GIESEPP	>3,500	[13]
NEXT-C	GIE	0.52–6.86	DART <sup>b</sup> /R&D	51,184	[89]
NASA T-220	HET	10.4	R&D	1,028	[90]
KM-10	HET	10.5	—	500	[91]
XR-12	HET	12.2	TSAT	400	[64]
AEPS ETU-2	HET	6.25, 8.33, 10.42, 12.5 <sup>c</sup>	PPE	730	[92]
HERMeS TDU-3	HET	6.25, 12.5 <sup>c</sup>	PPE/R&D	3,570	[87]
HT20k, DM1	HET	15, 20 <sup>c</sup>	CHEOPS	250	[11,93]
IT-500	GIE	17.8	—	2,018	[94]
NASA-300MS	HET	10, 15, 20 <sup>c</sup>	R&D	99	[95]
NEXIS	GIE	20.4	JIMO	2,020	[96]
HiPEP	GIE	20.8	JIMO	2,193	[97]
ESEX	Arcjet	27.8	ARGOS	>0.5 <sup>d</sup>	[98]
NASA-400M	HET	37 <sup>c</sup>	R&D	292	[99]

<sup>a</sup>Input power range was not directly available for the lifetime hours, so the power range given in [100] is used.

<sup>b</sup>Double Asteroid Redirection Test (DART) mission.

<sup>c</sup>Discharge power values are presented.

<sup>d</sup>ESEX lifetime is the total operational hours during the Advanced Research and Global Observation Satellite (ARGOS) mission.

operations testing. In HET lifetime testing, discharge channel wall erosion and external electromagnetic components are characterized. In GIE lifetime testing, developers focus on the degradation of the ion optics of the grid assembly and discharge chamber cathode orifice. Quite often, lifetime testing in a vacuum facility cannot be executed continuously due to limits on facility pumping capability or test operation anomalies and are generally segmented into sequential time intervals. In these situations, the same thruster must be operated for the entire duration of the test to accumulate operational hours. Since lifetime testing is essential for understanding the application of high-power devices for long-duration missions, we list in Table 7 the thrusters that have endured lifetime testing in ascending  $P_{in}$ , the driving mission if available, and their accumulated operational hours. For the cases in which lifetime testing was performed as part of scientific investigations, we denote the mission as research and development (R&D). We emphasize that the input power levels given in Table 7 may not necessarily be the maximum input power of the thruster and instead were a throttle point of interest for that test campaign.

From Table 7, the reader can see that high-power GIEs have proven to accumulate more lifetime hours than HETs. In fact, all the high-power GIEs identified in this review except one have completed more than 2000 h of constant thruster operations. Less than a third of high-power HETs embarked on a lifetime test campaign and varied between 99 h to more than 4000 h.

Figure 5 offers a broader perspective on the qualification state of high-power EP thrusters. This graphic depicts the number of high-power thrusters that have completed various acceptance tests up to SIT. Developers typically produce two replicates of a thruster design, utilizing one for lifetime testing and the other for qualification tests. From Fig. 5, the reader can see that the number of thrusters tested beyond lifetime drastically reduces. Mechanical qualification testing is the second most pursued qualification test, followed by thermal environment testing. Our study found seven thrusters that have achieved a mature qualification state by completing LT, ME, and TH acceptance tests: RIT 2X, NEXT-C, KM-10, HERMeS Technology Demonstration Units (TDUs), BHT-6000, AEPS Engineering Test Units (ETUs), and ESEX. Electrical qualification testing remains the least attained in this study, owing to the need for adequate mission-specific test parameter maturity and significant challenges, making such measurements inside metallic vacuum chambers. In this review, electrical qualification testing was conducted on four thrusters: T-220HT, NEXT-C, HERMeS, and ESEX. Of all the thrusters identified, only the 26 kW ESEX arcjet has achieved flight heritage after being successfully operated as an EP system on the ARGOS mission in 1999 [98].

The trends discussed in this section capture the SOA of high-power thruster performance across EP device types, time, and technological maturity for nominal input powers spanning from 5.65 to 200 kW. First, we discerned that HETs, GIEs, and arcjets all exhibit stark

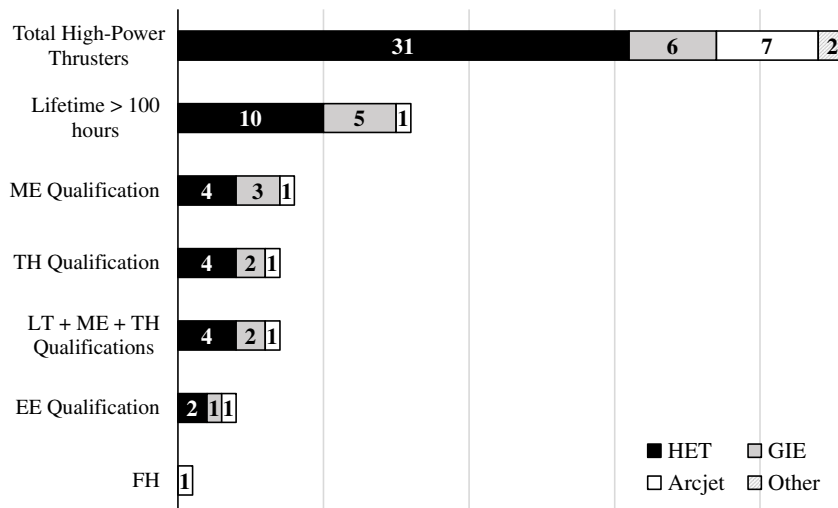


**Fig. 5** Number of high-power thrusters that have completed lifetime (LT), mechanical (ME), thermal (TH), and electrical (EE) qualification tests.

differences in  $T/P$ ,  $I_{sp}$ , and  $\eta_{tot}$  performance as summarized in Table 5 and depicted in Fig. 3. Second, high-power arcjet development is virtually inactive while HET and GIE thruster technologies have steadily flourished since the 1990s. The average total efficiency of high-power HETs and GIEs currently remains relatively constant at 62 and 72%, respectively. Lastly, the reader can see that although 46 high-power thrusters have been developed over the last 30 years, the regime remains technologically immature overall. As shown in Fig. 5, many EP devices perform lifetime testing to some degree but only seven thrusters are regarded as mature given their advancement in completing LT, ME, and TH acceptance tests. None of these thrusters have achieved flight heritage at input powers  $>6$  kW except for the 26 kW ESEX arcjet in 1999 on ARGOS. The high-power thrusters involved with EP string flight-qualification programs are discussed next.

## V. High-Power EP Strings

In this section, we introduce the high-power EP strings with flight heritage or in-development associated with the thrusters in Sec. IV. We define the criteria necessary to be considered a high-power string for this review. We provide some programmatic background about how the EP strings came to be and share their target performance throttle points. Then, we present the supporting cathode, PPU, and PMS segments, share their relevant performance metrics, and determine their hardware maturity when possible.

### A. EP String Criteria

For an EP string to be included in this review, the references explicitly mentioned development plans in maturing and/or qualifying any combination between the thruster, cathode, PPU, and/or PMS with total thruster input powers  $\geq 6$  kW. It is not necessary for the hardware to exist or for each of the segments to be technologically matured to the same degree. We found that all strings are being developed as part of a qualification program for a specific mission or space commercialization initiative. In many cases, program managers may choose to outsource or purchase commercially available PPU and/or PMS segments when qualifying the string. As an example, the NEXT-C string is qualifying all segments except for the PMS, which will be a commercially available xenon flow controller with significant hardware maturity [101].

### B. High-Power EP Strings

Table 8 captures the eight high-power EP strings in development or with flight heritage as of 2021. We include the string name, nominal input power, associated high-power thruster, mission, mission type, qualification state of the string when applicable, and primary developers responsible. The qualification state definitions from Sec. IV can be extrapolated to the string but includes the testing of the ensemble, SIT.

From our review, ESEX is the only high-power EP string that has achieved full qualification status by completing lifetime, mechanical, thermal, electrical, and flight operations by 1999 on the ARGOS mission [98,102]. The flight qualification program of the arcjet, PPU, and PMS string started in early 1995 and was finalized by mid-1998, lasting a little over three years. Mechanical acceptance tests included random vibration and a sine sweep based on mission specifications. Thermal acceptance testing exposed the ESEX string to a range of anticipated on-orbit temperatures using a thermal vacuum chamber. A fully integrated string test highlighted some of the challenges associated with testing high-mass flow rates in ample-sized vacuum chambers [102]. ESEX was designed to operate at a nominal flow rate of 240 mg/s on ammonia for 15-minute increments, but the integrated string test could not be maintained due to facility pumping limitations. Challenges such as arcing onto the PPU were experienced, further complicating ground-based string characterization. Of particular interest to the program were the electrical qualification tests that focused on EMI and EMC of ESEX string with the spacecraft. The military standards, MIL-STD-461C and MIL-STD-1541, were the driving documents for the electrical qualification tests.

NEXT-C, AEPS, and BHT-6000 follow as the most technologically mature high-power EP strings with active flight qualification programs as part of government-sponsored missions [6,101]. These strings are currently elevating the hardware maturity level of their thruster, cathode(s), and PPU. They are all planning to use commercially available xenon flow controllers as part of their PMS. The NEXT-C string has achieved the highest maturity level by completing all development and flight acceptance tests in preparation for DART science mission. Although technically NEXT-C was flown in November of 2021, it did so at a lower beam power throttle point of 2.76 kW and thus not considered a high-power string with flight heritage as defined herein. The NEXT-C is based on NASA's Evolutionary Xenon Thruster (NEXT), a GIE originally developed in 2002, and later commercialized by Aerojet Rocketdyne [101]. AEPS ETU thrusters are derived from the HERMeS 12.5 kW magnetically shielded HET [103]. The BHT-6000 is based upon the evolution of the BHT-5000 thruster to support the PPE science mission. The thruster segment of the three strings has been significantly matured with well-characterized performance mappings and lifetime, mechanical, and thermal acceptance tests. In addition to this, all three strings have completed or are engaged in preliminary system integration testing between the thruster, cathode(s), and PPU segments at least at a breadboard level or higher [6,101]. Also, the PPUs in these strings draw heavily from flight heritage units and have been customized to meet the mission requirements for their respective spacecraft buses [6,104,105]. Most segments of the BHT-6000 and AEPS strings have completed development testing, including environmental testing to qualification levels for engineering model (EM) hardware. The EM PPUs for AEPS and BHT-6000 thrusters are currently under development by Maxar and derived from their heritage PPU-140. Both strings are at a critical design review (CDR) level and are transitioning into formal qualification campaigns for the PPE

Table 8 High-power EP strings advancing their qualification state in ascending  $P_{in}$

EP string	$P_{in}$ , kW	Thruster	Mission/program	Mission type	Qualification state	Developers	References
NEXT-C	2.99–3.65	NEXT-C	DART	SCI	LT, ME, TH, EE, SIT	Aerojet Rocketdyne, ZIN Technologies, NASA GRC	[101,106]
—	1.77, 5.94	BBM4	ETS-9	GEO	—	IHI Aerospace, ISAS, JAXA	[88,107]
RIT 2X	2–6	RIT 2X	GIESEPP	GEO	—	ArianeGroup, Airbus DS Crisa	[13]
BHT-6000	3–6 <sup>a</sup>	BHT-6000	PPE	SCI	LT, ME, TH, SIT	Busek Co., Maxar	[8]
T7	2.7–6.4	T7	GIESEPP	GEO	—	QinetiQ, Airbus DS Crisa, AST	[12]
AEPS <sup>b</sup>	6.35–12.58	AEPS	PPE	SCI	LT, ME, TH, EE, SIT	Aerojet Rocketdyne, Maxar, NASA GRC, JPL, ZIN Technologies, VACCO, Moog	[6,108]
ESEX	26	ESEX	ARGOS	R&D	LT, ME, TH, EE, SIT, FH	AFRL, TRW, Olin Aerospace Corp., CTA Space Systems	[102,109]
XR-100	66–78.3 <sup>a,c</sup>	X3	NextSTEP	R&D	—	Aerojet Rocketdyne, University of Michigan, JPL, NASA GRC	[110]

<sup>a</sup>Thruster discharge power for the BHT-6000 and XR-100 is given.

<sup>b</sup>AEPS thruster designed and fabricated by Aerojet Rocketdyne is preceded by the NASA HERMeS thruster [8].

<sup>c</sup>XR-100 thermal equilibrium test for  $P_{in} > 50$  kW is shown; XR-100 was designed for total thruster input power of 100 kW [110].

mission. Despite this progress, AEPS and BHT-6000 strings have not completed flight qualification tests and are on-going as of 2022.

The BBM4 has matured through a series of design iterations and preliminary lifetime testing. The thruster design is on its fourth iteration, called BBM4, and completed a lifetime test of more than 4000 h as of late 2019 [88]. Another unit, designated BBM/STM, was fabricated and used to characterize thruster erosion rates and structural integrity with respect to the launch load environment. The unit has completed preliminary string testing using the BBM4 thruster, cathode, and breadboard model PPU, PPU-E [111]. The results of the BBM4/PPU-E coupling test in 2018 led to the design and fabrication of a mature engineering model for string acceptance testing. Engineering Test Satellite 9 (ETS-9) is the mission driving string flight qualification with a planned launch date sometime in 2023 [5].

The XR-100 is being matured to a TRL 4/5 to serve as a proof-of-concept demonstrating string operation in the 100 kW power levels for human space exploration architectures. The NASA Next Space Technologies for Exploration Partnerships, NextSTEP, program funded the development of the thruster, cathode, PPU, and PMS segments [110]. XR-100 completed a preliminary system integration test at NASA GRC in early 2019, demonstrating compatibility between early prototypes of all four string segments. The thruster used in this string is the X3, a 100 kW nested HET, and is the most powerful HET to date. The X3 is a proof-of-concept laboratory thruster that, with minor design changes, could be operated up to 200 kW. The breadboard level PPU and PMS prototype designs were based on the segments used on AEPS and XR-5 strings. A novel, high-amperage LaB<sub>6</sub> cathode in the 100-A's range was developed specifically for the X3 [112]. However, testing the XR-100 at its full power has not been successful due mechanical design issues [110].

The T7 and RIT 2X are currently in the early phases of string development. The Gridded Ion Engine Standardised Electric Propulsion Platform (GIESEPP) program is funding the initial phase of both high-power GIE strings to TRL 5 by 2024 [12,113]. Although we were only able to find limited performance data for both GIEs, the context surrounding these thrusters justified their candidacy as potential EP strings. Out of the two strings, the RIT 2X is more mature than the T7, and the developer, ArianeGroup, is currently manufacturing flight qualification strings. The RIT 2X is based on the RIT-22 RF GIE, which underwent significant hardware maturity, including a 3000 h lifetime test in 2005 [114]. ArianeGroup has produced two RIT 2X qualification units, QM1 and QM2, that are managed in parallel to complete lifetime, mechanical, thermal, and electrical acceptance tests. QM1 has accumulated more than 3500 h while QM2 has passed vibration, shock, and thermal cycling tests and is preparing to undergo EMC testing [13]. QinetiQ's T7 ion engine is a scaled-up version of the T6 midpower GIE that continues to operate nominally aboard the BepiColombo spacecraft [12]. An engineering model of the T7 is being manufactured with functional tests to follow [12]. Various space industry manufacturers are developing PPUs, PMSs, and cathodes to support these two thrusters. Most notably, Airbus DS Crisa is developing a modular PPU that can power both GIEs [67]. The difference in this qualification program is twofold: 1) these high-power strings will be made commercially available to GEO telecommunication and deep space exploration missions, and 2) the supporting segments are also intended to become commercially available to support other midpower EP strings such as the PPS<sup>®</sup>5000, SPT-140D, and XR-5 [67].

We remark that only HET and GIE technologies are being considered for high-power EP strings. Since ESEX in the late 1990s, no

other high-power arcjet strings were identified in this review. Additionally, devices classified as Other like the HEMP-T 30250 and VX-200 continue to mature at the thruster level with limited information on plans for a fully integrated EP string. Thus, we shift our focus to the discussion of HET and GIE high-power EP strings.

### C. Current SOA of High-Power Cathodes, PPUs, and PMSs

For the strings discussed in the previous subsection, we share their supporting cathode(s), PPU, and PMS segments as they constitute the SOA in the high-power regime. For each segment, we include the performance metrics relevant for each segment as discussed in Sec. II. Starting with the cathode,  $I_{dis}$ , emitter material, ignition method, and qualification state are shown in Table 9. The SOA high-power cathodes are mainly BaO-W and can generate up to 21 A at nominal string operation. The maximum demonstrated  $I_{dis}$  is the Gen3 LaB<sub>6</sub> cathode producing more than 300 A of current for the XR-100 string. All high-power cathodes use heaters as the ignition method.

For high-power PPUs, we determined that  $V_{dis}$ ,  $V_{beam}$ ,  $I_{dis}$ ,  $I_{beam}$ ,  $V_{in}$ ,  $\eta_{PPU}$ , and total PPU segment mass, in addition to the qualification state, are the relevant metrics. This information is given in Table 10. Note that the power values in the table represent total input power into the PPU,  $P_{tot}$ , for operating the entire string. We can draw the following conclusions regarding the SOA of high-power PPUs. First, each thruster required a customized PPU design to support the increase requirements in  $V_{dis}$ ,  $V_{beam}$ ,  $I_{dis}$ , and  $I_{beam}$ . Second, most of the PPUs were developed to be compatible with a wider range of spacecraft input voltages between 80 and 160 V. Third, the PPU total mass scales with thruster mass at a ratio of 2.6:1 but maintains  $\eta_{PPU} > 90\%$ . In terms of qualification state, the PPU lags its associated thruster.

The SOA of the PMS supporting high-power EP strings is captured in Table 11. Mass flow rate scales with string input power as thrusters operate at higher  $I_{dis}$  or  $I_{beam}$ . Many of these units were modified versions of their midpower counterparts with flight heritage in Table 4 except for XR-100 PMS segment. The XR-100 uses a newly developed propellant management unit and mass flow controllers due to its sufficiently high xenon flow rates ranging between 18 and 250 mg/s [115]. We included propellant compatibility to give readers a sense of the PMS's adaptability to gases other than xenon. Table 11 reveals that all SOA PMS segments in the high-power regime are based on xenon except for ESEX. This is especially interesting for developers experimenting with alternative propellants such as krypton and iodine.

## VI. Recent Advances in High-Power EP

Recent technological advances that have enabled the SOA of high-power EP are discussed in this section. We define *recent* to be within the last 15 years and *advances* as any hardware technology that has noticeably aided the research community in getting closer to flying high-power EP. Based on our review experience, we believe that programmatic factors are critical in understanding the technological maturity of these devices. As such, we first introduce the qualitative factors that facilitated the progress of high-power EP from a historical perspective. Then, we provide the technological advances that continue to enable the high-power regime.

### A. Factors Leading to the Current SOA of High-Power EP

From our literature review spanning the last 35 years of the community, we observed a few driving factors that started and/or

**Table 9** Current SOA of high-power cathodes in ascending  $I_{dis}$

Cathode	$I_{dis}$ , A	Emitter material	Ignition method	Developer	Qualification state	References
2X5 (RIT 2X Neutralizer)	1–5	BaO-W	Heater	ArianeGroup	LT	[116]
NEXT-C Neutralizer	1–3	BaO-W	Heater	NASA GRC	LT, ME, SIT	[101,117]
NEXT-C Discharge	4–24	BaO-W	Heater	NASA GRC	LT, ME, SIT	[101,117]
TDU (AEPS)	20.8	BaO-W	Heater	Aerojet Rocketdyne, NASA GRC	SIT	[118]
Gen3 (XR-100)	25–330	LaB <sub>6</sub>	Heater	JPL	SIT	[119]

**Table 10** Current SOA of high-power PPU in ascending  $P_{tot}$ 

EP string PPU	$P_{tot}$ , kW	$V_{dis}$ or $V_{beam}$ , V	$I_{dis}$ or $I_{beam}$ , A	$V_{in}$ , V	Mass, kg	$\eta_{PPU}\%$	Qualification state	Developers	References
NEXT-C (DART) <sup>a</sup>	3.2–4	936–1179	2.7	80, 100, 125	34.5	91–94	LT, ME, TH, EE, SIT	ZIN Technologies, Aerojet Rocketdyne, NASA GRC	[40,106]
RIT 2X/T7 <sup>b</sup>	3–6.1	1600	5	100	22–26	93	SIT	Airbus DS Crisa	[120]
BHT-6000	6.5	600	20	100	—	94	EE, SIT	Maxar	[8]
NEXT-C Baseline <sup>a</sup>	0.5–7	1800	3.52	80–160	34.5	95	LT, TH, SIT	NASA GRC, ZIN Technologies, Aerojet Rocketdyne	[40,105]
AEPS	6.7–13.5	300–630	10–20.8	95–140	62	95	SIT	NASA GRC, ZIN Technologies, Aerojet Rocketdyne, Maxar <sup>c</sup>	[6,104]
ESEX	30	90–130	200–288	160–240	48.4	95	LT, ME, TH, EE, SIT, FH	Pacific Electro Dynamics, Space Power Inc.	[121]
XR-100 <sup>d</sup>	73.7–85.4	300	78–141	94–140	~45	>95	SIT	Aerojet Rocketdyne	[110,115]

<sup>a</sup>Two PPU for the NEXT-C string have been fabricated: 1) the NEXT-C PPU (DART) has been flight-qualified for the DART mission to the performance metrics presented, and 2) NEXT-C Baseline PPU, a mature prototype developed to support the full-range of NEXT-C performance from 0.5 to 7 kW [40,106].

<sup>b</sup>Airbus DS Crisa is developing a modular high-power PPU that can support both the T7 and RIT 2X GIEs in a variety of cluster configurations.

<sup>c</sup>Aerojet Rocketdyne PPU performance is given. We expect the PPU supplier to change to Maxar, but delays in publication prevent us from sharing the new PPU performance values.

<sup>d</sup>XR-100 breadboard PPU performance during preliminary SIT testing is presented. Discharge power modules exhibited a wider performance range up to 100 kW as described in [115].

**Table 11** Current SOA of high-power PMS in ascending  $\dot{m}_a$ 

EP string PMS	$\dot{m}_a$ , mg/s	Compatible propellants	Qualification state	Developer	References
T7	0.15–10	Xe, Kr, Ar, He, N <sub>2</sub>	—	Advanced Space Technologies GmbH	[12,122]
AEPS	8–24	Xe	SIT, LT, ME, TH	VACCO <sup>a</sup>	[6,41]
ESEX	240 ± 5	NH <sub>3</sub>	SIT, LT, TH, ME, EE, FH	Rocket Research Company	[123]
XR-100	Up to 250	Xe	SIT	Aerojet Rocketdyne	[115]

<sup>a</sup>We expect a change in supplier to Moog, but delays in publishing this information prevent us from stating this in the table.

sustained the growth of high-power EP. The three main drivers responsible for the early development of high-power EP devices are 1) international collaboration and knowledge exchange between researchers and developers, 2) performance requirements set forth by premier space missions, and 3) national directives targeting technological advancement. This subsection will discuss each driver from a historical perspective, but not necessarily in chronological order, and their contribution to the evolution of high-power EP devices to the current SOA.

EP research collaboration at an international level disseminated the design scalability and manufacturability of high-power EP devices. Since the 1970s, various countries have engaged in the design and prototyping of high-power electrostatic and electrothermal devices producing thrusters such as the D-160 [124], TT1 [125], and the RIT-35 [126]. For instance, Bober et al. shared the preliminary performance of an entire suite of high-power HET prototypes with input powers up to 25 kW [127], while Loeb had developed a family of RF ion thrusters (RIT) exceeding 3 kW [128]. This was not the case in the United States, where the focus was more on developing high-power arcjets [129,130].

The end of the Cold War in the early 1990s marked a critical moment in the development timeline of high-power HETs in the United States as a technology exchange with Russia bridged a wide knowledge gap between the two nations. Before this technological research exchange, HETs were virtually nonexistent in the United States. In 1991, a cohort of American EP specialists traveled to Russia and had the opportunity to test the 1.35 kW SPT-100 [131]. The increasing spacecraft power budget for mission architectures of the time bolstered NASA and other American space companies to execute comprehensive R&D campaigns to study Russian HETs [68,84,132]. The efforts of this collaboration culminated in the development of the first Western high-power HET in 1997—the NASA T-220 [133]. This trend continued well into the 2000s with NASA GRC proving its ability to proficiently scale up HETs by producing the 20 kW NASA-300M [134], the 50 kW NASA-400M [99], and the 72 kW NASA 457Mv1 [135]. However, the testing of all

these high-power thrusters was performed in vacuum facilities outfitted with laboratory power supplies and gas flow control systems. None of these high-power HETs had an equivalent PMS or PPU developed for fully integrated system testing. From these reports, we can gather that the American objective was focused on understanding the HET design principles and scaling them up to tens of kilowatts range. The published performance of these HETs stimulated interest in the further development of this technology as observed in the evolution of the NASA T-220 into the T-220HT for EMI investigations [136]. In parallel, other Western organizations initiated fundamental plasma physics research to enhance the performance of high-power HETs. Notable thrusters produced were the H6 [137], H9 [138], X2 [139], X3 [140], BHT-8000 [141], BHT-20k [142], and HERMeS [143].

High-visibility space missions have proven to be essential catalysts in the pursuit of realizing high-power electrostatic devices in the United States and abroad. The success of Deep Space 1 in 1998, along with a renewed interest in the possibility of utilizing nuclear power for spacecraft, facilitated research focused on high-power GIEs. NASA's Solar Electric Propulsion Technology Applications Readiness (NSTAR) project was responsible for providing the Deep Space 1 spacecraft with a new 2.3 kW ion thruster [144]. Aside from an initial firing issue, the NSTAR GIE operated through 2001, accumulating more than 16,000 h and processing more than 70 kg of xenon [145]. The success of Deep Space 1 established GIE technology as one capable of achieving long operational hours and high propellant throughput for space exploration type missions. Soon after, the Jupiter Icy Moon Orbiter (JIMO) became the next high-visibility mission in the early 2000s that motivated the development of three next-generation, higher power GIEs: HiPEP [146], NEXIS [147], and NEXT [148]. All three ion thrusters leveraged NSTAR heritage as a baseline, were significantly matured, completed lifetime testing, and engaged in some form of mechanical and/or thermal cycling testing per NASA technology readiness standards by 2007 [96,97,149]. Of the three, NEXT became the most advanced in this endeavor through the mid-2000s. The first phase of the technological

development program for NEXT began in 2003, consisting of two gridded ion thrusters and breadboard PPU and PMS models. Over the course of 18 years, the NEXT GIE would be transitioned into the commercial space sector and renamed NEXT-C mainly focusing on spacecraft integration issues and considerable PPU architecture design modifications. As of today, NEXT-C is the most advanced EP string comprising of thruster and PPU flight models achieving  $FQ$  for the DART mission, albeit at input powers less than 6 kW [101].

The same pattern is also evident in the recent development of the RIT 2X and T7 high-power GIE strings. The 10 cm RF ion thruster, RIT-10, had two successful ESA missions that established its promise as an in-space propulsion device. The RIT-10 first flew as a technology demonstration unit in the 1992 EURECA mission [150], and then again in 2001 on ARTEMIS where it was repurposed to serve as the primary propulsion system after a postlaunch anomaly and successfully placed the spacecraft in its mission orbit [151]. The RIT-10 served as a baseline enabling its European developers to produce the 2.8 kW RIT-35 and 5 kW RIT-22. This extensive heritage with RF ion engine technology was used to develop the RIT 2X high-power GIE.

More recently, the successful BepiColombo flight in 2018 validated the performance of midpower, Kaufman-type T6 ion engine for interplanetary missions [57]. Before this, four T5 GIEs supported ESA's Gravity field and steady-state Ocean Circulation Explorer (GOCE), demonstrating variable thrust performance between 2009 and 2013 accumulating about 36,000 operational hours. These premier ESA missions and the space industry's push toward all-electric satellite platforms directly motivated the development of the 6.4 kW T7 [12]. We also noted that early high-power GIEs differed from HETs in that some of these programs did invest R&D efforts to produce breadboard prototypes of PMS, PPU, and cathode hardware.

In 1997, the U.S. Air Force launched ARGOS, a technology demonstration mission that ultimately qualified the 26 kW ESEX string. The arcjet was a scaled-up version of two 1.5-kW-class hydrazine arcjets [109]. The selection of the arcjet over other EP technologies at the time was primarily based on its lower design complexity, relatively mature PPU concepts for string operation, and high thrust performance [152]. Many of the mission concepts at the time planned on leveraging the high thrust performance of arcjets for LEO to GEO electric orbiting raising. These events made ESEX the first and only high-power EP string operating at discharge powers >6 kW to have flown as of the writing of this paper.

National initiatives for technology maturation have been and continue to be essential in the advancement of high-power EP thrusters. This was directly observed in the early 2000s with program initiatives like In-Space Transportation Program (ISTP) and Project Prometheus that investigated high-power EP as viable propulsion options in hopes of leveraging nuclear power capabilities in exploration-type missions. The ISTP directly sponsored R&D efforts raising the TRL from 3 to 4/5 of the 72 kW NASA-457M v1 HET, resulting in a second version, NASA-457M v2 by 2004 [153]. Project Prometheus was a significant stimulant to high-power devices like HiPEP, NEXIS, and NASA-400M as noted in [153,154]. In the United States, NASA's 2017 space policy directive and the culmination of work conducted under the Flight Technology Demonstrator 1 program (FTD-1), Asteroid Redirect Robotic Mission (ARRM), and now PPE set a strong foundation for the TRL of AEPS and BHT-6000 strings facilitating their current flight qualification programs [155]. Similar observations are made in Europe in late 2008 with the HiPER project—a project aimed at investigating innovative EP technologies for space transportation and exploration missions [156]. The HiPER project supported high-power EP initiatives in six different countries producing notable thrusters such as the PPS-20k ML [157], DS3G [158], and the 100 kW Alta MPDT [156]. Most recently, the European Union's research and innovation commission initiated two projects with the objective of further enabling high-power GIEs and HETs: GIESEPP and the Consortium for Hall Effect Orbital Propulsion System (CHEOPS). GIESEPP is directly supporting the string development of the RIT 2X and T7 for mid- and high-power applications primarily targeting the GEO telecommunication satellite

market [12,13]. CHEOPS is responsible for the continued maturity of the PPS<sup>®</sup>Dual-ML and HT20k HETs as well as PPU and cathode development [93].

These national initiatives and flagship space missions also motivated the private space sector to engage in high-power thruster development. Capable prototypes such as the BHT-5000 [159], BHT-8000 [141], BHT-20K [142], and the XR-12 [64] were developed demonstrating breadth in  $T$  and  $I_{sp}$  performance with the goal of supporting government space missions. However, R&D funding fluctuated as flight programs or requirements were either canceled or changed, making it more difficult to sustain these efforts long-term. Regardless, we can state that national technology maturity initiatives and premier space missions engage the commercial space sector, making them assets in further enabling high-power EP.

## B. Recent Technological Advances Enabling High-Power EP

In this subsection, we delineate the technological advances that have led us to the current SOA of high-power EP strings. For inclusion in this section, the technological advancement must have addressed the operational challenges observed in lifetime, thermal constraints, structural integrity, and/or electrical performance. All four segments of the string are reviewed separately and discussed below.

### 1. Thruster

The recent technological advances within the thruster segment are the ability to scale designs to high power levels and magnetic shielding to enhance lifetime operations. The HET and GIE prototype work developed in the late 1990s through 2010s served as design baselines for higher power thrusters. The first of the high-power HET's developed in the United States was the 10 kW NASA T-220. In addition, the T-220 is the first HET to undergo a magnetic-field characterization and lifetime performance testing [90,133]. The two main results of the initial T-220 test campaign are that the cathode placement and inner/outer magnetic coil operation settings effect the thruster's discharge efficiency [133]. A second test campaign focused on quantifying the erosion of the discharge channel wall over 1000 h of lifetime testing. During this test campaign, discharge current oscillations were also measured over time. They were seen to diminish beyond the 500 h mark, indicating that the discharge oscillations of a thruster are a function of structural erosion of the discharge channel [90]. This test was also the first to utilize full-circumferential and in situ laser profilometry to quantify discharge channel erosion as a function of time on a high-power HET [90]. Results showed asymmetric erosion coupled to the magnetic field topology. These findings were directly incorporated into the development of two 50 kW HETs, namely, the NASA-457M v1 [135] and NASA-457M v2 [160]. From a practical standpoint, this effort ultimately proved the EP community's ability to scale HETs up to the tens of kilowatts power level, manage vacuum facilities during high-power HET performance testing, and apply a range of diagnostics to characterize the structural and electrical properties of HETs.

The NASA-457M's test campaigns demonstrated the community's ability to incorporate magnetic-field design lessons learned into the 50 kW operating point in preparation for flight qualification environment testing and high-power operation on krypton. NASA-457M v1's magnetic-field design was based on the NASA-173M model, a midpower 5 kW HET prototype focused on high-discharge-voltage, high- $I_{sp}$  operations [135,153]. Furthermore, the NASA-457M v1 was the first high-power HET tested with krypton that included a full performance characterization test campaign [161]. The main challenges encountered during the NASA-457M v1 test campaign were primarily based on thermal, high-voltage electrical operation, mechanical, and magnetic field optimization issues. The experience gained from the NASA-457M v1 test campaign directly influenced the design of NASA-457M v2 and NASA-400M. The main goal of NASA-457M v2 was to incorporate the lessons learned from v1 and advance the TRL of this thruster to between 4 and 5 [160] to satisfy flight qualification environment

testing. The NASA-457M v2 test campaign also confirmed that HET design scaling is well-understood. The thruster in this test, however, was limited by cathode design limitations as the one used during this test could not operate at the performance requirement of 100 A for extended time periods [160]. The motivation for the NASA-400M was primarily focused on high-power, high-voltage operation on krypton to achieve  $I_{sp,dis}$  values up to 5000 s. The outcome during the NASA-400M tests was our ability to scale thruster power levels on propellants other than xenon.

HET magnetic shielding is a recent technological advancement that has ultimately reduced the physical degradation of the discharge channel and other critical components yielding longer operational lifetimes. Magnetic shielding has been investigated since the early 2010s and was first achieved and characterized on the BPT-4000 H all thruster during a qualification life test in which channel erosion essentially ceased after 5600 h of operation [162]. The results from this effort were transitioned into the midpower XR-5 Zero-Erosion™ thruster design [163]. Soon after, magnetic shielding was formally implemented and studied on the 6 kW H6MS laboratory thruster serving as a testbed for future thruster designs [164]. The theory behind magnetic shielding is beyond the scope of this review paper and best explained in [165]. In this review, we identified many high-power HETs that have implemented magnetic shielding design features such as the HERMeS [87], H9 [138], N30 [166], and HT20k [93]. The main result of this advancement is that discharge channel erosion concerns of high-power HETs have been mitigated for future flight applications.

## 2. Cathodes

The recent technological advances for cathodes are increased discharge current performance, emitter material characterization, and heaterless ignition methods for high-power EP thruster operation. Initial efforts in producing higher discharge current cathodes were associated with excessive erosion and thermal fatigue of critical components after long-duration operations [167]. Early work on a 90 A cathode indicated that erosion could be minimized using improved cathode orifice geometries for continuous operation lasting more than 100 h [167]. However, generating these high currents still resulted in cathode orifice tip temperatures between 1300 and 1400°C and above the 1150°C recommended threshold for >28,000 h operational life of BaO-W cathodes [168]. Various publications show that increasing the cathode flow rate, small cathode orifice diameters, and reduced thermal conductivity of the emitter material all contribute to higher orifice tip temperatures, thereby reducing cathode lifetime [168–170]. Kamhawi et al. considered these factors and produced a 100 A BaO-W laboratory cathode with a measured tip temperature of 1132°C with a theoretical lifetime of 30,000 h [168]. Similar efforts have been made for LaB<sub>6</sub> cathodes, which have proven steady-state discharge currents up to 300 A at the expense of higher cathode orifice tip temperatures approaching 2300°C [171]. The elevated temperatures observed in high-amperage LaB<sub>6</sub> cathodes require more heat-resistant components such as the sheathed heaters used for ignition [171].

Improved characterization of the cathode emitter material is another advancement that addresses the high-current levels and ignition energy requirements of high-power thrusters. As discussed in Sec. II, the two commonly used emitter materials are BaO-W and LaB<sub>6</sub>. Emission current density and chemical reactivity are the two main factors that distinguish the two emitter types. The emission current density is a material property of the emitter that quantifies how much electron current it can generate per unit area as a function of its surface temperature. The chemical composition of these thermionic emitters, which is used to characterize the emission current density, is inherently affected by its environment. Formally, this is known as cathode poisoning and can decrease the operational lifetime of the cathode [19]. Thus, the chemical reactivity of the emitter material as it interacts with its local environment is important to understand [172,173]. The LaB<sub>6</sub> emitter is a compelling option due to its high emission current densities in the 20–30 A/cm<sup>2</sup> range at a thermionic emission temperature greater than 1500°C, it is

chemically resilient to propellant impurities and exposure to air during ground testing [171], and it has flight heritage aboard many Russian EP platforms. BaO-W has been extensively characterized as an emitter for high-current cathodes up to 150 A due to its low work function, a material property that is proportional to its thermionic emission temperature that is empirically determined. BaO-W's low work function in the 2 eV range has demonstrated high emission current densities at temperatures less than 1000°C, requiring less input energy for ignition when compared to LaB<sub>6</sub>. This lower emission temperature alleviates technical and fabrication challenges in the cathode heater component that often represents a single-point failure for thrusters. Chapter 6 in [19] contains the emission current density as a function of  $T_{emit}$  plot for various emitter materials and can help supplement the information provided in this section.

Due to BaO-W's susceptibility to impurities in the propellant and complex chemical reactions at the surface and within the emitter substrate, handling and operating on BaO-W requires increased precautionary measures, which translates to higher program costs and time. Several investigations characterizing the performance of the two emitters have been conducted to date. In fact, two high-current cathodes were developed for the HERMeS thruster, one of each emitter material, to compare and contrast their performance [174]. The two cathodes had their performance well documented in [174,175]. This improved understanding of emitter materials' properties has allowed us to develop flight-representative cathodes for high-power thruster applications.

The ignition method for high-current cathodes is an important technological advancement in the high-power regime. Cathode ignition is the operational step where plasma is created inside the cathode tube before being extracted through the exit orifice by the electric field generated by the keeper electrode. A minimum amount of energy must be supplied to the cathode for plasma ignition based on cathode gas flow rate and its internal geometry. Developers typically characterize the input energy using ignition voltage–ampere curves for different flow rates as given in [175–177]. Therefore, ignition is a critical operational aspect of high-current cathodes required for successful thruster operation. More importantly, the ignition method of cathodes is a high-risk segment limiting the overall lifetime of the EP string. As part of this effort, many developers have made significant progress in mitigating this risk and providing alternative design options for cathode ignition. Currently, the two main ignition methods are heater and heaterless cathodes. Heater-based cathodes require energizing a resistive element inside the cathode that raises the emitter temperature to the thermionic emission temperature. Heaterless cathodes energize the keeper electrode and rely on pressure-induced breakdown [178]. Heater-based cathodes pose a significant risk due to thermal fatigue of the resistive element after being cycled multiple times in operating the thruster throughout the mission lifetime. Both heater and heaterless cathodes are being developed, with heater-based cathodes being the majority. Of particular interest is the heaterless high-current cathode as it is less complex in design and mechanical assembly and ultimately bypasses the inherent reliability of the resistive element in heater-based cathodes [178]. Within this subset of high-current cathodes, only a few organizations have made significant progress in characterizing the discharge current performance up to 55 A.

The EP community has successfully developed various high-current cathodes that incorporate many of these advancements. From the thrusters catalogued in the Appendix, the discharge/beam current ranges between 3 and 250 A. Thus, we thought it prudent to share 10 high-amperage laboratory prototype cathodes, in addition to those presented in Table 9, that have been developed to support the increased  $I_{dis}$  in Table 12. This information suggests a healthy abundance in high-current cathode research at an international level and on propellants other than xenon.

## 3. Power Processing Unit

The recent technological advances for PPU are power semiconductors in switch-mode DC/DC power converter electronics, PPU

**Table 12** Additional high-current cathodes in ascending  $I_{\text{dis}}$ 

Cathode	$I_{\text{dis}}$ , A	Emitter material	Ignition type	Compatible propellants	Developers	References
UoS-HHC	1–30	LaB <sub>6</sub>	Heaterless	Xe, Kr, Ar	University of Southampton	[178]
Mark II	25	BaO-W	Heater	Xe	NASA GRC	[179]
HC20	5–30	LaB <sub>6</sub>	Heater	Xe, Kr	SITAEL	[180]
TDU-1 (HERMeS)	7.5–31.5	LaB <sub>6</sub>	Heater	Xe	JPL	[175]
— —	<40	LaB <sub>6</sub>	Heater	Ar	Institut für Raumfahrtssysteme	[24]
HHC-M50M4	15–55	BaO-ScO-W <sup>a</sup>	Heaterless	Xe	Kharkov Aviation Institute	[157,181]
— —	5–60	LaB <sub>6</sub>	Heater	Xe	JPL	[171,175]
— —	30–70	LaB <sub>6</sub>	Heater	Xe	CNRS ICARE	[182]
HCPEE 625	1–100	— —	Heater	Xe, Ar	Electric Propulsion Laboratory	[136]
HC60	20–100	LaB <sub>6</sub>	Heater	Xe, Kr	SITAEL	[180,183]
— —	50–150	BaO-W	Heater	Xe	NASA GRC	[168]

<sup>a</sup>HHC-M50M4 cathode emitter material is composed of tungsten matrix impregnated with barium scandate oxide (BaO-ScO-W).

control logic and programmability to meet various thruster operating points, and power supply modularity in PPU architectures. First, we discuss switch-mode DC/DC power converter topologies and how they may be utilized in sizing the PPU for high-power EP thruster applications as background for the reader. Generally, a switched-mode DC/DC power converter changes the input voltage to the output voltage required by the electrical load. It is called “switch-mode” because the converter essentially uses a power semiconductor called a transistor to transfer energy by switching between two separate circuits to the load over a short time interval. The thruster, regarded as the electrical load, may require nominal discharge/beam voltages in the range of 300–6650 VDC. Thus, at a high level, the PPU must consist of a DC/DC converter that is able to step up the spacecraft bus voltages available, shown in this review to be between 36 and 160 VDC, to the operating voltages of the thruster. In practice, PPUs achieve these voltage conversions using various types of electrically isolated topologies like the buck, push-pull, full-bridge, and Weinberg, to name a few.

Recent technological demonstrations in power semiconductors show promise in their ability to support high-power thruster operations. Silicon metal-oxide-semiconductor field-effect transistors (Si MOSFETs) are commonly used power switches in DC/DC power converters. However, the EP community has experimented with other types of power switches, such as silicon-carbide MOSFETs (SiC MOSFET) and silicon-carbide junction field-effect transistors (SiC JFETs). Two PPU prototypes using these transistor derivatives were identified in our review. Fink et al. developed and tested a PPU prototype that utilized ten 1 kW DC/DC discharge supply modules using SiC MOSFETs to operate the 6 kW H6 thruster [184]. The result of this activity showed that SiC MOSFET-based power modules could be stacked in parallel to output a constant power of 3.2 kW with  $\eta_{\text{PPU}} > 97\%$  [184]. The second PPU prototype example is provided by Reese et al., who produced a 3.8 kW SiC JFET PPU specifically for high-voltage HET applications [185]. SiC MOSFETs have a higher breakdown voltage that can allow them to process more power from a high-voltage source and lower on-resistance values that can reduce conduction losses than comparable Si MOSFETs [185]. However, SiC MOSFETs are known to fail under single event effects in the MeV energy range. We also found active research in gallium nitride FETs (GaN FETs) for lower power DC/DC converters [186]. A good summary of the SOA of transistors and diodes as well as their application in PPU breadboard prototypes is given by Piñero et al. [187]. The most notable outcome from this work was a 15 kW SiC MOSFET breadboard discharge supply that was operated with the NASA-300M over a range of 3–15 kW and efficiencies  $> 97\%$  [187]. As a result of these efforts, power transistor technology is a recent advancement enabling PPU’s to meet thruster input power requirements in the high-power regime.

Next, we consider the programmable control loop techniques for operating the EP string stably. We focus on the load characteristics between all string segments and the PPU. Both digital and analog

filters must be implemented to minimize electrical noise sources throughout the string. Programmable digital control loops allow the user to configure parameters like mass flow rates to the anode and cathode(s),  $V_{\text{dis}}$ ,  $I_{\text{dis}}$ ,  $V_{\text{beam}}$ ,  $I_{\text{beam}}$ , and associated gain coefficients for a given PPU and thruster design. The flexibility of such control loops makes it easier for users to throttle the string in orbit to other operational points, given unplanned changes in spacecraft power availability. This is important because high-power thrusters have much wider performance envelopes and can operate over a range of voltages and currents as given in the Appendix. Second, design modifications can be made to both the PPU and thruster hardware during the flight qualification phase only, requiring the user to properly tune the digital control loop for the new set of output impedances and voltage/current ripples. Alternatively, the same PPU can be configured to operate another thruster altogether via control loop programming. An example of this technology development can be seen in the AEPS PPU, in which the digital control loop gain settings were tuned to reduce the discharge voltage ripple by 50% [104]. Ultimately, digital control loops facilitate PPU-thruster compatibility and allow us to access other throttle points within a thruster’s operating envelope.

Another advancement is in the design of the PPU architecture using modular power supplies to meet the high-power, high-voltage requirements of thrusters while maintaining PPU efficiencies above 95%. This is not exactly a technological advancement as this building-block concept has been implemented in heritage PPUs employed on NSTAR, XPC, PPU-140, XR-100, and many more. However, this PPU architecture approach must now be able to address the increased discharge voltages of high-power HETs from 300 to 1000 V and beam voltages of high-power GIEs from 900 to 6650 V. To support these higher electrical demands, developers have made much progress in designing power modules that can serve as building blocks to meet the increased voltage and current requirements. An early application of this concept was in the preparation of a breadboard PPU for the multi-kilowatt operation of the NASA-457M and NASA-173M HETs. A prototype 1 kW discharge power module weighing 0.765 kg was designed, built, and tested on the NASA-120M at 300V/3A with an efficiency greater than 96% [188]. The same is observed in the early design of the NEXT PPU that uses six parallel stacked 1.1 kW power modules [189]. A more recent example of this concept is given by the AEPS PPU that uses four 3.3 kW power modules to supply the 600 V and 20.83 A input power level for the thruster [104]. Modularity is also advantageous from a programmatic perspective as the PPU can be sized with flight qualified power modules instead of undergoing an entirely new PPU qualification program for missions that require different thruster power requirements. Thus, modularity also accommodates changes in thruster design and/or operating conditions as power supply modules can be added or withdrawn from the PPU segment and ultimately shorten the flight qualification timeline and reduce risk.

#### 4. Propellant Management System

The recent technological advances within the PMS segment that have enabled high-power EP strings are increased anode flow rates, versatile cathode flow fraction flow controllers, and alternative propellant testing. We focus on the anode flow rate range as it is the largest flow rate when compared to those of the cathode and neutralizer. Furthermore, the anode flow rates of HETs tend to be an order of magnitude larger than those of GIEs; thus, we focus on PMS segments catering to HETs. From this review, we noted that many of the available flow controllers with flight heritage could operate at higher xenon flow rates with slight modifications if any. As an example, we consider the PMS segment of AEPS that is a derivative design of the original Xenon Flow Control Module (XFCM) developed by VACCO for midpower EP thruster applications in 2012 [6]. The original XFCM was flight-qualified as an all-inclusive, two-channel, closed-loop feedback PMS specifically for HETs operating on xenon with a maximum anode flow rate of 7.9 mg/s [41]. However, the XFCM has been modified to achieve AEPS's anode flow rate range of 8–24 mg/s of xenon [6]. Two other examples include the RIT 2X and the T7 PMS segments that are also a derivative of previously qualified and commercially available flow control unit [12]. Lastly, Soenderker et al. developed a low-cost PMS architecture to meet the X3's total flow rate of up to 250 mg/s [115]. The primary objective in the design of the XR-100 PMS segment was to reduce the manufacturing cost of the unit by avoiding specialty machining processes and favoring larger tolerances for ease in assembly. In all these cases, the technological advancement of increasing the flow constrictor size to meet the increased flow rate ranges is well understood. Implementing this design modification is a low-risk activity given the well-defined qualification process of the PMS segment. This is an important fact to consider as a streamlined qualification process for these flow controllers facilitates the hardware maturity for high-power EP string applications. A representative qualification test matrix for the PMS segment that includes typical mechanical and thermal requirements can be found in the work of Cardin et al. qualification paper of their advanced XFCM [41].

Versatility in achieving different cathode flow rates for HETs is a recent advancement that may help address stability concerns for high-power thrusters. Lenguito et al. have developed and tested a xenon flow controller with a wider total flow rate range between 3 and 23 mg/s and the ability to support two cathode-flow-fractions (CFF), 5 and 9%, depending on the thruster operating condition [190]. The innovative flow controller endured SIT with a representative 4.5 kW SPT-140 string and successfully demonstrated its ability to switch between a CFF of 9–5% as the anode flow rate increased past a critical value of 6.05 mg/s. This is important because until now, most PMS flow controllers are sized to operate at predetermined flow rates and are not configurable. Adjustable CFF flow controllers like this can aid in our ability to conduct HET thruster stability studies at higher input powers.

Alternative propellants have been utilized in past test campaigns for high-power EP thrusters. From our literature review, krypton is the leading alternative propellant. The high-power HETs with krypton performance characterization data are H9 [191], NASA-300M [134], NASA-400M [99], NASA-457M v1 [161], BHT-8000 [141], BHT-20k [142], and the HT20k [93]. The second most tested propellant is bismuth and utilized by all the high-power TAL-type devices. The SOA in bismuth flow controllers is the breadboard prototype developed for the 36 kW VHITAL-160 R&D program demonstrating 5.8–9.8 mg/s [192]. Only one high-power HET was tested on iodine, the BHT-8000, with thruster performance measured up to 9 kW and flow rates between 9.7 and 21 mg/s [193]. Some PMS manufacturers have publicly announced investigative efforts in developing a baseline PMS design compatible with krypton for moderate anode flow rates. As an example, Harmann et al. introduce the miniaturized flow control unit ( $\mu$ FCU), a flow controller compatible with krypton as well as other working fluids [194]. However, performance metrics of krypton-based PMS flow controllers specific to high-power EP applications are rare.

## VII. Gaps in the SOA of High-Power EP

In this section, we identify the gaps in the current SOA of high-power EP. Gaps are defined to be areas of research where further investigation is needed to make high-power EP a viable propulsion option for future missions. The seven main gaps are structural design and scalability of high-power thruster, facility effects on thruster performance, enhanced plasma diagnostics appropriate for higher power thrusters, thrust measurement uncertainty and statistics, PPU-thruster dynamics, performance characterization on propellants other than xenon, and high-current cathode performance assessment.

### A. Structural Design and Scalability of High-Power Thrusters

The community needs to assess the structural and thermal design of thrusters and their ability to pass qualification testing as they continue to scale up in power for a range of mission applications. This is made significantly more challenging by the lack of a sufficiently mature spacecraft design, immature (if known at all) gimbal mechanisms that serve as the primary path for thruster dynamic loading, and a likely wide-ranging set of potential launch vehicles and mission profiles at the same time the thruster is being designed. These factors collectively contribute to complicating the thruster mechanical design envelope, which results in increased mass and cost.

From this perspective, the EP community must consider efforts aimed at developing modeling and simulation techniques capable of pinpointing potential thermal issues regarding heat deposition on critical thruster components, stresses/strains and displacements under dynamic loading, and single-point failure modes. We have successfully applied scaling laws to HETs and GIEs; however, little is understood regarding the practical limitations of these larger designs with respect to the material integrity of the components used in the assembly and manufacturability of the thruster. For example, a high-power HET with a larger-diameter boron nitride channel may face challenges as it endures mechanical qualification tests such as random vibration. The structural problem is most readily observed when learning about the design evolution of the NASA-457M v1 to v2 in 2004. It was found that commercial boron nitride vendors were limited in the single-piece manufacturing of the 0.457 m outer diameter of the discharge channel [195]. A segmented boron nitride channel was developed for the initial version of the NASA-457M, adding mechanical complexity to the 50 kW HET. Another issue encountered in this program was the displacements of structural components once exposed to high-temperature regions during thruster operations. As thruster discharge power levels increase, more heat is deposited via the current-carrying wires and along the plasma-exposed surfaces such as the discharge channel. Jacobson et al. discuss the use of finite element thermal models to estimate thermal-induced stresses on various components and validated these models by conducting experiments instrumented with thermocouples for the NASA-457M and NASA-173M HETs. It was found that the inner ceramic ring of the NASA-457M can reach temperatures near 800°C after 3.5 h of steady-state operation at 50 kW [153]. The lessons learned in NASA-457M v1 were incorporated into the design of version 2 and validated in [160]. Another approach to address the structural scaling of HETs has been to reduce the total surface area and mass of the thruster by nesting concentric discharge channels as implemented in [139,195,196]. Regardless, testing high-power EP devices at steady state in vacuum facilities may limit our ability to experimentally detect these issues and require advanced modeling techniques as a supplement.

Thermal effects on the thruster design and neutral gas flow are another research gap. From experience we know that high-power thrusters encounter thermal challenges as both power and voltage are increased. The higher power density must be rejected to keep critical thruster components like permanent magnets in GIEs and the electromagnets and ceramic discharge chamber of HETs from exceeding material allowable and qualification limits. Increased thermal radiation through high emissivity features and coatings as well as leveraging spacecraft capability to conduct and radiate heat from high-power thrusters are a few means to address these thermal challenges. As

$P_{in}$  increases, so does the temperature profiles of the anode, which typically serves as the gas distributor for many EP devices. The neutral gas inlet temperature is proportional to the temperature of the thruster discharge chamber and, thus, increases in time until it achieves thermal equilibrium. Elevated neutral gas temperatures increase the thermal velocity of xenon atoms, thereby affecting discharge oscillations. The EP research community will need to consider how higher thermal velocities of the gas affect ionization, acceleration zones, and discharge oscillations as this directly influences performance in thrust and stability of HETs.

Electromechanical issues also arise due to the higher voltages used in high-power EP thrusters. The NASA-400M experienced anode isolation problems during 600 V operations [99]. Visible arc damage to internal components was also observed in the postinspection of the NEXIS ion thruster [96]. As thrusters increase in power, proper electrical isolation should be included in the design. If not done properly, stray current pathways may alter the measured performance of the thruster. Based on this, we believe that a set of best practices is needed for experimentalist in academia and manufacturers in the industry to verify the electrical configuration of the thruster during ground-based testing and thruster performance data reduction.

### B. Facility Effects on High-Power Thruster Performance and Stability

Characterizing the difference between thruster operation in ground test facilities and the space environment is a research gap for enabling high-power EP. Given the disparity between the two operating environments, the current challenge lies in quantifying the effects vacuum facilities have on the performance of a thruster and decoupling them to ascertain its performance in space. These effects are formally called facility effects and can be divided into three categories: 1) pressure, 2) electrical, and 3) contamination.

The effects that pressure levels inside vacuum chambers have on the measured performance and stability of thrusters are known as pressure facility effects. Vacuum chambers are limited by the SOA in vacuum pump technology, maintaining facility operational pressures in the  $10^{-6}$  Torr range and orders of magnitude larger than the  $10^{-14}$  Torr estimate in GEO orbit [197]. Investigations of this sort generally consist of varying the facility background pressure either by injecting propellant via an auxiliary feed system or changing the number of active vacuum pumps while operating the thruster at a constant discharge power and voltage condition to obtain thrust versus facility backpressure curves [82,198]. These curves are used to extrapolate thruster performance at zero pressure as an estimate of the performance in the space environment. Studies on midpower HETs show that elevated facility pressures allow the thruster to ingest the background neutral gas as propellant, thereby augmenting the measured thrust. Recent investigations by Snyder et al. show that SPT-140 thrust measurements increase from 278 mN to almost 300 mN as the facility pressure increased by an order of magnitude at the constant 4.5 kW, 300 V operating condition [82,108]. In addition, elevated facility pressures can also enhance erosion rates of thruster components due to larger populations of charge-exchange (CEX) ions, change plasma properties of the thruster plume, affect discharge oscillations, and vary the location of the acceleration zone in HETs [199–201].

The sensitivity of high-power thrusters to elevated facility pressures is not well-understood. Only three high-power HETs have undergone pressure facility effects characterization experiments. HERMeS TDU-1 and AEPS behaved similarly in that both thrust and discharge oscillations were largely invariant to facility backpressure as the pressure was controlled between 4 and  $15 \times 10^{-6}$  Torr-Xe at the 12.5 kW, 600 V throttle point. Thrust measurements then decreased as the facility backpressure was elevated to the  $10^{-5}$  Torr-Xe range. However, thrust measurements monotonically decreased as facility pressures increased for other throttle points such as 9.7 kW, 800 V, contrary to the behavior observed in midpower thrusters [202]. The 20 kW HT20K exhibited the opposite trend as thrust measurements increased when facility

backpressure increased with no adjustment to  $\dot{m}_a$  [198]. For high-power EP qualification testing, facility operational pressure requirements should be revisited as well as the standard processes currently employed for quantifying CEX ion effects on thrust measurements, plasma diagnostic measurements, discharge oscillations, and erosion rates.

Studies of electrical facility effects focus on the electrical configuration of the thruster-cathode system and the resulting coupling between its plasma plume and the surrounding metallic vacuum chamber. The electrically grounded facility imposes a voltage boundary condition of 0 V that the plasma plume must satisfy at the chamber wall that is absent in the space environment. Thus, conductive vacuum chambers alter ion–electron recombination pathways in ground-based testing as electrons emitted from the cathode can complete the main plasma discharge circuit via a current pathway through nearby chamber surfaces and effectively neutralize the ion beam without having to do so in the exhausted plume. It was first shown by Walker et al. that a 3.4 kW HET's discharge electrically couples to the conductive chamber walls as a function of the relative position of the cathode with respect to the HET centerline registering global changes in plume properties and discharge oscillations behavior [203]. Consequently, as the discharge current of a thruster increases, so will its degree of electrical coupling to the grounded chamber walls, impacting its performance, measured plume properties, and discharge oscillation behavior. The HERMeS TDU-1 is the only high-power thruster that has engaged in efforts aimed at characterizing the electrical configuration of the thruster with respect to a grounded vacuum chamber. Peterson et al. showed that HERMeS TDU-1's electrically conductive thruster body, composed of graphite, and its electrical configuration with respect to the chamber and cathode influence performance in thrust, total efficiency, and peak-to-peak discharge oscillations. For the graphite thruster body tied to chamber ground test case, thrust and total efficiency increased by 4 and 5%, respectively, at the 12.5 kW, 600 V discharge condition accompanied by the largest peak-to-peak discharge current oscillation of 18 A [204]. And although the grounded thruster body configuration is not representative of flight operation, it should compel the EP community to assess the physics enabling the enhanced thruster performance in electrically grounded test facilities.

The study of residual gases and backspattered materials inherent in vacuum facilities and their impact on thruster operations and lifetime are called contamination facility effects. Previous work has shown that residual gases such as air constituents and hydrocarbons have artificially reduced thruster erosion rates by developing a protective layer over GIE screen grids, cathode keeper electrode, or HET discharge channel surfaces [205]. Efforts by Garner et al. were the first to document a decrease in the erosion rates of NSTAR's screen grid optics by a factor of 20 due to the presence of 2%  $N_2$  by mass in xenon flow rates in 1990 [206]. In addition, sputtered material from chamber surfaces like graphite, a crystalline form of carbon, that deposits back onto the thruster have also shown to reduce grid and discharge channel erosion rates. This process, known as backspattering, becomes increasingly important for high-power thrusters with beam/discharge voltages in the kilovolt range because energetic ions exhausted from the thruster will impinge on various chamber surfaces, thereby generating higher concentrations of sputtered material within the facility. The sputtering yields of graphite, stainless steel, and aluminum all increase by a factor of 4 as the ion energy increases from 200 to 600 eV [207]. Furthermore, the buildup of backspattered, electrically conductive material on thruster electrodes may even lead to electrical shorts on grids or spark events in HETs during thruster operation [208,209]. An accelerated carbon backspattering test campaign captured more than 3000 spark events on the H6MS, with some leading to anomalous thruster shutdowns [209].

Various analytical models have been developed to estimate the sputter yield of materials as a function of ion energy levels and vacuum facility wall composition and geometry, backspattered carbon deposition rates, and carbon film growth on thruster surfaces [199,207,210]. These models are compared against measured backspattered carbon deposition using quartz crystal microbalance

(QCM) sensors [209,211]. The design, thermal management, relative position with respect to the thruster, and sampling frequency of QCM devices have varied across test campaigns, with the most insight provided by Crofton et al. [211]. Many high-power GIEs have endured carbon backsputtering effects on grid erosion rate studies [207,211]. The H6MS and HERMeS TDU-1 were the only high-power HETs that have engaged in such investigations [92,209]. Although there is some progress along this front, there is no consensus on the best practices for measuring backsputtered carbon deposition rates, acceptable facility wall lining materials, or facility internal structure geometries to minimize these contamination effects on thruster lifetime assessments. Alternative methods such as pumping on or containing sputtered contaminants may be attractive options as the community shifts toward high-power EP.

### C. Plasma Diagnostics with High-Power Thrusters

As we continue to scale up in high-power thrusters, we believe that it is essential to revisit the plasma diagnostics required to assess the performance of these devices. The five most used invasive plasma diagnostic probes are ExB or Wien filter, Faraday, Langmuir, retarding potential analyzer (RPA), and emissive. We should revisit the assumptions and limitations of utilizing such probes to characterize the plume properties of the plasma jet exhausted by high-power EP devices. First, we determine which plasma state properties remain constant as we scale up in power. We note that the plasma density of the plume and the electron temperature are independent of thruster input power. The plasma number density remains relatively constant even though the thruster exhausts more mass; it does so with a higher volumetric flow rate that also scales with  $\dot{m}_{\text{tot}}$  for high-power EP devices. The electron temperature is determined by the plasma potential that can be shown to be approximately constant for HETs operating at the same discharge voltage. Based on this, we have determined that the ion energy distribution, as measured by an RPA, and ion species population, as measured by the ExB probe, to be the plasma properties that change as at this power regime.

As we test higher power EP devices, the increased vacuum facility pressures not only affect the plume via elastic and inelastic collisions with background neutrals but will also affect the sheath formation inside RPA and ExB probes challenging the current theory and analysis of the plasma state. Consider the geometry of a typical RPA probe, with a focus on the segment between the collector electrode and the ion repulsion grid. As the background facility pressure increases, the neutral number density within this segment will increase. As ions originating from the thruster flux through the ion repulsion grid, the number of charge exchange collisions will increase in this segment. The collector will eventually register both CEX ions and the original thruster ions without being able to distinguish between the two. Therefore, measuring the ion energy distribution will be difficult. In a higher facility pressure environment, the high-energy ions fluxing through the ExB probe will collide with thermal neutrals inside the probe cavity. In these events, the charged particles will be influenced by the Lorentz force. The net effect is that a sheath will form between the two electrodes, generating an electric field in the main cavity. This will result in attenuation and ultimate blocking of the external electric field, thus causing incident thruster ions to only experience the magnetic field effects. The sheath physics of ExB probes and higher power thrusters will affect our ability to appropriately measure the ion species distribution.

### D. Statistical Analysis of High-Power Thrust Diagnostic

There is a significant gap in the community's general practice of thrust diagnostics for measuring the performance of high-power devices. Furthermore, thrust measurements are necessary to quantify total efficiency and specific impulse—metrics important to mission designers and satellite operators. The two leading thrust diagnostics used in EP are the null-type inverted pendulum and the torsional-balance-type thrust stands [212]. Throughout our review, we seldom encountered publications with an adequate discussion of uncertainty regarding thrust measurements. In the few papers that did include

thrust measurement statistics, usually uncertainty attributed to equipment random error is considered. The application of rigorous statistics to experimentally determined thrust values is needed to better quantify the implications of changes in thruster design, magnetic field topology, cathode placement, flow rates, thruster body materials, facility pressure, and/or facility electrical boundary conditions to name a few. Secondly, it is not clear if the current SOA of thrust diagnostics is well-suited for high-power life tests. Therefore, we believe that the EP community should develop a standard for quantifying the uncertainty in thrust measurements to enhance our understanding of the sources of error contributing to overall performance. Such a formal uncertainty analysis requires a systematic breakdown of all the error sources associated with the diagnostic in both short- and long-duration experimental measurements.

In 2018, Mackey et al. published a conference paper providing a framework for quantifying the uncertainty sources and propagation for a null-type inverted pendulum thrust stand [213]. However, the study does not investigate thrust stand repeatability and only considers single-measurement sources of error. A similar study for a torsional balance or hanging pendulum thrust stand was not found during this review. As the community shifts to higher power thrusters, we recommend revisiting the sources of error in the diagnostics used and environmental factors such as facility operating pressure, elevated thruster temperatures, and electrical boundary conditions imposed by the facility and thruster hardware.

### E. PPU Architectures and Thruster Dynamics

Another gap is in our understanding of PPU-thruster dynamics at higher power levels. The PPU will have to mitigate higher power noise disturbances such as discharge current oscillations generated by high-power HETs. To this end, advanced control methodologies for power supplies are needed to handle these larger disturbances in discharge currents. Additionally, the high switching frequencies of PPU power converters coupled with thruster discharge oscillations will ultimately be a source of conducted and radiated EMI. We recommend investigating the effects of the emissions generated by both these power converters and time-varying plasma properties evident in high-power devices on overall thruster performance and the spacecraft. One way to control thruster oscillations was demonstrated in 2015 by Tamida et al., who discovered that HET discharge current oscillations would synchronize to the frequency of a time-varying input voltage signal [214]. The study utilized a modified DC/DC boost converter circuit to superpose a 50 V square waveform with the nominal 200 VDC voltage output. This demonstration showed that HET discharge current oscillations may be controlled by the PPU if it is designed to output variable discharge voltages with frequencies in the range of the discharge oscillations. In controlling the HET oscillations, the efficiency of the thruster was also shown to increase [214]. Although not practical in the design of PPUs for flight applications, this experiment may enhance our understanding of PPU-thruster dynamics and control.

There is a need to improve the specific power of converters as the overall PPU mass is projected to increase as thruster input power levels increase. We recommend focusing on reducing the mass and footprint of the magnetics as they can account for 30–40% of the PPU mass. To this end, design trades between magnetic material geometry such as ferrite E and drum cores, inductance, mass, PPU efficiency, and magnetic material temperature limits are required. Additionally, advances in wide-band gap power devices (e.g., GaN FETs, SiC MOSFETs, and Schottky diodes) provide high levels of efficiency with a smaller footprint. Mass and volume savings can also be obtained by leveraging recent advancements in passive electrical storage devices like capacitors.

In our discussion of the PPU segment thus far, we have assumed a DC spacecraft bus regulated down to a moderate voltage supplied by solar arrays, but there are alternative methods of spacecraft power generation that ultimately affect the PPU architecture. As an example, for AC spacecraft power buses, the PPU segment design must be reconsidered to support high-power EP strings. In 2005, Piñero et al. designed, fabricated, and tested an AC/DC power converter for the

30 kW Herakles GIE prototype assuming a fission-based AC power source aboard the Prometheus-1 spacecraft [215]. The outcome of this effort was a breadboard AC/DC PPU that takes in three-phase  $400 \pm 40$  V AC at 2.25 kHz and outputs the DC voltages necessary to operate the Herakles thruster. When tested at 17.5 kW, the beam supply was able to convert 400 VAC to the 6500 VDC at an efficiency  $>94\%$  [215]. This design posed different challenges to the PPU segment developers as they needed to balance electromechanical design complexity of AC/DC converters versus output DC power for GIEs. Design trades included transformer sizes, diode rectifier modules, and output capacitor sizes. Performance focused on minimizing output voltage and current ripple for DC thruster operation [215].

Another example different from the regulated DC spacecraft power bus is powering EP strings directly from the solar arrays, thereby reducing PPU segment complexity and mass. This concept is known as “direct-drive” and was demonstrated by Gooder as early as 1977, first with a 30 cm, mercury-based GIE in [216] then again by Hamley et al. on a 1-kW-class HET in 1997 [217]. The primary challenge in these applications was the large perturbations in the solar array  $I$ - $V$  characteristic curves when operating the HET. However, three recent direct-drive demonstrations show its promise as an alternative power option. In 2011, JPL was the first to report stable direct-drive operation of the H6 HET over  $V_{\text{dis}}$  range of 200–450 V and power levels between 1 and 10.4 kW [218]. Soon after, Piñero et al. developed and tested a breadboard level direct-drive unit (DDU) for a 300 V HET in 2013 [219]. Most recently, Reza et al. successfully demonstrated direct drive on the 5-kW-class HET, HT5k, using a solar simulator to assess the feasibility of this power option as solar array power production varies throughout mission orbit [220]. Our recommendation is to investigate and understand the feasibility of implementing these new PPU architectures, such as direct-drive, to high-power thrusters at power levels  $>10$  kW and orbits beyond GEO.

PPU segment should reconsider the fault detection, recovery, and recycle circuitry to protect high-power thrusters and the PPU from short-circuit faults. Short-circuit faults in GIEs, commonly known as recycles, are caused by electrical short across the grid electrodes causing the high voltage from the PPU to restart. Faults in HETs, sometimes referred to as spark events, are a result from abrupt reductions in the impedance of the main discharge causing the discharge to extinguish. From extensive experience in on-orbit operations, the EP community already practices FDIR circuitry in PPUs to manage short-circuit faults when operating midpower thrusters. In fact, GIEs often short between grids in high-thrust mode. An excellent example of this can be seen in the post-test inspection analysis of the NEXIS GIE. Snyder et al. recorded a total of 33,000 recycles over the 2000 h lifetime test when NEXIS was operating at 20.4 kW and 4760 V screen grid condition [96]. For the high operational voltages and currents in the high-power regime, developers will need to design PPUs with circuitry to handle these fault events and recover to constant thruster operations. DC/DC converters typically use primary current-limit functions to achieve this protection, but alternative FDIR techniques should be explored to support high-power EP strings.

#### F. High-Power Thruster Operation with Alternative Propellants

New propellants should be tested with high-power thrusters to meet the growing demands of future space architectures. Human exploration architectures for Mars have considered EP systems in the hundreds of kilowatts to multiple megawatts and xenon usage in tens of tons to multiple hundreds of tons. These xenon loads, while feasible from an engineering perspective, employ long-term stockpiling contracts that face significant programmatic obstacles [221]. Due to roughly  $10\times$  yield from air separation plant production, alternatives such as krypton have been considered for such high-propellant need applications. However, krypton does not store as densely, and the decrease in performance offsets the alternative propellant benefits from a spacecraft size and packaging perspective. Additionally, many studies have been conducted on krypton as

a higher specific impulse propellant for HETs. However, extensive analysis of the performance of HETs on krypton has yet to be investigated. Green propellants are attractive to meet the hybrid propulsion requirements of near-future spacecraft designs. The Air Force has developed a novel green propellant called the Advanced Spacecraft Energetic Non-Toxic (ASCENT) propellant and has demonstrated its viability in space on the Green Propellant Infusion Mission (GPIM) in 2019. Testing high-power thrusters on ASCENT would significantly reduce the volume and mass of hybrid propulsion systems as both chemical and EP subsystems would operate on the same propellant. We also believe that there is an opportunity to synergize with the MPDT community, who actively operate high-power thrusters with propellants such as argon, ammonia, methane, and hydrogen. The proven propellant flexibility of MPDTs can shed insight on fluid management processes and energy conversion mechanisms. Ultimately, alternative propellants may alter the design and operation of high-power EP devices based on their chemical properties and interaction with the thruster components.

#### G. High-Current Cathode Performance Characterization

We believe that the present means of characterizing high-current cathodes to be a gap as thrusters continue to scale up in power. There are several high-current density cathodes available for high-power EP thruster devices; however, their long-term functional characteristics are not well understood. Aside from AEPS and NEXT-C cathodes, other high discharge current cathode designs have not been extensively tested. From our review, we did not encounter a formally recognized cathode performance test procedure within the community. When independently testing the cathode, an external conductive surface serves as the discharge current detector. However, the electro- and magnetodynamics of electron flow from the cathode to the detector plate are not reflective of the real thruster-cathode-facility environment. This is especially a problem when attempting to understand the plume-to-cathode coupling effect on thruster and cathode performance. Only recently have cathode performance test campaigns included Hall-thruster-like magnetic field effects [222].

Heaterless cathodes as a viable option for high-power EP thrusters reveal another gap in this review. The risk involved in operating heaterless cathodes is significantly decreased due to the reduction in electromechanical parts needed for cathode operation. Operating an EP string using a heaterless cathode would ultimately reduce the risk posture of the EP subsystem for mission planning. However, the community must engage in more studies to determine the lifetime and discharge current reliability of heaterless cathodes.

### VIII. Conclusions

A thorough review of high-power thrusters and EP strings since 1990 with  $P_{\text{in}} \geq 6$  kW has been presented. Our review identified 46 high-power EP devices: 31 HETs, 6 GIEs, 7 arcjets, and 2 thrusters classified as other. The current SOA of high-power HETs ranges from 5.9 to 98.7 kW, 290 to 5420 mN, and 1120 to 3472 s, with total efficiencies between 57 and 67%. The current SOA of high-power GIEs ranges from 5.7 to 20.8 kW, 175 to 446 mN, and 3555 to 7650 s, with total efficiencies between 68 and 78%. High-power arcjets demonstrate performance between 9.8 and 100 kW, 568 and 4000 mN, 400 and 1400 s, and 14 and 37% total efficiency. Although many high-power devices exist, there is a significant gap in maturing high-power thrusters through a fully integrated EP string. As of the end of 2021, seven EP strings are actively being matured in TRL and/or undergoing flight qualification programs, whereas only one has flown at a power level greater than 6 kW. It was observed that various programmatic factors, such as R&D collaborations, flagship space missions, and national initiatives to advance the TRL of a thruster could either support or stymie its transition to an EP string. The PPU and PMS segments of the string significantly lag the hardware maturity of the high-power thruster and are at varying levels of maturity.

Over the last 20 years, the EP community has primarily focused on developing and maturing HETs and GIEs from thruster prototypes to fully operational EP strings. Many technological advancements have been made in the high-power regime extending thruster lifetime, design scalability, and modularity of segment components. However, many gaps exist in the current SOA of high-power EP. The seven main gaps are structural design and scalability of high-power

thrusters, facility effects on high-power thruster performance and stability, enhanced plasma diagnostics appropriate for higher power thrusters, statistical analysis of high-power thrust diagnostics, PPU-thruster dynamics and architectures, performance characterization on propellants other than xenon, and high-current cathode performance assessment. Addressing these gaps will further enable the realization of high-power EP for future space applications.

## Appendix: High-Power Thruster Performance Metrics

**Table A1** Current SOA of high-power HETs in ascending nominal  $P_{in}$

Thruster	Type	Propellant	$P_{in}$ , kW	$T$ , mN	$I_{sp, tot}$ , s	$\eta_{tot}$ , %	$\dot{m}_a$ , mg/s	Hardware maturity level	Developers	References
BBM	HET	Xe	5.98 (1.77–5.98)	383 (92.7–392.3)	1897 (1400–1940)	59.8 (47.9–62.7)	18.8 (4.6–18.8)	EU	IHI Aerospace, JAXA ISAS	[107,223]
X2	HET	Xe	6 <sup>a</sup> (5–6) <sup>a</sup>	460 (112–720)	1230 <sup>a</sup> (700–2870) <sup>a</sup>	46 <sup>a</sup> (25–71) <sup>a</sup>	11/27 <sup>a</sup> (4/10–12/30) <sup>a</sup>	BB	University of Michigan, AFRL, JPL	[139]
BHT-6000	HET	Xe	6 <sup>b</sup>	290	2505	60.5 <sup>b,c</sup>	11.6 <sup>c</sup>	FQ	Busek Co., Inc., Maxar	[8]
H6	HET	Xe	6.03 (1.1–6.2)	401 (84–410)	1950 (711–1955)	63.5	19.7 (10–20)	BB	University of Michigan, AFRL, JPL	[137,164]
H6MS	HET	Xe	6.05 (6–9.1)	384.2	2000 (2000–3020)	62.4 (60–68)	18.35 (12–19)	BB	University of Michigan, AFRL, JPL	[164,224]
SPT-200	HET	Xe	6.15 <sup>c</sup> (2.1–13.4)	379 <sup>c</sup> (135–552)	1896 <sup>c</sup> (1423–2980)	57.3 <sup>c</sup> (44–63)	19.8 <sup>c</sup> (8–20)	BB	Fakel	[225]
BHT-8000	HET	Xe, Kr, I	8.1 (Xe) (2–10)	507 (Xe) (143–508)	1884 (Xe) (1293–3060)	58 (Xe) (47–63)	24.9 <sup>c</sup> (Xe) (9–27.3)	BB	Busek Co., Inc.	[141,193]
T-220HT	HET	Xe	9 (2–22)	— (100–1000)	— (1300–2600)	—	—	BB	Pratt & Whitney Space Propulsion	[136,226]

<sup>a</sup>X2 is a nested HET. The discharge power  $P_{dis}$ , discharge specific impulse  $I_{sp, dis}$ , and discharge efficiency  $\eta_{dis}$  for dual inner + outer channel operation are presented.

<sup>b</sup>BHT-6000 discharge power  $P_{dis}$  and discharge efficiency  $\eta_{dis}$  are presented.

<sup>c</sup>Calculated from reported data points.

**Table A2** Current SOA of high-power HETs in ascending nominal  $P_{in}$

Thruster	Type	Propellant	$P_{in}$ , kW	$T$ , mN	$I_{sp, tot}$ , s	$\eta_{tot}$ , %	$\dot{m}_a$ , mg/s	Hardware maturity level	Developers	References
H9	HET	Xe, Kr	9.1 (Xe) <sup>b</sup> (4.5–9.1) <sup>a</sup>	391 (Xe) (290–436)	2950 (Xe) (1950–2950)	63.4 (Xe) (60–63.4)	12.7 (Xe) (12.7–18)	BB	University of Michigan, AFRL, JPL	[138,191]
NASA T-220	HET	Xe	10.39 (4.6–10.7)	512.5 (278–524)	2356 (1644–2379)	57 (46–57)	20.2 (15.7–22)	BB	TRW, Space Power, Inc., NASA GRC	[81,90]
KM-10	HET	Xe	10.43 <sup>b</sup> (1.5–12.5) <sup>a</sup>	517 (80–590)	2550 (1450–3380)	62 (38–66)	19.9 <sup>b</sup> (5–24)	EU	Keldysh Research Center	[91]
XR-12	HET	Xe	12.16 <sup>b</sup> (2–12) <sup>a</sup>	815 (232–815)	1961 (1100–2300)	64.5 <sup>b</sup> (40–65)	38.5 (10–38.5)	BB	Aerojet Rocketdyne	[64]
AEPS ETU-2	HET	Xe	12.58 <sup>b</sup> (6.3–12.6) <sup>b</sup>	609.3 (396–609)	2811 (1968–2811)	66.8 (60–66.8)	20.7 <sup>b</sup> (19–21)	FQ	Aerojet Rocketdyne, NASA GRC, JPL	[108]
HERMeS TDU-3	HET	Xe	12.64 <sup>b</sup> (2.7–13.1)	612.9 (167–630)	2826 (1760–2897)	67.2 (51–67.5)	20.7 <sup>b</sup> (12–28)	EU	NASA GRC, JPL	[227]
D-150	HET/TAL	Xe	15 (0.9–15)	794.3 (68–794)	2455 <sup>a</sup> (886–3099) <sup>a</sup>	64 <sup>a</sup> (32–66) <sup>a</sup>	33 (7.9–33)	BB	TsNIIMASH	[228]
SPT-290	HET	Xe	18 <sup>a</sup> (12–25) <sup>a</sup>	1000 (420–1100)	2006 <sup>b</sup> (1500–3200)	— (34–70)	50 (20–50)	BB	Fakel	[229]
HT20k DM2	HET	Xe, Kr	20 (Xe) <sup>a,b</sup> (15–22.5) <sup>a</sup>	995 (Xe) (760–1175)	2418 (Xe) (1985–2585) <sup>a</sup>	63 (Xe) <sup>a</sup> (53–63) <sup>a</sup>	39 (Xe) (36–60)	EU	SITAEL	[230]

<sup>a</sup>Discharge power  $P_{dis}$ , discharge specific impulse  $I_{sp, dis}$ , and/or discharge efficiency  $\eta_{dis}$  values are presented.

<sup>b</sup>Calculated from reported data points.

**Table A3 Current SOA of high-power HETs in ascending nominal  $P_{in}$**

Thruster	Type	Propellant	$P_{in}$ , kW	$T$ , mN	$I_{sp,tot}$ , s	$\eta_{tot}$ , %	$\dot{m}_a$ , mg/s	Hardware maturity level	Developers	References
BHT-20K	HET	Xe, Kr	20.07 <sup>c</sup> (Xe) (5.2–22.4)	980 (Xe) (242–1100)	2630 (Xe) (1430–2630)	63 (Xe) (49–64)	35.3 <sup>c</sup> (Xe) (10–59)	BB	Busek Co., Inc.	[142]
NASA-300M	HET	Xe, Kr	20.32 <sup>c</sup> (Kr) (5–20) <sup>a</sup> 20.53 <sup>c</sup> (Xe) (2.5–20.3) <sup>a</sup>	840 (Kr) (560–860) 1018 (Xe) (240–1130)	2909 (Kr) (1550–3223) 2701 (Xe) (1470–2916)	59 (Kr) (38–63) 66 (Xe) (45–67)	27.4 <sup>c</sup> (Kr) (10–51.4) 35.4 <sup>c</sup> (Xe) (9.4–52.2)	BB	NASA GRC	[134]
NASA-300MS	HET	Xe	20.7 <sup>c</sup> (2.5–20) <sup>a</sup>	921 <sup>c</sup> (136–1032)	2883 (1800–3130) <sup>a</sup>	63 (47–71) <sup>a</sup>	30 (7–41)	BB	NASA GRC, JPL	[95]
PPS-20k ML	HET	Xe	22.4 (2.6–23.5)	1050 (70–1060)	2610 <sup>c</sup> (420–2700) <sup>a</sup>	60 (38–68)	39.6 <sup>c</sup> (5–43)	BB	Safran	[157]
TAL-200 (D-200)	HET/TAL	Bi	25 (10–34)	1130 (147–1130)	3000 (2000–5200)	67	<38.4 <sup>c</sup> (10–38.4)	BB	TsNIIMASH	[231]
SPT-230	HET	Xe	25 <sup>a</sup>	Up to 1070	Up to 3200	—	—	BB	Fakel	[232]
TM-50	HET/TAL	Xe	25.4 (2.1–25.4)	966 (147–966)	3166 <sup>c</sup> (1270–3166) <sup>c</sup>	59 <sup>c</sup> (44–67) <sup>a</sup>	29.6 (10–30)	BB	TsNIIMASH	[132]
N30	HET	Xe	32.4 <sup>b</sup> (16–32.3) <sup>b</sup>	—	—	—	—	BB	University of Michigan, JPL	[166]
VHITAL-160	HET/TAL	Bi	36.8 <sup>a</sup> (6.7–36.8) <sup>a</sup>	618 (205–618)	7667 <sup>a</sup> (3500–7667) <sup>a</sup>	63 <sup>a</sup> (51–63)	8 (5.8–9.8)	BB	TsNIIMASH, JPL	[192]

<sup>a</sup>Discharge power  $P_{dis}$ , discharge specific impulse  $I_{sp,dis}$ , and/or discharge efficiency  $\eta_{dis}$  values are presented.

<sup>b</sup>N30 theoretical discharge power range presented; only inner channel performance has been measured up to discharge power of 9 kW and reported in [166].

<sup>c</sup>Calculated from reported data points.

**Table A4 Current SOA of high-power HETs in ascending nominal  $P_{in}$**

Thruster	Type	Propellant	$P_{in}$ , kW	$T$ , mN	$I_{sp,tot}$ , s	$\eta_{tr}$ , %	$\dot{m}_a$ , mg/s	Hardware maturity level	Developers	References
D-160	HET/TAL	Bi	39.6 <sup>a</sup> (20–140) <sup>a</sup>	1128 (153–1128)	5505 <sup>a</sup> (4000–8000) <sup>a</sup>	75 <sup>a</sup> (60–80) <sup>a</sup>	21.4 (4.4–26)	BB	TsNIIMASH	[124]
NASA-400M	HET	Xe, Kr	47 <sup>a</sup> (Xe) (3.6–47) <sup>a</sup> 64.5 <sup>a</sup> (Kr) (5.1–64.5) <sup>a</sup>	2118 (Xe) (271–2118) 1915 (Kr) (265–1915)	2995 <sup>a</sup> (Xe) (1322–3372) <sup>a</sup> 4377 <sup>a</sup> (Kr) (2171–4943) <sup>a</sup>	66 <sup>a</sup> (Xe) (46–72) <sup>a</sup> 64 <sup>a</sup> (Kr) (47–68) <sup>a</sup>	72.1 (Xe) (20–72.1) 44.6 (Kr) (11–44.6)	BB	NASA GRC	[99]
NASA-457M v2	HET	Xe	50.1 <sup>b</sup> (5–50) <sup>a</sup>	2300 (330–2300)	2740 (1420–2740)	61.7 <sup>b</sup> (51–66)	79.2 <sup>b</sup> (17–82)	BB	NASA GRC	[160]
NASA-457M v1	HET	Xe, Kr	72.5 <sup>a</sup> (Kr) (7.8–72.5) <sup>a</sup> 73.2 (Xe) (10–73.2)	2473 (Kr) (390–2473) 2950 (Xe) (371–2950)	3472 (Kr) (2039–4495) <sup>a</sup> 2929 (Xe) (1557–2929)	64 <sup>a</sup> (Kr) (48–64) <sup>a</sup> 58 (Xe) (34–58)	66 (Kr) (19.5–66) 92.7 (Xe) (15–92.7)	BB	NASA GRC	[135,161]
X3	HET	Xe	98.7 (4.9–101) <sup>a</sup>	5420 (350–5420)	2340 (1800–2650)	63 (54–67)	220.7 <sup>b</sup> (18–250)	BB	University of Michigan, NASA GRC, JPL	[233]

<sup>a</sup>Discharge power  $P_{dis}$ , discharge specific impulse  $I_{sp,dis}$ , and/or discharge efficiency  $\eta_{dis}$  values are presented.

<sup>b</sup>Calculated from reported data points.

**Table A5 Current SOA of high-power GIEs in ascending nominal  $P_{in}$**

Thruster	Type	Propellant	$P_{in}$ , kW	$T$ , mN	$I_{sp,tot}$ , s	$\eta_{tot}$ , %	$\dot{m}_a$ , mg/s	Hardware maturity level	Developers	References
RIT 2X <sup>a</sup> (RIT-22)	GIE	Xe	5.65 (2–7.5)	175 (70–215)	4750 (2500–6400)	72	3.4	EU	ArianeGroup	[13,100,114]
T7 <sup>b</sup>	GIE	Xe	6.4 (2.7–6.4)	250 (97–250)	3555 (3117–3984)	68 (66–70)	7.2 <sup>c</sup>	BB	QinetiQ, Mars Space Limited	[12]
NEXT-C	GIE	Xe	6.86 (0.53–6.86)	237 (25–237)	4190 (1395–4310)	71 (32–70)	4.9 <sup>c</sup> (1.2–4.9)	FQ	Aerojet Rocketdyne, NASA GRC	[89,234]
IT-500	GIE	Xe	17.8 (17.8–35)	390 (375–750)	7250 <sup>c</sup> (≥ 7000) <sup>a</sup>	78 <sup>c</sup>	<5.5 <sup>c</sup> (5.5–11) <sup>c</sup>	EU	Keldysh Research Center	[94]
NEXIS	GIE	Xe	20.4 (16–28)	446 (403–531)	7050 (6040–8730)	75.7 (74–81)	5.4 (5.1–5.7)	EU	JPL	[147]
HiPEP	GIE	Xe	20.8 (6–39.3)	428 (240–670)	7650 (5970–9620)	77 (72–80)	4.6 <sup>c</sup> (3.2–4.6)	EU	NASA GRC	[97,235]

<sup>a</sup>RIT 2X performance is proprietary, so its predecessor, RIT-22, performance data are presented.

<sup>b</sup>The theoretical performance values of the T7 are presented. The measured performance in  $T$ ,  $I_{sp}$ , and  $\eta_{tot}$  have not been reported.

<sup>c</sup>Calculated from reported data points.

**Table A6** Current SOA of high-power arcjets in ascending nominal  $P_{in}$ 

Thruster	Type	Propellant	$P_{in}$ , kW	$T$ , mN	$I_{sp,tot}$ , s	$\eta_{tot}$ , %	$\dot{m}_a$ , mg/s	Hardware maturity level	Developers	References
MARC 6	Arcjet	H <sub>2</sub>	9.8 (5–9.8)	567 (493–567)	1280 (1112–1280)	36 (36–49)	45.2	BB	Institut für Raumfahrt-systeme	[15]
—	Arcjet	NH <sub>3</sub>	10 (3.1–12)	1118 (299–1452)	650 (394–730)	36 (29–37)	170 (43–305)	BB	JPL	[236,237]
—	Arcjet	H <sub>2</sub>	11.3 (7.8–11.3)	742	1200	37 (34–38)	63 (46–63)	BB	Electric Propulsion Laboratory, Inc.	[238]
—	Arcjet	CH <sub>4</sub>	11.4 (6.2–11.4)	588 (373–588)	550 (430–590)	13.9 (12–15.6)	109 (76–109)	BB	Busek Co., Inc.	[239]
TT1	Arcjet	Ar, N <sub>2</sub> , H <sub>2</sub> , N <sub>2</sub> H <sub>2</sub>	12.8 (Ar) (1.3–12.8)	1500 (Ar) (250–1500)	400 (Ar) (150–510)	30 (Ar) (21–30)	300 (Ar) (100–400)	BB	BPD, Institut für Raumfahrt-systeme	[125]
ESEX	Arcjet	NH <sub>3</sub>	27.8	1930	786	26.7	240	FQ	Rocket Research Co., TRW, AFRL	[240]
HIPARC-R	Arcjet	H <sub>2</sub>	99.7 (17–107)	4000 (1200–4000)	1400 (800–2100)	28 (25–30)	300 (150–300)	BB	Institut für Raumfahrt-systeme	[241]

**Table A7** Current SOA of high-power Other thrusters in ascending nominal  $P_{in}$ 

Thruster	Type	Propellant	$P_{in}$ , kW	$T$ , mN	$I_{sp,tot}$ , s	$\eta_{tot}$ , %	$\dot{m}_a$ , mg/s	Hardware maturity level	Developers	References
HEMP-T 30250 DM2	Other	Xe	10 (0.8–10.8)	332 (40–332)	3154 (1300–3600)	51.5 (29–51.5)	10.8 (3–11.8)	BB	Thales Electron Devices	[242]
VX-200	Other	Ar	200 (28–200)	5800 (600–5800)	4900	72 (10–72)	100	BB	Ad Astra Co.	[243]

### Acknowledgments

The authors would like to thank Luis Piñero and Dragos Dinca at NASA Glenn Research Center for their invaluable insight and guidance throughout this paper. Additionally, the authors greatly appreciate Vlad Hruby and the Hall thruster team at Busek Co., Inc., for their open cooperation in the data collection of this paper. Lastly, the authors would like to thank Benjamin Jorns, Jorge Delgado, Jaime Perez Luna, Antonio Piragino, Javier Torres Cabañuz, Heiko Dartsch, Thierry Scalais, Kristof Holste, Hans Leiter, and Gen Ito for their support in completing the data segment of this review.

### References

- [1] Surampudi, R., Blosiu, J., Stella, P., Elliott, J., Castillo, J., Yi, T., Lyons, J., Piszczor, M., McNatt, J., Taylor, C., Gaddy, E., Liu, S., Plichta, E., Iannello, C., Beauchamp, P., and Cutts, J. A., "Solar Power Technologies for Future Planetary Science Missions," NASA/Jet Propulsion Lab. Rept. JPL D-101316, Dec. 2017.
- [2] Feuerborn, S. A., Perkins, J., and Neary, D. A., "Finding a Way: Boeing's 'All Electric Propulsion Satellite,'" *49th AIAA/ASME/SAE/ASEE Joint Propulsion Conference*, AIAA Paper 2013-4126, 2013. <https://doi.org/10.2514/6.2013-4126>
- [3] Autric, J.-M., Escourrou, P., and Laine, I., "Telecom Spacecraft Mission Design: Electric Orbit Raising for Airbus Communications Satellites," *2018 SpaceOps Conference*, AIAA Paper 2018-2601, 2018. <https://doi.org/10.2514/6.2018-2601>
- [4] Johnson, I., Santiago, G., Li, J., and Baldwin, J., "100,000 hrs of On-Orbit Electric Propulsion and MAXAR's First Electric Orbit Raising," *AIAA Scitech 2020 Forum*, AIAA Paper 2020-0189, 2020. <https://doi.org/10.2514/6.2020-0189>
- [5] Nishi, K., Ozawa, S., Fukatsu, T., Hatooka, Y., Sano, T., Nishijo, K., Otani, F., and Kohama, T., "Conceptual Design of Japan's Engineering Test Satellite-9," *35th AIAA International Communications Satellite Systems Conference*, AIAA Paper 2017-5427, 2017. <https://doi.org/10.2514/6.2017-5427>
- [6] Jackson, J., Miller, S., Cassady, J., Soendker, E., Welander, B., Barber, M., and Peterson, P., "13 kW Advanced Electric Propulsion Flight System Development and Qualification," *36th International Electric Propulsion Conference*, IEPC Paper 2019-692, 2019.
- [7] Ticker, R., Gates, M., Manzella, D., Biaggi-Labiosa, A., and Lee, T., "The Gateway Power and Propulsion Element: Setting the Foundation for Exploration and Commerce," *AIAA Propulsion and Energy 2019 Forum*, AIAA Paper 2019-3811, 2019. <https://doi.org/10.2514/6.2019-3811>
- [8] Herman, D. A., Johnson, T. G., Kerl, I. T., Lee, T., and Silva, T., "The Application of Advanced Electric Propulsion on the NASA Power and Propulsion Element (PPE)," *36th International Electric Propulsion Conference*, IEPC Paper 2019-651, 2019.
- [9] Giannetti, V., Ferrato, E., Piragino, A., Reza, M., Faraji, F., Andreucci, M., and Andreussi, T., "HT5k Thruster Unit Development History, Status and Way Forward," *36th International Electric Propulsion Conference*, IEPC Paper 2019-878, 2019.
- [10] Duchemin, O., Rabin, J., Balika, L., Diome, M., Lonchard, J.-M., Cavelan, X., Boniface, C., and Liénart, T., "Development Status of the PPS®5000 Hall Thruster Unit," *35th International Electric Propulsion Conference*, IEPC Paper 2017-415, 2017.
- [11] Piragino, A., Leporini, A., Giannetti, V., Pedrini, D., Rossodivita, A., Andreussi, T., Andreucci, M., and Estublier, D., "Characterization of a 20 kW-Class Hall Effect Thruster," *35th International Electric Propulsion Conference*, IEPC Paper 2017-381, 2017.
- [12] Luna, J. P., Lewis, R. A., Park, N., Boshier, J., Guarducci, F., and Cannat, F., "T7 Thruster Design and Performance," *36th International Electric Propulsion Conference*, IEPC Paper 2019-356, 2019.
- [13] Leiter, H.-J., Lauer, D., Bauer, P., Berger, M., and Rath, M., "The Ariane Group Electric Propulsion Program 2019-2020," *36th International Electric Propulsion Conference*, IEPC Paper 2019-592, 2019.
- [14] Petro, E. M., and Sedwick, R. J., "Survey of Moderate-Power Electric Propulsion Systems," *Journal of Spacecraft and Rockets*, Vol. 54, No. 3, 2017, pp. 529–541. <https://doi.org/10.2514/1.A33647>
- [15] Wollenhaupt, B., Le, Q. H., and Herdrich, G., "Overview of Thermal Arcjet Thruster Development," *Aircraft Engineering and Aerospace Technology*, Vol. 90, No. 2, 2018, pp. 280–301. <https://doi.org/10.1108/AEAT-08-2016-0124>
- [16] Lev, D., Myers, R. M., Lemmer, K. M., Kolbeck, J., Koizumi, H., and Polzin, K., "The Technological and Commercial Expansion of Electric Propulsion," *Acta Astronautica*, Vol. 159, June 2019, pp. 213–227. <https://doi.org/10.1016/j.actaastro.2019.03.058>
- [17] Dale, E., Jorns, B., and Gallimore, A., "Future Directions for Electric Propulsion Research," *Aerospace*, Vol. 7, No. 9, 2020, Paper 120. <https://doi.org/10.3390/aerospace7090120>
- [18] Jahn, R. G., *Physics of Electric Propulsion*, Dover, Mineola, NY, 2006, Chap. 1.
- [19] Goebel, D. M., and Katz, I., *Fundamentals of Electric Propulsion: Ion and Hall Thrusters*, 1, Wiley, Hoboken, NJ, 2008, Chaps. 1–3.

- [20] Kodys, A., and Choueiri, E. Y., "A Critical Review of the State-of-the-Art in the Performance of Applied-Field Magnetoplasmadynamic Thrusters," *41st AIAA/ASME/SAE/ASEE Joint Propulsion Conference & Exhibit*, AIAA Paper 2005-4247, 2005.  
<https://doi.org/10.2514/6.2005-4247>
- [21] Cong, Y., Li, Y., Wei, Y., Zhou, C., Ding, F., Wang, B., Wang, L., Tian, H., Yang, N., and Sun, K., "The Experimental Performances of the 100 kW MPD Thruster with Applied Magnetic Field," *36th International Electric Propulsion Conference*, IEPC Paper 2019-310, 2019.
- [22] Boxberger, A., and Herdrich, G., "Integral Measurements of 100 kW Class Steady State Applied-Field Magnetoplasmadynamic Thruster SX3 and Perspectives of AF-MPD Technology," *35th International Electric Propulsion Conference*, IEPC Paper 2017-339, 2017.
- [23] Ide, S., Tsukizaki, R., Nishiyama, K., and Kuninaka, H., "Performance of Applied Field MPD Thruster with Various Propellants," *36th International Electric Propulsion Conference*, IEPC Paper 2019-A450, 2019.
- [24] Boxberger, A., Behnke, A., and Herdrich, G., "Current Advances in Optimization of Operative Regimes of Steady State Applied Field MPD Thrusters," *36th International Electric Propulsion Conference*, IEPC Paper 2019-585, 2019.
- [25] Ichihara, D., Uno, T., Kataoka, H., Jeong, J., Iwakawa, A., and Sasoh, A., "Ten-Ampere-Level, Applied-Field-Dominant Operation in Magnetoplasmadynamic Thrusters," *Journal of Propulsion and Power*, Vol. 33, No. 2, 2017, pp. 360–369.  
<https://doi.org/10.2514/1.B36179>
- [26] Dailey, C. L., and Lovberg, R. H., "The PIT MkV Pulsed Inductive Thruster," NASA CR-191155, July 1993.
- [27] Polzin, K., Martin, A., Little, J., Promislow, C., Jorns, B., and Woods, J., "State-of-the-Art and Advancement Paths for Inductive Pulsed Plasma Thrusters," *Aerospace*, Vol. 7, No. 8, 2020, Paper 105.  
<https://doi.org/10.3390/aerospace7080105>
- [28] Polzin, K. A., "Comprehensive Review of Planar Pulsed Inductive Plasma Thruster Research and Technology," *Journal of Propulsion and Power*, Vol. 27, No. 3, 2011, pp. 513–531.  
<https://doi.org/10.2514/1.B34188>
- [29] Dankanich, J., and Polzin, K., "Mission Assessment of the Faraday Accelerator with Radio-Frequency Assisted Discharge (FARAD)," *44th AIAA/ASME/SAE/ASEE Joint Propulsion Conference & Exhibit*, AIAA Paper 2008-4517, 2008.  
<https://doi.org/10.2514/6.2008-4517>
- [30] Rostoker, N., and Qerushi, A., "Classical Transport in a Field Reversed Configuration," *Plasma Physics Reports*, Vol. 29, No. 7, 2003, pp. 626–630.  
<https://doi.org/10.1134/1.1592562>
- [31] Weber, T. E., Slough, J. T., and Kirtley, D., "The Electrodeless Lorentz Force (ELF) Thruster Experimental Facility," *Review of Scientific Instruments*, Vol. 83, No. 11, 2012, Paper 113509.  
<https://doi.org/10.1063/1.4759000>
- [32] Kazeev, M. N., and Kozlov, V. F., "Ablation-Fed Discharge Characteristics," *31st International Electric Propulsion Conference*, IEPC Paper 2009-249, 2009.
- [33] Snyder, J. S., Randolph, T. M., Hofer, R. R., and Goebel, D. M., "Simplified Ion Thruster Xenon Feed System for NASA Science Missions," *31st International Electric Propulsion Conference*, IEPC Paper 2009-064, 2009.
- [34] Fearn, D. G., and Philip, C. M., "An Investigation of Physical Processes in a Hollow Cathode Discharge," *AIAA Journal*, Vol. 11, No. 2, 1973, pp. 131–132.  
<https://doi.org/10.2514/3.50441>
- [35] Lev, D. R., Mikellides, I. G., Pedrini, D., Goebel, D. M., Jorns, B. A., and McDonald, M. S., "Recent Progress in Research and Development of Hollow Cathodes for Electric Propulsion," *Reviews of Modern Plasma Physics*, Vol. 3, No. 1, 2019, Paper 6.  
<https://doi.org/10.1007/s41614-019-0026-0>
- [36] Goebel, D. M., Watkins, R. M., and Jameson, K. K., "LaB6 Hollow Cathodes for Ion and Hall Thrusters," *Journal of Propulsion and Power*, Vol. 23, No. 3, 2007, pp. 552–558.  
<https://doi.org/10.2514/1.25475>
- [37] Sengupta, A., "Magnetic Confinement in a Ring-Cusp Ion Thruster Discharge Plasma," *Journal of Applied Physics*, Vol. 105, No. 9, 2009, Paper 093303.  
<https://doi.org/10.1063/1.3106087>
- [38] Delgado, J. J., Baldwin, J. A., and Corey, R. L., "Space Systems Loral Electric Propulsion Subsystem: 10 Years of On-Orbit Operation," *34th International Electric Propulsion Conference*, IEPC Paper 2015-04, 2015.
- [39] Piñero, L. R., and Benson, S. W., "NEXT Engineering Model PPU Development, Progress and Plans," *47th AIAA/ASME/SAE/ASEE Joint Propulsion Conference & Exhibit*, AIAA Paper 2011-5659, 2011.  
<https://doi.org/10.2514/6.2011-5659>
- [40] Bontempo, J. J., Brigeman, A. N., Fain, H. B., Gonzalez, M. C., Piñero, L. R., Birchenough, A. G., Aulisio, M. V., Fisher, J., and Ferraiuolo, B., "The NEXT-C Power Processing Unit: Lessons Learned from the Design, Build, and Test of the NEXT-C PPU for APL's DART Mission," *AIAA Propulsion and Energy 2020 Forum*, AIAA Paper 2020-3641, 2020.  
<https://doi.org/10.2514/6.2020-3641>
- [41] Cardin, J. M., Cook, W., and Bhandari, R., "Qualification of an Advanced Xenon Flow Control Module," *33rd International Electric Propulsion Conference*, IEPC Paper 2013-382, 2013.
- [42] Bennett, D. C., and Stellrecht, E. J., "A Low Power Proportional Flow Control Valve for Electric Propulsion Systems for Satellite Applications," *35th International Electric Propulsion Conference*, IEPC Paper 2017-278, 2017.
- [43] Oh, D. Y., Snyder, J. S., Goebel, D. M., Hofer, R. R., and Randolph, T. M., "Solar Electric Propulsion for Discovery-Class Missions," *Journal of Spacecraft and Rockets*, Vol. 51, No. 6, 2014, pp. 1822–1835.  
<https://doi.org/10.2514/1.A32889>
- [44] Racca, G. D., "SMART-1 from Conception to Moon Impact," *Journal of Propulsion and Power*, Vol. 25, No. 5, 2009, pp. 993–1002.  
<https://doi.org/10.2514/1.36278>
- [45] Sackheim, R. L., "Overview of United States Space Propulsion Technology and Associated Space Transportation Systems," *Journal of Propulsion and Power*, Vol. 22, No. 6, 2006, pp. 1310–1332.  
<https://doi.org/10.2514/1.23257>
- [46] Sovey, J. S., Rawlin, V. K., and Patterson, M. J., "Ion Propulsion Development Projects in U.S.: Space Electric Rocket Test I to Deep Space 1," *Journal of Propulsion and Power*, Vol. 17, No. 3, 2001, pp. 517–526.  
<https://doi.org/10.2514/2.5806>
- [47] Tighe, W., Chien, K.-R., Solis, E., Rebello, P., Goebel, D. M., and Snyder, J. S., "Performance Evaluation of the XIPS 25-cm Thruster for Application to NASA Discovery Missions," *42nd AIAA/ASME/SAE/ASEE Joint Propulsion Conference & Exhibit*, AIAA Paper 2006-4666, 2006.  
<https://doi.org/10.2514/6.2006-4666>
- [48] Snyder, J. S., Goebel, D. M., Hofer, R. R., Polk, J. E., Wallace, N. C., and Simpson, H., "Performance Evaluation of the T6 Ion Engine," *Journal of Propulsion and Power*, Vol. 28, No. 2, 2012, pp. 371–379.  
<https://doi.org/10.2514/1.B34173>
- [49] Castellini, F., Bellei, G., and Budnik, F., "BepiColombo Orbit Determination Activities During Electric Propulsion Arcs," *AIAA Scitech 2020 Forum*, AIAA Paper 2020-1701, 2020.  
<https://doi.org/10.2514/6.2020-1701>
- [50] Delgado, J. J., Corey, R. L., Murashko, V. M., Koryakin, A. I., and Pridanikov, S. Y., "Qualification of the SPT-140 for Use on Western Spacecraft," *50th AIAA/ASME/SAE/ASEE Joint Propulsion Conference*, AIAA Paper 2014-3606, 2014.  
<https://doi.org/10.2514/6.2014-3606>
- [51] Casaregola, C., "Electric Propulsion for Station Keeping and Electric Orbit Raising on Eutelsat Platforms," *34th International Electric Propulsion Conference*, IEPC Paper 2015-97, 2015.
- [52] Fisher, J., Wilson, A., King, D., Meyer, S., de Grys, K., and Werthman, L., "The Development and Qualification of a 4.5 kW Hall Thruster Propulsion Subsystem," *39th AIAA/ASME/SAE/ASEE Joint Propulsion Conference & Exhibit*, AIAA Paper 2003-4551, 2003.  
<https://doi.org/10.2514/6.2003-4551>
- [53] Mueller, M. J., "Lessons from the AEHF-1 Bipropellant Maneuver Anomaly with Recurring Themes," *51st AIAA/SAE/ASEE Joint Propulsion Conference*, AIAA Paper 2015-3955, 2015.  
<https://doi.org/10.2514/6.2015-3955>
- [54] Bober, A., Kozubsky, K., Komarow, G., Maslennikov, N., Kozlov, A., and Romashko, A., "Development and Qualification Test of a SPT Electric Propulsion System for 'GALS' Spacecraft," *23rd International Electric Propulsion Conference*, IEPC Paper 1993-008, 1993.
- [55] Lyszyk, M., Klinger, E., Sécheresse, O., Bugeat, J., Valentian, D., Cadiou, A., Beltan, T., and Gelas, C., "Qualification Status of the PPS 1350 Plasma Thruster," *35th Joint Propulsion Conference & Exhibit*, AIAA Paper 1999-2278, 1999.  
<https://doi.org/10.2514/6.1999-2278>
- [56] Hutchins, M., Simpson, H., and Jiménez, J. P., "QinetiQ's T6 and T5 Ion Thruster Electric Propulsion System Architectures and Performances," *34th International Electric Propulsion Conference*, IEPC Paper 2015-131, 2015.
- [57] Randall, P. N., Lewis, R. A., Clark, S. D., Chan, K. K., Gray, H., Striedter, F., and Steiger, C., "BepiColombo—MEPS Commissioning Activities and T6 Ion Thruster Performance During Early Mission

- Operations," *36th International Electric Propulsion Conference*, IEPC Paper 2019-615, 2019.
- [58] Chien, K.-R., Tighe, W. G., Bond, T. A., and Spears, R., "An Overview of Electric Propulsion at L-3 Communications, Electron Technologies Inc.," *42nd AIAA/ASME/SAE/ASEE Joint Propulsion Conference & Exhibit*, AIAA Paper 2006-4322, 2006.  
<https://doi.org/10.2514/6.2006-4322>
- [59] Goebel, D. M., Martínez-Lavin, M., Bond, T. A., and King, A. M., "Performance of XIPS Electric Propulsion in On-Orbit Station Keeping of the Boeing 702 Spacecraft," *38th AIAA/ASME/SAE/ASEE Joint Propulsion Conference & Exhibit*, AIAA Paper 2002-4348, 2002.  
<https://doi.org/10.2514/6.2002-4348>
- [60] Wilson, F., King, D., Willey, M., Aadland, R., Tilley, D., and de Grys, K., "Development Status of the BPT Family of Hall Current Thrusters," *35th Joint Propulsion Conference & Exhibit*, AIAA Paper 1999-2573, 1999.  
<https://doi.org/10.2514/6.1999-2573>
- [61] Hoskins, A. W., Cassady, J. R., Morgan, O., Myers, R. M., Wilson, F., King, D. Q., and de Grys, K., "30 Years of Electric Propulsion Flight Experience at Aerojet Rocketdyne," *33rd International Electric Propulsion Conference*, IEPC Paper 2013-439, 2013.
- [62] Tilley, D. L., Willmes, G. F., Myers, R. M., and Smith, R. D., "Flight Hollow Cathode for Hall Thruster Applications," *34th AIAA/ASME/SAE/ASEE Joint Propulsion Conference & Exhibit*, AIAA Paper 1998-3339, 1998.  
<https://doi.org/10.2514/6.1998-3339>
- [63] Polk, J. E., Goebel, D. M., and Tighe, W., "Ongoing Wear Test of a XIPS<sup>®</sup>25-cm Thruster Discharge Cathode," *44th AIAA/ASME/SAE/ASEE Joint Propulsion Conference & Exhibit*, AIAA Paper 2008-4913, 2008.  
<https://doi.org/10.2514/6.2008-4913>
- [64] Welander, B., Monheiser, J., Meckel, N., de Grys, K., Peterson, P., and Khayms, V., "Demonstration of the XR-12 Hall Current Thruster," *33rd International Electric Propulsion Conference*, IEPC Paper 2013-451, 2013.
- [65] Bourguignon, E., and Fraselle, S., "Power Processing Unit Activities at Thales Alenia Space in Belgium," *36th International Electric Propulsion Conference*, IEPC Paper 2019-584, 2019.
- [66] Glogowski, M. J., Kodys, A. D., Pilchuk, J. W., Hartmann, J. W., Lentati, A., Kadakkal, V., Pulido, C., Trescott, J. A., Pucci, J. M., and Koch, B. A., "Design, Qualification, and Initial Flight Operations of the GEOStar-3<sup>TM</sup> Electric Propulsion System," *2018 Joint Propulsion Conference*, AIAA Paper 2018-4719, 2018.  
<https://doi.org/10.2514/6.2018-4719>
- [67] Pintó, F., Palencia, J., Glorieux, G., and Wagner, N., "Airbus Defence and Space Power Processing Units: New HET and GIT PPU Developments Qualification Status," *35th International Electric Propulsion Conference*, IEPC Paper 2017-266, 2017.
- [68] Day, M., Maslennikov, N., Randolph, T., and Rogers, W., "SPT-100 Subsystem Qualification Status," *32nd Joint Propulsion Conference & Exhibit*, AIAA Paper 1996-2713, 1996.  
<https://doi.org/10.2514/6.1996-2713>
- [69] Gollor, M., Franke, A., Schwab, U., Dechent, W., Glorieux, G., Wagner, N., Pintó, F., Palencia, J., Galantini, P., Tuccio, G., and Bourguignon, E., "Electric Propulsion Electronics Activities in Europe 2016," *52nd AIAA/SAE/ASEE Joint Propulsion Conference*, AIAA Paper 2016-5032, 2016.  
<https://doi.org/10.2514/6.2016-5032>
- [70] Clark, S., Randall, P., Lewis, R., Marangone, D., Goebel, D. M., Chaplin, V., Gray, H., Kempkens, K., and Wallace, N., "BepiColombo—Solar Electric Propulsion System Test and Qualification Approach," *36th International Electric Propulsion Conference*, IEPC Paper 2019-586, 2019.
- [71] de Grys, K., Welander, B., DiMicco, J. L., Wenzel, S., Kay, B., Khayms, V., and Paisley, J., "4.5 kW Hall Thruster System Qualification Status," *41st AIAA/ASME/SAE/ASEE Joint Propulsion Conference & Exhibit*, AIAA Paper 2005-3682, 2005.  
<https://doi.org/10.2514/6.2005-3682>
- [72] Kay, R. J., Fisher, J. R., Meyer, S. D., DiMicco, J. L., Hobson, D. C., Homiak, D., and Stolzenburg, S., "The Development of a 4.5 kW Hall Thruster Propulsion System Power Processing Unit," *27th International Electric Propulsion Conference*, IEPC Paper 2001-333, 2001.
- [73] Clayton, P., Staley, M., Tomescu, B., Waranauskas, J., Kendall, J., Saghri, S., Esquivias, J., Malone, S., Delgado, J., and Nelson, N., "High Efficiency, Versatile Power Processing Units for Hall-Effect Plasma Thrusters," *2018 Joint Propulsion Conference*, AIAA Paper 2018-4642, 2018.  
<https://doi.org/10.2514/6.2018-4642>
- [74] Gray, H. L., and Sutherland, O., "Development and Qualification Status of the Electric Propulsion System for the BepiColombo Mission," *33rd International Electric Propulsion Conference*, IEPC Paper 2013-114, 2013.
- [75] Di Cara, D. M., and Estublier, D., "SMART-1: An Analysis of Flight Data," *Acta Astronautica*, Vol. 57, Nos. 2–8, July–Oct. 2005, pp. 250–256.  
<https://doi.org/10.1016/j.actaastro.2005.03.036>
- [76] Beattie, J. R., Matossian, J. N., and Robson, R. R., "Status of Xenon Ion Propulsion Technology," *Journal of Propulsion and Power*, Vol. 6, No. 2, 1990, pp. 145–150.  
<https://doi.org/10.2514/3.23236>
- [77] Barbarits, J. K., "Xenon Pressure Regulator," *34th AIAA/ASME/SAE/ASEE Joint Propulsion Conference & Exhibit*, AIAA Paper 1998-3493, 1998.  
<https://doi.org/10.2514/6.1998-3493>
- [78] Gnizdor, R., Kozubsky, K., Koryakin, A., Maslennikov, N., Pridannikov, S., and Day, M., "SPT100 Life Test with Single Cathode up to Total Impulse Two Million N-Sec," *34th AIAA/ASME/SAE/ASEE Joint Propulsion Conference & Exhibit*, AIAA Paper 1998-3790, 1998.  
<https://doi.org/10.2514/6.1998-3790>
- [79] Bushway, E. D., III, King, P. T., Engelbrecht, C., and Werthman, L., "A Xenon Flowrate Controller for Hall Current Thruster Applications," *27th International Electric Propulsion Conference*, IEPC Paper 2001-315, 2001.
- [80] Corey, R. L., and Pidgeon, D. J., "Electric Propulsion at Space Systems/Loral," *31st International Electric Propulsion Conference*, IEPC Paper 2009-270, 2009.
- [81] Hargus, W., Jr., Fife, J. M., Mason, L., Jankovsky, R., Haag, T., Piñero, L., and Snyder, J. S., "Preliminary Performance Results of the High Performance Hall System SPT-140," *36th AIAA/ASME/SAE/ASEE Joint Propulsion Conference & Exhibit*, AIAA Paper 2000-3250, 2000.  
<https://doi.org/10.2514/6.2000-3250>
- [82] Snyder, J. S., Lenguito, G., Frieman, J. D., Haag, T. W., and Mackey, J. A., "Effects of Background Pressure on SPT-140 Hall Thruster Performance," *Journal of Propulsion and Power*, Vol. 36, No. 5, 2020, pp. 668–676.  
<https://doi.org/10.2514/1.B37702>
- [83] Kim, V., Popov, G., Arkhipov, B., Murashko, V., Gorshkov, O., Koroteyev, A., Garkusha, V., Semenkin, A., and Tverdokhlebov, S., "Electric Propulsion Activity in Russia," *27th International Electric Propulsion Conference*, IEPC Paper 2001-05, 2001.
- [84] Jankovsky, R., Tverdokhlebov, S., and Manzella, D., "High Power Hall Thrusters," *35th Joint Propulsion Conference & Exhibit*, AIAA Paper 1999-2949, 1999.  
<https://doi.org/10.2514/6.1999-2949>
- [85] Hirshorn, S. R., Voss, L. D., and Bromley, L. K., "NASA Systems Engineering Handbook," NASA SP-2016-6105 Rev 2, Feb. 2017.
- [86] Roe, R. R., "Payload Test Requirements," NASA STD-7002 Rev B, June 2018.
- [87] Frieman, J. D., Kamhawi, H., Mackey, J., Haag, T., Peterson, P. Y., Herman, D. A., Gilland, J. H., and Hofer, R. R., "Completion of the Long Duration Wear Test of the NASA HERMeS Hall Thruster," *AIAA Propulsion & Energy 2019 Forum*, AIAA Paper 2019-3895, 2019.  
<https://doi.org/10.2514/6.2019-3895>
- [88] Funaki, I., Cho, S., Sano, T., Fukatsu, T., Tashiro, Y., Shiiki, T., and Nakamura, Y., "Hall Thruster Breadboard Model Development for ETS-9," *32nd International Symposium on Space Technology and Science*, ISTS Paper 2019-b-003, 2019.
- [89] Shastry, R., Herman, D. A., Soulas, G. C., and Patterson, M. J., "End-of-Test Performance and Wear Characterization of NASA's Evolutionary Xenon Thruster (NEXT) Long-Duration Test," *50th AIAA/ASME/SAE/ASEE Joint Propulsion Conference*, AIAA Paper 2014-3617, 2014.  
<https://doi.org/10.2514/6.2014-3617>
- [90] Mason, L. S., Jankovsky, R. S., and Manzella, D. H., "1000 Hours of Testing on a 10 Kilowatt Hall Effect Thruster," *37th Joint Propulsion Conference & Exhibit*, AIAA Paper 2001-3773, 2001.  
<https://doi.org/10.2514/6.2001-3773>
- [91] Shashkov, A. S., and Lovtsov, A. S., "Laboratory Tests of 10.5 kW Hall Thruster with External Layer," *36th International Electric Propulsion Conference*, IEPC Paper 2019-392, 2019.
- [92] Frieman, J. D., Kamhawi, H., Huang, W., Mackey, J., Ahern, D. M., Peterson, P. Y., Gilland, J., Hall, S. J., Hofer, R. R., Inaba, D., Dao, H., Zubair, J., Neuhoff, J., and Branch, N. A., "Wear Test of the 12.5-kW Advanced Electric Propulsion System Engineering Test Unit Hall Thruster," *AIAA Propulsion and Energy 2020 Forum*, AIAA Paper 2020-3625, 2020.  
<https://doi.org/10.2514/6.2020-3625>

- [93] Piragino, A., Giannetti, V., Reza, M., Faraji, F., Ferrato, E., Kitaeva, A., Pedrini, D., Andreussi, T., Andrenucci, M., and Paganucci, F., "Development Status of SITAEL's 20 kW Class Hall Thruster," *AIAA Propulsion and Energy 2019 Forum*, AIAA Paper 2019-3812, 2019. <https://doi.org/10.2514/6.2019-3812>
- [94] Lovtsov, A. S., Selivanov, M. Y., and Kostin, A. N., "Qualification Status of High Power Ion Thruster and Flow Control Unit," *Acta Astronautica*, Vol. 169, April 2020, pp. 150–157. <https://doi.org/10.1016/j.actaastro.2019.12.009>
- [95] Kamhawi, H., Huang, W., Haag, T., Shastry, R., Soulas, G., Smith, T., Mikellides, I., and Hofer, R., "Performance and Thermal Characterization of the NASA-300MS 20 kW Hall Effect Thruster," *33rd International Electric Propulsion Conference*, IEPC Paper 2013-444, 2013.
- [96] Snyder, J. S., Goebel, D. M., Polk, J. E., Schneider, A. C., and Sengupta, A., "Results of a 2000-Hour Wear Test of the NEXIS Ion Engine," *29th International Electric Propulsion Conference*, IEPC Paper 2005-281, 2005.
- [97] Williams, G. J., Foster, J. E., Miller, J. R., Haag, T. W., Fong, D., Noord, J. L. V., Malone, S. P., Hickman, T. A., Crable, V. J., and Patterson, M. J., "Wear-Testing of a 21 kW 7600 s Ion Thruster," *41st AIAA/ASME/SAE/ASEE Joint Propulsion Conference & Exhibit*, AIAA Paper 2005-4396, 2005. <https://doi.org/10.2514/6.2005-4396>
- [98] Bromaghim, D. R., LeDuc, J. R., Salasovich, R. M., Spanjers, G. G., Fife, J. M., Dulligan, M. J., Schilling, J. H., White, D. C., and Johnson, L. K., "Review of the Electric Propulsion Space Experiment (ESEX) Program," *Journal of Propulsion and Power*, Vol. 18, No. 4, 2002, pp. 723–730. <https://doi.org/10.2514/2.6009>
- [99] Peterson, P. Y., Jacobson, D. T., Manzella, D. H., and John, J. W., "The Performance and Wear Characterization of a High-Power High-Isp NASA Hall Thruster," *41st AIAA/ASME/SAE/ASEE Joint Propulsion Conference & Exhibit*, AIAA Paper 2005-4243, 2005. <https://doi.org/10.2514/6.2005-4243>
- [100] Leiter, H.-J., Kuhmann, J., Kukies, R., Porst, J.-P., Berger, M., and Rath, M., "Results from the RIT-22 Technology Maturity Demonstration Activity," *50th AIAA/ASME/SAE/ASEE Joint Propulsion Conference*, AIAA Paper 2014-3421, 2014. <https://doi.org/10.2514/6.2014-3421>
- [101] Fisher, J., Ferraiuolo, B., Monheiser, J., Goodfellow, K., Hoskins, A., Myers, R., Bontempo, J., McDade, J., O'Malley, T., Soulas, G., Shastry, R., and Gonzalez, M., "NEXT-C Flight Ion System Status," *AIAA Propulsion and Energy 2020 Forum*, AIAA Paper 2020-3604, 2020. <https://doi.org/10.2514/6.2020-3604>
- [102] Sutton, A. M., Bromaghim, D. R., and Johnson, L. K., "Electric Propulsion Space Experiment (ESEX) Flight Qualification & Operations," *31st Joint Propulsion Conference & Exhibit*, AIAA Paper 1995-2503, 1995. <https://doi.org/10.2514/6.1995-2503>
- [103] Zubair, J., Dao, H., Branch, N., Inaba, D., Welander, B., Frieman, J. D., Kamhawi, H., Lobbia, R., and Hofer, R., "12.5 kW Advanced Electric Propulsion System Thruster Development Testing," *AIAA Propulsion and Energy 2020 Forum*, AIAA Paper 2020-3628, 2020. <https://doi.org/10.2514/6.2020-3628>
- [104] Soendker, E., Hablitzel, S., Haynie, C., Hesterman, B., Poehls, A., Bachand, K., Dinca, D., Boomer, K., Piñero, L., and Birchenough, A., "13 kW Advanced Electric Propulsion System Power Processing Unit Development," *36th International Electric Propulsion Conference*, IEPC Paper 2019-A930, 2019
- [105] Aulisio, M. V., Piñero, L. R., White, B. L., Hickman, T. A., Bontempo, J. J., Hertel, T. A., and Birchenough, A. G., "Status of the Development of Flight Power Processing Units for the NASA's Evolutionary Xenon Thruster—Commercial (NEXT-C) Project," *14th International Energy Conversion Engineering Conference*, AIAA Paper 2016-4519, 2016. <https://doi.org/10.2514/6.2016-4519>
- [106] Thomas, R. E., Aulisio, M. V., Badger, A. R., Heistand, C. C., Thompson, D. S., Liang, R., John, J. W., Goodfellow, K. D., and Bontempo, J. J., "NEXT Single String Integration Tests in Support of the Double Asteroid Redirection Test Mission," *36th International Electric Propulsion Conference*, IEPC Paper 2019-853, 2019.
- [107] Funaki, I., Cho, S., Sano, T., Fukatsu, T., Tashiro, Y., Shiiki, T., Nakamura, Y., Watanabe, H., Kubota, K., Matsunaga, Y., and Fuchigami, K., "Development of a 6-kW-class Hall Thruster for Geostationary Missions," *Acta Astronautica*, Vol. 170, May 2020, pp. 163–171. <https://doi.org/10.1016/j.actaastro.2019.08.029>
- [108] Frieman, J. D., Kamhawi, H., Huang, W., Mackey, J., Ahern, D. M., Peterson, P. Y., Gilland, J. H., Hall, S. J., Hofer, R. R., Inaba, D., Dao, H., Zubair, J., Neuhoﬀ, J., and Branch, N. A., "Characterization Test of the 12.5-kW Advanced Electric Propulsion System Engineering Test Unit Hall Thruster," *AIAA Propulsion and Energy 2020 Forum*, AIAA Paper 2020-3626, 2020. <https://doi.org/10.2514/6.2020-3626>
- [109] Vaughan, C. E., Cassady, R. J., Aadland, R. S., and Kay, R. J., "Integrated Mission Simulation of a 26 kW Flight Arcjet Propulsion System," *29th Joint Propulsion Conference & Exhibit*, AIAA Paper 1993-2395, 1993. <https://doi.org/10.2514/6.1993-2395>
- [110] Shark, S. W. H., Hall, S. J., Jorns, B. A., Hofer, R. R., and Goebel, D. M., "High Power Demonstration of a 100 kW Nested Hall Thruster System," *AIAA Propulsion and Energy 2019 Forum*, AIAA Paper 2019-3809, 2019. <https://doi.org/10.2514/6.2019-3809>
- [111] Funaki, I., Sano, T., Fukatsu, T., Tashiro, Y., Shiiki, T., Cho, S., Matsunaga, Y., Goto, D., and Watanabe, H., "Development Status of 6-kW-Class Hall Thrusters at JAXA," *36th International Electric Propulsion Conference*, IEPC Paper 2019-441, 2019.
- [112] Goebel, D. M., Becatti, G., Reilly, S., Tilley, K., and Hall, S., "High Current Lanthanum Hexaboride Hollow Cathode for 20-200 kW Hall Thrusters," *35th International Electric Propulsion Conference*, IEPC Paper 2017-303, 2017.
- [113] Porst, J.-P., Altmann, C., Arnold, C., Kuhmann, J., Syring, C., Leiter, H.-J., Berger, M., Soto, A., Herty, F., Scholze, F., Eichhorn, C., and Bundesmann, C., "The RIT 2X Propulsion System: Current Development Status," *35th International Electric Propulsion Conference*, IEPC Paper 2017-505, 2017.
- [114] Leiter, H.-J., Kukies, R., Killinger, R., Bonelli, E., Scaranzin, S., and Scortecchi, F., "RIT-22 Ion Engine Development—Endurance Test and Life Prediction," *42nd AIAA/ASME/SAE/ASEE Joint Propulsion Conference & Exhibit*, AIAA Paper 2006-4667, 2006. <https://doi.org/10.2514/6.2006-4667>
- [115] Soendker, E. H., Hablitzel, S., Tolentino, A., Welander, B., Shark, S., Allen, M., Jackson, J., and Pencil, E., "Power Processing and Flow Control for a 100 kW Hall Thruster System," *2018 Joint Propulsion Conference*, AIAA Paper 2018-4419, 2018. <https://doi.org/10.2514/6.2018-4419>
- [116] Altmann, C., Kraus, S., and Valles, P., "Ariane Group 5A Neutralizer Qualification Status," *36th International Electric Propulsion Conference*, IEPC Paper 2019-896, 2019.
- [117] Yim, J. T., Soulas, G. C., Shastry, R., Choi, M., Mackey, J. A., and Sarver-Verhey, T. R., "Update of the NEXT Ion Thruster Service Life Assessment with Post-Test Correlation to the Long-Duration Test," *35th International Electric Propulsion Conference*, IEPC Paper 2017-061, 2017.
- [118] Hofer, R., Polk, J., Mikellides, I., Ortega, A. L., Conversano, R., Chaplin, V., Lobbia, R., Goebel, D., Kamhawi, H., Verhey, T., Williams, G., Mackey, J., Huang, W., Yim, J., Herman, D., and Peterson, P., "Development Status of the 12.5 kW Hall Effect Rocket with Magnetic Shielding (HERMeS)," *35th International Electric Propulsion Conference*, IEPC Paper 2017-231, 2017.
- [119] Becatti, G., Goebel, D. M., Yoke, C. V., Ortega, A. L., and Mikellides, I. G., "High Current Hollow Cathode for the X3 100-kW Class Nested Hall Thruster," *36th International Electric Propulsion Conference*, IEPC Paper 2019-371, 2019.
- [120] Pintó, F., Velasco, R., and Guidoux, E., "Airbus DS PPU Qualification Status for HET, GIT and New Space Technologies," *36th International Electric Propulsion Conference*, IEPC Paper 2019-888, 2019.
- [121] Cassady, R. J., Hoskins, W. A., and Vaughan, C. E., "Development and Flight Qualification of a 26-Kilowatt Arcjet Propulsion Subsystem," *Journal of Propulsion and Power*, Vol. 18, No. 4, 2002, pp. 740–748. <https://doi.org/10.2514/2.6027>
- [122] Rothaus, S., Harmann, H.-P., and Kopp, T., "µFCU—Results of a Prequalification Test Campaign," *33rd International Electric Propulsion Conference*, IEPC Paper 2013-228, 2013.
- [123] Vaughan, C. E., and Morris, J. P., "Propellant Feed Subsystem for a 26 kW Flight Arcjet Propulsion System," *29th Joint Propulsion Conference & Exhibit*, AIAA Paper 1993-2400, 1993. <https://doi.org/10.2514/6.1993-2400>
- [124] Grishin, S. D., Erofeev, V. S., Zharinov, A. V., Naumkin, V. P., and Saftonov, I. N., "Characteristics of a Two-Stage Ion Accelerator with an Anode Layer," *Journal of Applied Mechanics and Technical Physics*, Vol. 19, No. 2, 1978, pp. 166–173. <https://doi.org/10.1007/BF00850027>
- [125] Kurtz, H. L., Auweter-Kurtz, M., Glocker, B., Merke, W., and Schrade, H. O., "A 15 kW Experimental Arcjet," *20th International Electric Propulsion Conference*, IEPC Paper 1988-107, 1988.

- [126] Lang, H., and Loeb, H. W., "Mission Capabilities of the RIT Engines," *10th Electric Propulsion Conference*, AIAA Paper 1973-1073, 1973. <https://doi.org/10.2514/6.1973-1073>
- [127] Bober, A., Maslennikov, N., Day, M., Popov, G., and Rylov, Y., "Development and Application of Electric Propulsion Thrusters in Russia," *23rd International Electric Propulsion Conference*, IEPC Paper 1993-001, 1993.
- [128] Loeb, H. W., "Electric Propulsion Technology Status and Development Plans—European Programs," *Journal of Spacecraft and Rockets*, Vol. 11, No. 12, 1974, pp. 821–828. <https://doi.org/10.2514/3.62183>
- [129] Schmidt, W. M., and Andrews, J. C., "Interests in Electric Propulsion," *20th International Electric Propulsion Conference*, IEPC Paper 1988-005, 1988.
- [130] Haag, T. W., and Curran, F. M., "High-Power Hydrogen Arcjet Performance," *27th Joint Propulsion Conference*, AIAA Paper 1991-2226, 1991. <https://doi.org/10.2514/6.1991-2226>
- [131] Garner, C. E., Brophy, J. R., Polk, J. E., and Pless, L. C., "A 5,730-Hr Cyclic Endurance Test of the NASA-300M," *31st Joint Propulsion Conference & Exhibit*, AIAA Paper 1995-2667, 1995. <https://doi.org/10.2514/6.1995-2667>
- [132] Jacobson, D., and Jankovsky, R., "Performance Evaluation of a 50 kW Hall Thruster," *37th Aerospace Sciences Meeting & Exhibit*, AIAA Paper 1999-0457, 1999. <https://doi.org/10.2514/6.1999-457>
- [133] Jankovsky, R., McLean, C., and McVey, J., "Preliminary Evaluation of a 10 kW Hall Thruster," *37th Aerospace Sciences Meeting & Exhibit*, AIAA Paper 1999-0456, 1999. <https://doi.org/10.2514/6.1999-456>
- [134] Kamhawi, H., Haag, T. W., Jacobson, D. T., and Manzella, D. H., "Performance Evaluation of the NASA-300M 20 kW Hall Effect Thruster," *47th AIAA/ASME/SAE/ASEE Joint Propulsion Conference & Exhibit*, AIAA Paper 2011-5521, 2011. <https://doi.org/10.2514/6.2011-5521>
- [135] Manzella, D., Jankovsky, R., and Hofer, R., "Laboratory Model 50 kW Hall Thruster," *38th AIAA/ASME/SAE/ASEE Joint Propulsion Conference & Exhibit*, AIAA Paper 2002-3676, 2002. <https://doi.org/10.2514/6.2002-3676>
- [136] McVey, J. B., Britt, E. J., Engelman, S. F., Gulczinski, F. S., Beiting, E. J., and Pollard, J. E., "Characteristics of the T-220HT Hall-Effect Thruster," *39th AIAA/ASME/SAE/ASEE Joint Propulsion Conference & Exhibit*, AIAA Paper 2003-5158, 2003. <https://doi.org/10.2514/6.2003-5158>
- [137] Brown, D. L., "Investigation of Low Discharge Voltage Hall Thruster Characteristics and Evaluation of Loss Mechanisms," Ph.D. Dissertation, Dept. of Aerospace Engineering, Univ. of Michigan, Ann Arbor, MI, 2009.
- [138] Hofer, R. R., Cusson, S. E., Lobbria, R. B., and Gallimore, A. D., "The H9 Magnetically Shielded Hall Thruster," *35th International Electric Propulsion Conference*, IEPC Paper 2017-232, 2017.
- [139] Liang, R., "The Combination of Two Concentric Discharge Channels into a Nested Hall-Effect Thruster," Ph.D. Dissertation, Dept. of Aerospace Engineering, Univ. of Michigan, Ann Arbor, MI, 2013.
- [140] Florenz, R., Gallimore, A. D., and Peterson, P. Y., "Developmental Status of a 100-kW Class Laboratory Nested Channel Hall Thruster," *32nd International Electric Propulsion Conference*, IEPC Paper 2011-246, 2011.
- [141] Szabo, J., Pote, B., Byrne, L., Paintal, S., Hruby, V., Tedrake, R., Kolencik, G., Freeman, C., and Gatsonis, N., "Eight Kilowatt Hall Thruster System Characterization," *33rd International Electric Propulsion Conference*, IEPC Paper 2013-317, 2013.
- [142] Szabo, J., Pote, B., Hruby, V., Byrne, L., Tedrake, R., Kolencik, G., Kamhawi, H., and Haag, T. W., "A Commercial One Newton Hall Effect Thruster for High Power In-Space Missions," *47th AIAA/ASME/SAE/ASEE Joint Propulsion Conference & Exhibit*, AIAA Paper 2011-6152, 2011. <https://doi.org/10.2514/6.2011-6152>
- [143] Kamhawi, H., Huang, W., Haag, T., Yim, J., Chang, L., Clayman, L., Herman, D., Shastry, R., Thomas, R., Griffith, C., Myers, J., Williams, G., Mikellides, I., Hofer, R., Polk, J., and Goebel, D., "Overview of the Development of the Solar Electric Propulsion Technology Demonstration Mission 12.5-kW Hall Thruster," *50th AIAA/ASME/SAE/ASEE Joint Propulsion Conference*, AIAA Paper 2014-3898, 2014. <https://doi.org/10.2514/6.2014-3898>
- [144] Rawlin, V., Sovey, J., Anderson, J., and Polk, J., "NSTAR Flight Thruster Qualification Testing," *34th AIAA/ASME/SAE/ASEE Joint Propulsion Conference & Exhibit*, AIAA Paper 1998-3936, 1998. <https://doi.org/10.2514/6.1998-3936>
- [145] Sengupta, A., Anderson, J. A., Garner, C., Brophy, J. R., de Groh, K. K., Banks, B. A., and Thomas, T. A. K., "Deep Space 1 Flight Spare Ion Thruster 30,000-Hour Life Test," *Journal of Propulsion and Power*, Vol. 25, No. 1, 2009, pp. 105–117. <https://doi.org/10.2514/1.36549>
- [146] Foster, J. E., Williams, G. J., and Patterson, M. J., "Characterization of an Ion Thruster Neutralizer," *Journal of Propulsion and Power*, Vol. 23, No. 4, 2007, pp. 828–835. <https://doi.org/10.2514/1.22591>
- [147] Polk, J. E., Goebel, D. M., Snyder, J. S., Schneider, A. C., Johnson, L. K., and Sengupta, A., "A High Power Ion Thruster for Deep Space Missions," *Review of Scientific Instruments*, Vol. 83, No. 7, 2012, Paper 073306. <https://doi.org/10.1063/1.4728415>
- [148] Patterson, M. J., Foster, J. E., Haag, T. W., Rawlin, V. K., Soulas, G. C., and Roman, R. F., "NEXT: NASA's Evolutionary Xenon Thruster," *38th AIAA/ASME/SAE/ASEE Joint Propulsion Conference & Exhibit*, AIAA Paper 2002-3832, 2002. <https://doi.org/10.2514/6.2002-3832>
- [149] Patterson, M. J., and Benson, S. W., "NEXT Ion Propulsion System Development Status and Performance," *43rd AIAA/ASME/SAE/ASEE Joint Propulsion Conference & Exhibit*, AIAA Paper 2007-5199, 2007. <https://doi.org/10.2514/6.2007-5199>
- [150] Bassner, H., Berg, H.-P., Kukies, R., and Mueller, H., "Flight Test and Ground Investigation Results of the RITA Experiment on EURECA," *30th Joint Propulsion Conference & Exhibit*, AIAA Paper 1994-2848, 1994. <https://doi.org/10.2514/6.1994-2848>
- [151] Killinger, R., Kukies, R., Surauer, M., Saccoccia, G., and Gray, H., "Final Report on the ARTEMIS Salvage Mission Using Electric Propulsion," *39th AIAA/ASME/SAE/ASEE Joint Propulsion Conference & Exhibit*, AIAA Paper 2003-4546, 2003. <https://doi.org/10.2514/6.2003-4546>
- [152] Sanks, T. M., Jones, J. M., and Andrews, J. C., "The Electric Propulsion Program at the Astronautics Laboratory," *21st International Electric Propulsion Conference*, AIAA Paper 1990-2657, 1990. <https://doi.org/10.2514/6.1990-2657>
- [153] Jacobson, D. T., Manzella, D. H., Hofer, R. R., and Peterson, P. Y., "NASA's 2004 Hall Thruster Program," *40th AIAA/ASME/SAE/ASEE Joint Propulsion Conference & Exhibit*, AIAA Paper 2004-3600, 2004. <https://doi.org/10.2514/6.2004-3600>
- [154] Oleson, S., and Katz, I., "Electric Propulsion for Project Prometheus," *39th AIAA/ASME/SAE/ASEE Joint Propulsion Conference & Exhibit*, AIAA Paper 2003-5279, 2003. <https://doi.org/10.2514/6.2003-5279>
- [155] Herman, D. A., Tofil, T., Santiago, W., Kamhawi, H., Polk, J. E., Snyder, J. S., Hofer, R. R., Picha, F., Jackson, J., and Allen, M., "Overview of the Development and Mission Application of the Advanced Electric Propulsion System (AEPS)," *35th International Electric Propulsion Conference*, IEPC Paper 2017-284, 2017.
- [156] Casaregola, C., Cesaretti, G., and Andreucci, M., "The European HiPER Programme: High Power Electric Propulsion Technology for Space Exploration," *32nd International Electric Propulsion Conference*, IEPC Paper 2011-209, 2011.
- [157] Zurbach, S., Cornu, N., and Lasgorceix, P., "Performance Evaluation of a 20 kW Hall Effect Thruster," *32nd International Electric Propulsion Conference*, IEPC Paper 2011-020, 2011.
- [158] Coletti, M., and Gabriel, S. B., "Design of a Dual Stage Ion Engine for the HiPER Project," *46th AIAA/ASME/SAE/ASEE Joint Propulsion Conference & Exhibit*, AIAA Paper 2010-7113, 2010. <https://doi.org/10.2514/6.2010-7113>
- [159] Mullins, C., Hruby, V., Pote, B., Blake, K., and Lenguito, G., "Development of a 5 kW Class Hall Thruster," *36th International Electric Propulsion Conference*, IEPC Paper 2019-492, 2019.
- [160] Soulas, G. C., Haag, T. W., Herman, D. A., Huang, W., Kamhawi, H., and Shastry, R., "Performance Test Results of the NASA-457M v2 Hall Thruster," *48th AIAA/ASME/SAE/ASEE Joint Propulsion Conference & Exhibit*, AIAA Paper 2012-3940, 2012. <https://doi.org/10.2514/6.2012-3940>
- [161] Jacobson, D. T., and Manzella, D. H., "50 kW Class Krypton Hall Thruster Performance," *39th AIAA/ASME/SAE/ASEE Joint Propulsion Conference & Exhibit*, AIAA Paper 2003-4550, 2003. <https://doi.org/10.2514/6.2003-4550>
- [162] Mikellides, I. G., Katz, I., Hofer, R. R., Goebel, D. M., Grys, K. D., and Mathers, A., "Magnetic Shielding of the Acceleration Channel Walls in a Long-Life Hall Thruster," *46th AIAA/ASME/SAE/ASEE Joint Propulsion Conference & Exhibit*, AIAA Paper 2010-6942, 2010. <https://doi.org/10.2514/6.2010-6942>

- [163] Brown, N. P., and Walker, M. L. R., "Review of Plasma-Induced Hall Thruster Erosion," *Aerospace*, Vol. 10, No. 11, 2020, Paper 3775. <https://doi.org/10.3390/app10113775>
- [164] Hofer, R. R., Goebel, D. M., Mikellides, I. G., and Katz, I., "Design of a Laboratory Hall Thruster with Magnetically Shielded Channel Walls, Phase II: Experiments," *48th AIAA/ASME/SAE/ASEE Joint Propulsion Conference & Exhibit*, AIAA Paper 2012-3788, 2012. <https://doi.org/10.2514/6.2012-3788>
- [165] Mikellides, I. G., Katz, I., Hofer, R. R., and Goebel, D. M., "Magnetic Shielding of a Laboratory Hall Thruster. I. Theory and Validation," *Journal of Applied Physics*, Vol. 115, No. 4, 2014, Paper 043303. <https://doi.org/10.1063/1.4862313>
- [166] Cusson, S. E., Hofer, R. R., Goebel, D. M., Georgin, M. P., Vazsonyi, A. R., Jorns, B. A., Gallimore, A. D., and Boyd, I. D., "Development of a 30-kW Class Magnetically Shielded Nested Hall Thruster," *36th International Electric Propulsion Conference*, IEPC Paper 2019-266, 2019.
- [167] Carpenter, C. B., and Patterson, M. J., "High-Current Hollow Cathode Development," *27th International Electric Propulsion Conference*, IEPC Paper 2001-274, 2001.
- [168] Kamhawi, H., and Noord, J. V., "Development and Testing of High Current Hollow Cathodes for High Power Hall Thrusters," *48th AIAA/ASME/SAE/ASEE Joint Propulsion Conference & Exhibit*, AIAA Paper 2012-4080, 2012. <https://doi.org/10.2514/6.2012-4080>
- [169] John, J. W., Sarver-Verhey, T., Jacobson, D. T., and Kamhawi, H., "High Current Cathode Development for 50 kW Class Hall Thrusters," *41st AIAA/ASME/SAE/ASEE Joint Propulsion Conference & Exhibit*, AIAA Paper 2005-4244, 2005. <https://doi.org/10.2514/6.2005-4244>
- [170] Noord, J. L. V., Kamhawi, H., and McEwen, H. K., "Characterization of a High Current, Long Life Hollow Cathode," *29th International Electric Propulsion Conference*, IEPC Paper 2005-321, 2005.
- [171] Goebel, D. M., and Chu, E., "High-Current Lanthanum Hexaboride Hollow Cathode for High-Power Hall Thrusters," *Journal of Propulsion and Power*, Vol. 30, No. 1, 2014, pp. 35–40. <https://doi.org/10.2514/1.B34870>
- [172] Sharma, A. K., Chopra, A. K., and Mathew, R., "Emission Poisoning Studies on Impregnated Tungsten Dispenser Cathode Under CO<sub>2</sub> and O<sub>2</sub> Environment," *Applied Surface Science*, Vol. 40, Nos. 1–2, 1989, pp. 97–101. [https://doi.org/10.1016/0169-4332\(89\)90163-3](https://doi.org/10.1016/0169-4332(89)90163-3)
- [173] Gallagher, H. E., "Poisoning of LaB<sub>6</sub> Cathodes," *Journal of Applied Physics*, Vol. 40, No. 1, 1969, pp. 44–51. <https://doi.org/10.1063/1.1657092>
- [174] Sarver-Verhey, T. R., Kamhawi, H., Goebel, D. M., Polk, J. E., Peterson, P. Y., and Robinson, D. A., "Hollow Cathode Assembly Development for the HERMeS Hall Thruster," *52nd AIAA/SAE/ASEE Joint Propulsion Conference*, AIAA Paper 2016-5026, 2016. <https://doi.org/10.2514/6.2016-5026>
- [175] Goebel, D. M., Polk, J. E., and Ho, A. K., "Lanthanum Hexaboride Hollow Cathode Performance and Wear Testing for the Asteroid Redirect Mission Hall Thruster," *52nd AIAA/SAE/ASEE Joint Propulsion Conference*, AIAA Paper 2016-4835, 2016. <https://doi.org/10.2514/6.2016-4835>
- [176] Arkhipov, B. A., Kudriavtsev, S. S., Maslennikov, N. A., Murashko, V. M., and Turgeneva, I. A., "The Development Investigation of the Cathode-Compensator of Stationary Plasma Thrusters for Discharge Currents of up to 50 A," *24th International Electric Propulsion Conference*, IEPC Paper 1995-230, 1995.
- [177] Fearn, D. G., and Patterson, S. W., "Characterisation of the High Current Hollow Cathode for the T6 Ion Thruster," *34th AIAA/ASME/SAE/ASEE Joint Propulsion Conference & Exhibit*, AIAA Paper 1998-3346, 1998. <https://doi.org/10.2514/6.1998-3346>
- [178] Daykin-Iliopoulos, A., Golosnoy, I. O., Gabriel, S., and Bosi, F., "Characterisation of a 30 A Heaterless Hollow Cathode," *36th International Electric Propulsion Conference*, IEPC Paper 2019-802, 2019
- [179] Hall, S. J., Gray, T. G., Yim, J. T., Choi, M., Mooney, M. M., Sarver-Verhey, T. R., and Kamhawi, H., "The Effect of Anode Position on Operation of a 25-A Class Hollow Cathode," *36th International Electric Propulsion Conference*, IEPC Paper 2019-299, 2019.
- [180] Becatti, G., Pedrini, D., Saravia, M. M., Paganucci, F., Andreussi, T., and Andreucci, M., "5-100 A LaB<sub>6</sub> Hollow Cathodes for High-Power Hall Thrusters," *36th International Electric Propulsion Conference*, IEPC Paper 2019-760, 2019.
- [181] Loyan, A., Koshelev, N., Ribalov, O., Dudeck, M., and Zurbach, S., "Results of Tests of High-Current Cathode for High-Power Hall Thruster," *32nd International Electric Propulsion Conference*, IEPC Paper 2011-197, 2011.
- [182] Mazouffre, S., Jousset, R., Vincent, B., Tsikata, S., Oriol, S., and Masson, F., "Characterization of a 100 A-class LaB<sub>6</sub> Hollow Cathode for High-Power Hall Thrusters," *36th International Electric Propulsion Conference*, IEPC Paper 2019-776, 2019.
- [183] Kitaeva, A., Andreussi, T., Pedrini, D., Andreucci, M., and Becatti, G., "Development of a 10-30 kW Augmented Field MPD Thruster at SITAEL," *36th International Electric Propulsion Conference*, IEPC Paper 2019-872, 2019.
- [184] Fink, D. A., Butler, N. R., Planck, P. V., Phillips, R. A., DelPriore, G. A., Gaudreau, M. P. J., Blakely, J. M., Lobbia, R. B., and Brown, D. L., "Development and Test Results of a High Efficiency Low Weight DC-DC SiC FET Based PPU Prototype for Hall Thrusters," *60th JANNAF Propulsion Meeting*, JANNAF Paper AF071-278, 2013.
- [185] Reese, B., McPherson, B., Schupbach, M., and Lostetter, A., "Silicon Carbide Power Processing Unit for Hall Effect Thrusters," *2012 IEEE Aerospace Conference*, 2012. <https://doi.org/10.1109/AERO.2012.6187244>
- [186] Mallmann, A., Forrissi, F., Mache, E., Blaser, M., and Hall, K. W., "High Voltage Power Supply for T5 Gridded Ion Thruster," *36th International Electric Propulsion Conference*, IEPC Paper 2019-A512, 2019.
- [187] Piñero, L. R., Scheidegger, R. J., Aulisio, M. V., and Birchenough, A. G., "High Input Voltage Discharge Supply for High Power Hall Thrusters Using Silicon Carbide Devices," *33rd International Electric Propulsion Conference*, IEPC Paper 2013-388, 2013.
- [188] Piñero, L. R., Peterson, P. Y., and Bowers, G. E., "High Performance Power Module for Hall Effect Thrusters," *38th AIAA/ASME/SAE/ASEE Joint Propulsion Conference & Exhibit*, AIAA Paper 2002-3947, 2002. <https://doi.org/10.2514/6.2002-3947>
- [189] Phelps, T. K., Wiseman, S., Komm, D. S., Bond, T., and Piñero, L., "Development of the NEXT Power Processing Unit," *39th AIAA/ASME/SAE/ASEE Joint Propulsion Conference & Exhibit*, AIAA Paper 2003-4867, 2003. <https://doi.org/10.2514/6.2003-4867>
- [190] Lenguito, G., Neff, K., Barbarits, J., Snyder, J. S., and Chaplin, V., "Versatile Xenon Flow Controller for Extended Hall Effect Thruster Power Range," *36th International Electric Propulsion Conference*, IEPC Paper 2019-303, 2019.
- [191] Su, L. L., Vazsonyi, A. R., and Jorns, B. A., "Performance of a 9-kW Magnetically-Shielded Hall Thruster with Krypton," *AIAA Propulsion and Energy 2020 Forum*, AIAA Paper 2020-3617, 2020. <https://doi.org/10.2514/6.2020-3617>
- [192] Zakharenkov, L., Semenkin, A., Tverdokhlebov, S., Sengupta, A., and Marrese-Reading, C., "Development and Study of the Very High Specific Impulse Bismuth TAL," *30th International Electric Propulsion Conference*, IEPC Paper 2007-128, 2007
- [193] Szabo, J., Robin, M., Paintal, S., Pote, B., Hruby, V., and Freeman, C., "Iodine Propellant Space Propulsion," *33rd International Electric Propulsion Conference*, IEPC Paper 2013-311, 2013.
- [194] Harmann, H.-P., Rothaus, S., and Wanot, G., "μFCU—A Miniaturized Flow Control Unit for Xenon," *33rd International Electric Propulsion Conference*, IEPC Paper 2013-227, 2013.
- [195] Jacobson, D. T., John, J. W., Kamhawi, H., Manzella, D. H., and Peterson, P. Y., "An Overview of Hall Thruster Development at NASA's John H. Glenn Research Center," *41st AIAA/ASME/SAE/ASEE Joint Propulsion Conference & Exhibit*, AIAA Paper 2005-4242, 2005. <https://doi.org/10.2514/6.2005-4242>
- [196] Hall, S. J., Cusson, S. E., and Gallimore, A. D., "30-kW Performance of a 100-kW Class Nested-Channel Hall Thruster," *34th International Electric Propulsion Conference*, IEPC Paper 2015-125, 2015.
- [197] Østgaard, N., Mende, S. B., Frey, H. U., Gladstone, G. R., and Lauche, H., "Neutral Hydrogen Density Profiles Derived from Geocoronal Imaging," *Journal of Geophysical Research*, Vol. 108, No. A7, 2003, Paper 1300. <https://doi.org/10.1029/2002JA009749>
- [198] Piragino, A., Faraji, F., Reza, M., Ferrato, E., Piraino, A., and Andreussi, T., "Background Pressure Effects on the Performance of a 20 kW Magnetically Shielded Hall Thruster Operating in Various Configurations," *Aerospace*, Vol. 8, No. 3, 2021, Paper 69. <https://doi.org/10.3390/aerospace8030069>
- [199] Soulas, G. C., "The Impact of Back-Sputtered Carbon on the Accelerator Grid Wear Rates of the NEXT and NSTAR Ion Thrusters," *33rd International Electric Propulsion Conference*, IEPC Paper 2013-157, 2013.
- [200] Diamant, K. D., Liang, R., and Corey, R. L., "The Effect of Background Pressure on SPT-100 Hall Thruster Performance," *50th AIAA/ASME*

- SAE/ASEE Joint Propulsion Conference, AIAA Paper 2014-3710, 2014.  
<https://doi.org/10.2514/6.2014-3710>
- [201] Nakles, M. R., and Hargus, W. A., Jr., "Background Pressure Effects on Ion Velocity Distribution Within a Medium-Power Hall Thruster," *Journal of Propulsion and Power*, Vol. 27, No. 4, 2011, pp. 737–743.  
<https://doi.org/10.2514/1.48027>
- [202] Huang, W., Kamhawi, H., Haag, T. W., Ortega, A. L., and Mikellides, I. G., "Facility Effect Characterization Test of NASA's HERMeS Hall Thruster," *52nd AIAA/SAE/ASEE Joint Propulsion Conference*, AIAA Paper 2016-4828, 2016.  
<https://doi.org/10.2514/6.2016-4828>
- [203] Walker, J. A., Frieman, J. D., Walker, M. L. R., Khayms, V., King, D., and Peterson, P. Y., "Electrical Facility Effects on Hall-Effect-Thruster Cathode Coupling: Discharge Oscillations and Facility Coupling," *Journal of Propulsion and Power*, Vol. 32, Jan. 2016, pp. 844–855.  
<https://doi.org/10.2514/1.B35835>
- [204] Peterson, P. Y., Kamhawi, H., Huang, W., Yim, J., Herman, D., Williams, G., Gilland, J., and Hofer, R., "NASA HERMeS Hall Thruster Electrical Configuration Characterization," *52nd AIAA/SAE/ASEE Joint Propulsion Conference*, AIAA Paper 2016-5027, 2016.  
<https://doi.org/10.2514/6.2016-5027>
- [205] Randolph, T., Kim, V., Kaufman, H., Kozubsky, K., Zhurin, V., and Day, M., "Facility Effects on Stationary Plasma Thruster Testing," *23rd International Electric Propulsion Conference*, IEPC Paper 1993-093, 1993.
- [206] Garner, C. E., Brophy, J. R., Pless, L. C., and Barnett, J. W., "The Effect of Nitrogen on Xenon Ion Engine Erosion," *21st International Electric Propulsion Conference*, AIAA Paper 1990-2591, 1990.  
<https://doi.org/10.2514/6.1990-2591>
- [207] Noord, J. L. V., and Soulas, G. C., "A Facility and Ion Thruster Back Sputter Survey for Higher Power Ion Thrusters," *41st AIAA/ASME/SAE/ASEE Joint Propulsion Conference & Exhibit*, AIAA Paper 2005-4067, 2005.  
<https://doi.org/10.2514/6.2005-4067>
- [208] Hanna, J., Doerner, R. P., Tynan, G. R., Yu, J. H., Oyarzabal, E., and Taylor, K. J., "Carbon Film Deposition and Flaking Studies in Ion Thruster Environments," *41st AIAA/ASME/SAE/ASEE Joint Propulsion Conference & Exhibit*, AIAA Paper 2005-3524, 2005.  
<https://doi.org/10.2514/6.2005-3524>
- [209] Lobbia, R. B., Polk, J. E., Hofer, R. R., and Chaplin, V. H., "Accelerating 23,000 hours of Ground Test Backsputtered Carbon on a Magnetically Shielded Hall Thruster," *AIAA Propulsion and Energy 2019 Forum*, AIAA Paper 2019-3898, 2019.  
<https://doi.org/10.2514/6.2019-3898>
- [210] Gilland, J. H., Williams, G. J., Burt, J. M., and Yim, J. T., "Carbon Back Sputter Modeling for Hall Thruster Testing," *52nd AIAA/SAE/ASEE Joint Propulsion Conference*, AIAA Paper 2016-4941, 2016.  
<https://doi.org/10.2514/6.2016-4941>
- [211] Crofton, M. W., Nocerino, J. C., Young, J. A., and Patterson, M. J., "NEXT Ion Engine Plume Deposition Rates: QCM Measurements," *52nd Aerospace Sciences Meeting*, AIAA Paper 2014-0140, 2014.  
<https://doi.org/10.2514/6.2014-0140>
- [212] Polk, J. E., Pancotti, A., Haag, T., King, S., Walker, M., Blakely, J., and Ziemer, J., "Recommended Practice for Thrust Measurement in Electric Propulsion Testing," *Journal of Propulsion and Power*, Vol. 33, No. 3, 2017, pp. 539–555.  
<https://doi.org/10.2514/1.B35564>
- [213] Mackey, J., Haag, T., Kamhawi, H., Hall, S., and Peterson, P., "Uncertainty in Inverted Pendulum Thrust Measurements," *2018 Joint Propulsion Conference*, AIAA Paper 2018-4516, 2018.  
<https://doi.org/10.2514/6.2018-4516>
- [214] Tamida, T., Osuga, H., Yamamoto, N., Takegahara, H., Aoyagi, J., and Kuriki, K., "Performance Improvement of Hall Thrusters Using a Pulse-Synchronous Driver System," *Journal of Propulsion and Power*, Vol. 31, No. 3, 2015, pp. 956–961.  
<https://doi.org/10.2514/1.B35273>
- [215] Piñero, L. R., Hill, G. M., Aulisio, M., Gerber, S., Griebeler, E., Hewitt, F., and Scina, J., "Status of a Power Processor for the Prometheus-1 Electric Propulsion System," *41st AIAA/ASME/SAE/ASEE Joint Propulsion Conference & Exhibit*, AIAA Paper 2005-3895, 2005.  
<https://doi.org/10.2514/6.2005-3895>
- [216] Gooder, S. T., "Operational Compatibility of 30-Centimeter-Diameter Ion Thruster with Integrally Regulated Solar Array Power Source," NASA TN-D-8428, July 1977.
- [217] Hamley, J. A., Sankovic, J. M., Miller, J. R., O'Neill, M. J., Lynn, P., and Oleson, S. R., "Hall Thruster Direct Drive Demonstration," *33rd Joint Propulsion Conference & Exhibit*, AIAA Paper 1997-2787, 1997.  
<https://doi.org/10.2514/6.1997-2787>
- [218] Snyder, J. S., Brophy, J. R., Hofer, R. R., Goebel, D. M., and Katz, I., "Experimental Investigation of a Direct-Drive Hall Thruster and Solar Array System," *Journal of Spacecraft and Rockets*, Vol. 51, No. 1, 2014, pp. 360–373.  
<https://doi.org/10.2514/1.A32479>
- [219] Piñero, L. R., Bozak, K. E., Santiago, W., Scheidegger, R. J., and Birchenough, A. G., "Development of High-Power Hall Thruster Power Processing Units at NASA GRC," *51st AIAA/SAE/ASEE Joint Propulsion Conference*, AIAA Paper 2015-3921, 2015.  
<https://doi.org/10.2514/6.2015-3921>
- [220] Reza, M., Faraji, F., and Andreussi, T., "Characterization of a High-Power Hall Thruster Operation in Direct-Drive," *Acta Astronautica*, Vol. 178, Jan. 2021, pp. 392–405.  
<https://doi.org/10.1016/j.actaastro.2020.09.008>
- [221] Herman, D. A., and Unfried, K. G., "Xenon Acquisition Strategies for High-Power Electric Propulsion NASA Missions," GRC-E-DAA-TN23198, June 2015.
- [222] Hall, S. J., Gray, T. G., Yim, J. T., Choi, M., Mooney, M. M., Sarver-Verhey, T. R., and Kamhawi, H., "The Effect of a Hall Thruster-like Magnetic Field on Operation of a 25-A Class Hollow Cathode," *36th International Electric Propulsion Conference*, IEPC Paper 2019-300, 2019.
- [223] Funaki, I., Cho, S., Sano, T., Fukatsu, T., Tashiro, Y., Shiiki, T., Nakamura, Y., Watanabe, H., Kubota, K., Matsunaga, Y., and Fuchigami, K., "1,000-hours Demonstration of a 6-kW-class Hall Thruster for All-Electric Propulsion Satellite," *Transactions of the Japan Society for Aeronautical and Space Sciences, Aerospace Technology Japan*, Vol. 17, No. 5, 2019, pp. 589–595.  
<https://doi.org/10.2322/tastj.17.589>
- [224] Mikellides, I. G., Hofer, R. R., Katz, I., and Goebel, D. M., "Magnetic Shielding of Hall Thrusters at High Discharge Voltages," *Journal of Applied Physics*, Vol. 116, No. 5, 2015, Paper 053302.  
<https://doi.org/10.1063/1.4892160>
- [225] Arhipov, B., Krochak, L., Maslennikov, N., and Scortecchi, F., "Investigation of SPT-200 Operating Characteristics at Power Levels up to 12 kW," *25th International Electric Propulsion Conference*, IEPC Paper 1997-132, 1997.
- [226] Britt, E. J., and McVey, J. B., "Electric Propulsion Activities in U.S. Industries," *38th AIAA/ASME/SAE/ASEE Joint Propulsion Conference & Exhibit*, AIAA Paper 2002-3559, 2002.  
<https://doi.org/10.2514/6.2002-3559>
- [227] Hofer, R., Lobbia, R., Chaplin, V., Ortega, A. L., Mikellides, I., Polk, J., Kamhawi, H., Frieman, J., Huang, W., Peterson, P., and Herman, D., "Completing the Development of the 12.5 kW Hall Effect Rocket with Magnetic Shielding (HERMeS)," *36th International Electric Propulsion Conference*, IEPC Paper 2019-193, 2019.
- [228] Semenkin, A. V., Tverdokhlebov, S. O., Garkusha, V. I., Kochergin, A. V., Chislov, G. O., Shumkin, B. V., Solodukhin, A. V., and Zakharenkov, L. E., "Operating Envelopes of Thrusters with Anode Layer," *27th International Electric Propulsion Conference*, IEPC Paper 2001-013, 2001.
- [229] Arkhipov, B. A., Bober, A. S., Maslennikov, N. A., and Popov, G. A., "Electric Propulsion System for Spacecraft Acceleration and Maneuvering During Flight to Asteroids," *24th International Electric Propulsion Conference*, IEPC Paper 1995-231, 1995.
- [230] Piragino, A., Ferrato, E., Faraji, F., Reza, M., Giannetti, V., Kitaeva, A., Pedrini, D., Andreucci, M., and Andreussi, T., "SITAE's Magnetically Shielded 20 kW Hall Thruster Tests," *36th International Electric Propulsion Conference*, IEPC Paper 2019-879, 2019.
- [231] Tverdokhlebov, S., Semenkin, A., and Polk, J., "Bismuth Propellant Option for Very High Power TAL Thruster," *40th AIAA Aerospace Sciences Meeting & Exhibit*, AIAA Paper 2002-0348, 2002.  
<https://doi.org/10.2514/6.2002-348>
- [232] Gnizdor, R., Komarov, A., Pridannikov, S., and Savchenko, K., "Investigation of the Thrust Vector Angle Stability of the Stationary Plasma Thrusters," *35th International Electric Propulsion Conference*, IEPC Paper 2017-041, 2017.
- [233] Hall, S. J., Jorns, B. A., Gallimore, A. D., Kamhawi, H., Haag, T. W., Mackey, J. A., Gilland, J. H., Peterson, P. Y., and Baird, M. J., "High-Power Performance of a 100-kW Class Nested Hall Thruster," *35th International Electric Propulsion Conference*, IEPC Paper 2017-228, 2017.
- [234] Herman, D. A., Soulas, G. C., and Patterson, M. J., "Performance Evaluation of the Prototype-Model NEXT Ion Thruster," *43rd AIAA/ASME/SAE/ASEE Joint Propulsion Conference & Exhibit*, AIAA Paper 2007-5212, 2007.  
<https://doi.org/10.2514/6.2007-5212>
- [235] Foster, J. E., Haag, T., Kamhawi, H., Patterson, M., Malone, S., Elliot, F., Williams, G. J., Sovey, J. S., and Carpenter, C., "The High Power

- Electric Propulsion (HiPEP) Ion Thruster," *40th AIAA/ASME/SAE/ASEE Joint Propulsion Conference & Exhibit*, AIAA Paper 2004-3812, 2004.  
<https://doi.org/10.2514/6.2004-3812>
- [236] Goodfellow, K. D., and Polk, J. E., "Design and Development of a 3 to 10 kW Ammonia Arcjet," *23rd International Electric Propulsion Conference*, IEPC Paper 1993-078, 1993.
- [237] Polk, J. E., and Goodfellow, K. D., "Results of a 1462 Hour Ammonia Arcjet Endurance Test," *28th Joint Propulsion Conference & Exhibit*, AIAA Paper 1992-3833, 1992.  
<https://doi.org/10.2514/6.1992-3833>
- [238] Aston, G., Aston, M. B., Kolts, J. B., Miller, T. M., and Seaworth, G. B., "5-15 kW High Performance Hydrogen and Ammonia Arcjets," *30th AIAA/ASME/SAE/ASEE Joint Propulsion Conference & Exhibit*, AIAA Paper 1994-2871, 1994.  
<https://doi.org/10.2514/6.1994-2871>
- [239] Hruby, V., Kolencik, J., Martinez-Sanchez, M., Dvorn, D., Annen, K. D., and Brown, R. C., "Methane Arcjet Development," *25th International Electric Propulsion Conference*, IEPC Paper 1997-014, 1997.
- [240] Fife, J. M., Bromaghim, D. R., Chart, D. A., Hoskins, W. A., Vaughan, C. E., and Johnson, L. K., "Orbital Performance Measurements of Air Force Electric Propulsion Space Experiment Ammonia Arcjet," *Journal of Propulsion and Power*, Vol. 18, No. 4, 2002, pp. 749-753.  
<https://doi.org/10.2514/2.6028>
- [241] Goelz, T. M., Auweter-Kurtz, M., and Kurtz, H. L., "Development and Testing of a 100 kW Radiation Cooled Thermal Hydrogen Arcjet Thruster," *23rd International Electric Propulsion Conference*, IEPC Paper 1993-221, 1993.
- [242] Kornfeld, G., Koch, N., Harmann, H.-P., Micheli, P., Meusemann, H., and Gengembre, E., "High Power HEMP-Thruster Module, Status and Results of a DLR and ESA Development Program," *42nd AIAA/ASME/SAE/ASEE Joint Propulsion Conference & Exhibit*, AIAA Paper 2006-4476, 2006.  
<https://doi.org/10.2514/6.2006-4476>
- [243] Squire, J. P., Olsen, C. S., Chang Díaz, F. R., Cassady, L. D., Longmier, B. W., Ballenger, M. G., Carter, M. D., Glover, T. W., McCaskill, G. E., and Bering, E. A., III, "VASIMR®VX-200 Operation at 200 kW and Plume Measurements: Future Plans and an ISS EP Test Platform," *32nd International Electric Propulsion Conference*, IEPC Paper 2011-154, 2011.

J. J. Szabo  
 Associate Editor